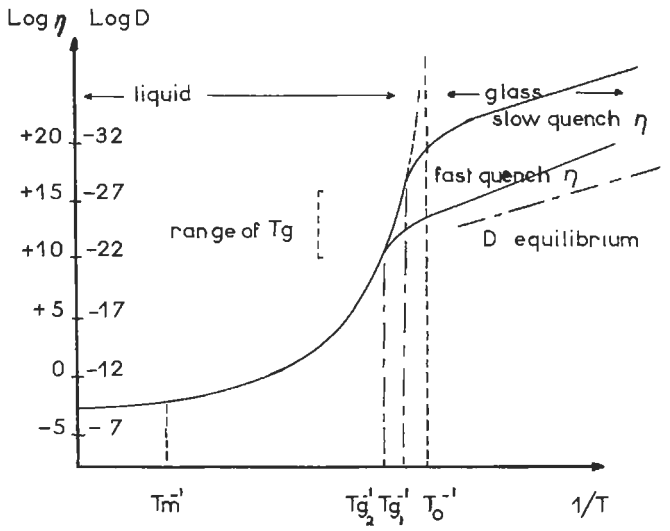

Fig. 22. Viscosity (η) and diffusion (D) evolutions during two rapid quenches of a liquid. Above T_g, in the liquid range, η and D obey the Stokes–Einstein relation. Below T_g, depending on the quench rate, the isoconfigurationnal viscosity evolves according to the "slow" or the "fast" curve. The Stokes–Einstein relationship is no longer obeyed, the diffusion being generally much underestimated.

9.1.1. Experimental portrait of the diffusion behaviour

I) At first, a thermally activated equilibrium diffusion can be defined in all these materials, after a proper annealing. One of the most intriguing characteristics of the diffusion in A.M.A. is its "normal" behaviour: diffusion is arrhenian versus T (but on a quite limited temperature range), and not dispersive (penetration plots are gaussian and D does not depend on time). Apparently D is controlled by a single activation energy Q, or by a very narrow distribution (but see § 9.3), in contradiction with local measurements (see above, § 2.2).

In table 12 a non exhaustive set of tracer determinations of self-and-solute diffusion measurements in various alloys have been gathered. They have been choosen according to the level of confidence the present authors can reasonably have in them. A few of them displaying quite unrealistic diffusion parameters have however been kept in order to give a clue to the possible uncertainty remaining in the other ones.

II) In the first class the best measurements have converged toward i) a Q value of the order of 0.7 to 0.8 of an equivalent solute solvent couple in the crystalline state, ii) the D_0 are within ± 2 orders of magnitude of the corresponding terms. Nevertheless in the first row the D_0 value of the P^{32} tracer (5.10^{-15} m^2/sec!) is a reminiscence of the stone age in the studies of glassy metals during which the D_0 where supposed to be able to cover 38 (!) orders of magnitude (LIMOGE *et al.* [1982]). The same comment applies probably also to P diffusion in the second row; in both cases the value of the P *diffusion coefficient* is nevertheless *in the same range* as the one of the other tracers.

III) In the second class the diffusion of the late T.M. (Fe, Co, Ni, Cu), small atoms,

occurs with a Q nearly equal to the one prevailing in the α-Zr, but not in the α-Ti matrix, and a D_0 of the same order, albeit a bit smaller. A marked correlation has been found (HAHN and AVERBACK [1988]) between the value of D and the size of the solute, reminiscent of the one observed in the crystalline α-Zr or α-Ti matrices (HOOD [1978]). The diffusivity of small solutes is orders of magnitude larger than the diffusivity of big ones. With regard to the mobility of the early T.M. (big atoms) the situation is quite confusing: as probably the mobility is related to the size of the tracer, the results for Au, Ag, Zr and Hf in the various Zr-rich alloys are not consistent, contrarily to the Ti-based alloys, where the recent results are more in line with the behaviour of the first group (row 10). More generally neither for the small nor for the big solutes is the consistency between nearby alloys in the same laboratory (rows 11 and 12) or for similar systems in different laboratories (rows 7, 8 and 9) satisfactory. The possibility to deduce from these results safe values for the activation energies, and even more for the D_0, is not obvious.

Among the experiments which cast a specific light on the possible atomic mechanisms the following results have been obtained.

IV) The isotopic effect has been measured for Co diffusion in a CoFeNbB alloy; it decreases during the relaxation, from 0.5 to 0.1 in a well-relaxed glass (RÄTZKE *et al.* [1992]).

V) The activation volume has been determined in a FeNiPb glass for chemical diffusion yielding a value of 1 Ω (LIMOGE [1987], [1990]), in a CoFeNbB alloy for the Co tracer, yielding a result of $-0.06\ \Omega$ (RÄTZKE and FAUPEL [1992]), and last in a series of NiZr alloys in which the activation volume for the Co tracer varies rather strongly with the concentration from 0.8 to 1.6 Ω (HÖFLER *et al.* [1993]).

VI) Under irradiation, diffusion is enhanced. This has been shown in the first group, using either electron irradiation, that is producing only isolated Frenkel pairs and excluding cascade mixing, (BARBU and LIMOGE [1983]), or heavy ions (TYAGI *et al.* [1991a]), and also in the second group using electrons (LIMOGE [1987]) or heavy ions too (AVERBACK and HAHN [1988]). When measured, the flux dependence is sublinear, of the order of 1/2, pointing *in crystals* to a recombination regime (see § 8.3.1.3). Irradiations at low temperature (30 K) followed by isochronal annealings produce stages similar to the ones in crystalline metals (AUDOUARD and JOUSSET [1979]).

VII) Positron annihilation spectroscopy, possibly due to the competition between vacancy trapping and a high level of volume trapping, does not provide a clear answer, but the results are not incompatible with the existence of vacancy defects in both kind of alloys (TRIFTHÄUSER and KÖGEL [1987]).

VIII) As sketched on the figure 22, the Stokes–Einstein relationship is not obeyed *below* T_g. On the contrary, the viscosity deduced from creep measurements evolves as t^{-1} whatever the duration of the experiment (LIMOGE *et al.* [1882], LIMOGE and BREBEC [1988]), at least in the first group of alloys: with regard to the deformation there is no "equilibrium" structure on any accessible time scale. But the activation energies of diffusion and viscosity are generally very similar.

IX) Hydrogen diffusion has been reviewed by KIRCHEIM [1988]. It has been much studied in PdSi and NiTi alloys by various methods. The main characteristic is that D

Table 12
Diffusion parameters in various metallic glasses.

Alloy	Tracer	D_0 m²/sec	Q_{eV}	$Q_{crystal}$ (eV)	Reference
$Fe_{40}Ni_{40}P_{14}B_6$	Fe^{59}	1.0×10^{-3}	2.0	2.9	a
	P^{32}	5.5×10^{-15}	.81		a
	Fe^{56}	2.7×10^{-2}	2.4	2.9	b
$Fe_{40}Ni_{40}B_{20}$	P^{32}	$1.0\times10^{+4}$	3.1		b
	Ni^{63}	4.0×10^{-4}	2.14		c
	Au	1.9×10^{-4}	2.09		d
$Fe_{80}B_{20}$	Fe^{59}	4.6×10^{-5}	2.1		e
$Pd_{77}Cu_6Si_{17}$	Au	1.2×10^{-5}	1.78		d
	Fe^{59}	3.1×10^{-7}	1.5		e
$Fe_{91}Zr_9$	Zr^{95}	2.1×10^{-3}	2.5		e
	Co^{57}	8.0×10^{-7}	1.52		f
$Co_{89}Zr_{11}$	Au^{195}	7.9×10^{-1}	2.84		
$Co_{74}Ti_{26}$	B^{11}	1.77×10^{-7}	1.63		g
	Co^{60}	3.7×10^{-7}	1.42	1.52 (α Zr)	h
	Ni^{63}	1.7×10^{-7}	1.47	.8 (α Zr)	h
$Ni_{50}Zr_{50}$	Cu	1.2×10^{-6}	1.69		i
	Au	4.8×10^{-6}	2.09		i
	Hf	8×10^{-17}	.75		j
	Ag	1.2×10^{-14}	.82		k
$Cu_{50}Zr_{50}$	Au	1.3×10^{-7}	1.55		k
$Ni_{40}Ti_{60}$	B	7.4×10^{-4}	2.05		l
	Be	1.7×10^{-3}	2.2		l
	Fe	2.5×10^{-3}	2.33	1.2 (α-Ti)	l
	Si	5.8×10^{-4}	2.35		l
$Fe_{28}Zr_{72}$	Fe^{59}	2.6×10^{1}	2.6		e
	Fe^{59}	6.0×10^{-1}	2.3	< 1	e
$Fe_{24}Zr_{76}$	Zr^{95}	7.0×10^{6}	3.2	3.1	e

[a] VALENTA *et al.* [1981]; [b] HORVATH *et al.* [1985]; [c] TYAGI *et al.* [1991b]; [d] AKTHAR *et al.* [1982]; [e] HORVATH *et al.* [1988]; [f] DÖRNER and MEHRER [1991]; [g] LA VIA *et al.* [1992]; [h] HOSHINO *et al.* [1988]; [i] HAHN and AVERBACK [1988]; [j] WU [1991]; [k] STELTER and LAZARUS [1987]; [l] SHARMA *et al.* [1993].

increases with the H concentration with a concomitant decrease of both activation energy and D_0 term. The diffusion in a $Pd_{81}Si_{19}$ alloy can be lower at low concentration than in the crystalline phase, but higher at high concentration (LEE and STEVENSON [1985]). These results can be understood by assuming a distribution of site energies for H, the lowest being filled first and acting like traps which decrease D. A gaussian distribution is usually assumed (KIRCHHEIM *et al.* [1982]), although in-elastic and quasi-elastic neutron scattering are more in agreement with bimodal distributions (RUSH *et al.* [1989]). This bimodal distribution has been seen by H permeation studies in a NiTi system (KIM and STEVESON[1988]).

References: p. 651.

9.1.2. Mechanism proposals

We enter here a more subjective part. Three possibilities are presently explored, namely the so-called collective mechanism, the point defect route and the free volume approach. Lacking space, we will not present here the free volume approach (COHEN and TURNBULL [1961], SPAEPEN [1981]) since in its present state, it is basically an inconsistent *vacancy model* (LIMOGE [1992a)]), which moreover contradicts point VIII) above (among others).

Five reasons are generally invoked to support the proposal of a collective mechanism: i) the difficulty to figure out a defect in the absence of a lattice, ii) the extreme values of the D_0's, iii) the arrhenian behaviour, iv) the small value of the isotope effect, v) the slightly negative value observed for the activation volume in one alloy. The D_0's have been shown particularly to be correlated with the Q's, with a correlation coefficient quite different from the one prevailing in crystals, obtained through Zener's model (§ 3.3.3). This unusual coefficient has been taken as the indication of a new mechanism at work (SHARMA *et al.* [1989]). The points i) ii) iii) iv) will be developed in the next two paragraphs. We have no explanation for the experimental contradictions on point v), except that diffusion under pressure is an extremely difficult task in itself, and *systematic errors* (surface oxidation, thermal gradients, ...) are not easy to avoid, particularly in the glassy systems for the reasons given above. Moreover negative activation volumes are difficult to understand in compact phases. We nevertheless have the feeling that the strongest motivation for that proposal is simply that the glassy state can be obtained in a continuous evolution from the liquid state, making the transposition very natural, despite the break in the D versus 1/T plot in fig. 22. No proposal has been made for describing the diffusion event at an atomic level.

The defect proposal is based on the following ideas: i) a sufficient amount of *local order* in amorphous metallic alloys for defining a defect, ii) a close analogy for D_0 and Q between crystalline and credible results in many glasses, for similar compositions, iii) the existence of irradiation effects, iv) the activation volume measurements, v) from point VIII) above different defects are involved in diffusion and creep, vi) the defect viewed as an energy density fluctuation which must exist in a glass as in any other thermodynamic system. A vacancy defect has been proposed for the first group of alloys and possibly for the large atoms in the second, and an interstitial defect for the small solutes in the second group.

We have no room here to discuss these proposals in detail and the interested reader can find quite extensive developments in the reviews quoted at the beginning, or in the general references given at the end. We would like to emphasize that almost all of these arguments are mere *analogies*. In order to get firmer conclusions we need to develop a better understanding of the atomic mechanism itself, and of its statistical properties. This is the purpose of the following two paragraphs, chiefly in the case of the vacancy proposal for which the most developed studies have been done.

9.2. Simulation approach of the self-diffusion process

The direct simulation of the diffusion, generally by Molecular Dynamics, is a delicate

task since the lowest accessible values of D are of the order of 10^{-11} m^2/s given the present-day limitations of the computing possibilities, to be compared to the 10^{-20} m^2/s which is the typical goal. The direct simulations are therefore limited to the *liquid* range, giving few informations on the *solid* one. The other way is to devise a (and of course if possible all) probable atomic mechanism(s), involving a defect or not, and to study its properties, coming back to macroscopic diffusion using the proper statistical theory.

In the first approach it has been shown several times recently that when the diffusion becomes of the order of 10^{-11} m^2/s, the diffusion *in the liquid* turned progressively from a collective behaviour to a jump one, involving three to five atoms (MIYAGAWA *et al.* [1988], WAHNSTROM [1991]). In the absence of any activation energy determination for these jumps, it is not possible to determine wether they are still active at the much lower temperatures which are of interest here, and which role they could play in diffusion. It is also not possible to build a proper statistical theory for them.

Several works have attempted to characterize point defects in simple models of glasses, using mostly Lennard–Jones interactions (BENNETT *et al.* [1979], DOYAMA *et al.* [1981], LAAKONEN and NIEMINEN [1988, 1990]). These studies generally denied any interest in the notions of interstitial or vacancy, since the latter disappeared quite rapidly after their introduction into a model glass at a non-zero temperature. However, given the small size of the systems studied in simulation, and the possibility that a glass contains sources and sinks for the various possible defects, this elimination is possibly normal if the temperature is high enough to allow the defect to jump (LIMOGE and BREBEC [1988]). This is indeed what has been observed in a careful statistical study of the properties of vacancies in a Lennard–Jones glass: it has been shown that it is possible to define a vacancy defect in this simple model glass (DELAYE and LIMOGE [1992, 1993a, 1993b]). These vacancies are associated with a high level of local order, of a spherical nature in this case. They can jump as soon as the temperature is high enough, and these jumps are frequently collective like those observed in crystalline metals at high temperature, involving from three to five atoms. The least ordered regions in the glass act as defect sources and sinks, and this characteristic feature persists over duration quite long with respect to the duration of a jump sequence. The thermodynamical properties of the vacancy (formation and migration energies, entropies and volumes) were shown to be in quite good agreement with the knowledge gained in actual glasses. We have shown in figure 23 an example of these thermodynamic properties.

Using the results of the theory of the random walk on a random lattice (see § 9.4) LIMOGE [1992b)] and LIMOGE *et al.* [1993] have been able to build a model for the vacancy-mediated diffusion in amorphous metals in reasonable agreement with the experimental results.

The goal now is to check wether the other mechanisms which can be imagined, can be characterized and inserted in a statistical model in a similar way, to compare them with the experiments.

9.3. Random walk on a random array

Due to the lack of translational symmetry, in an amorphous solid the local properties

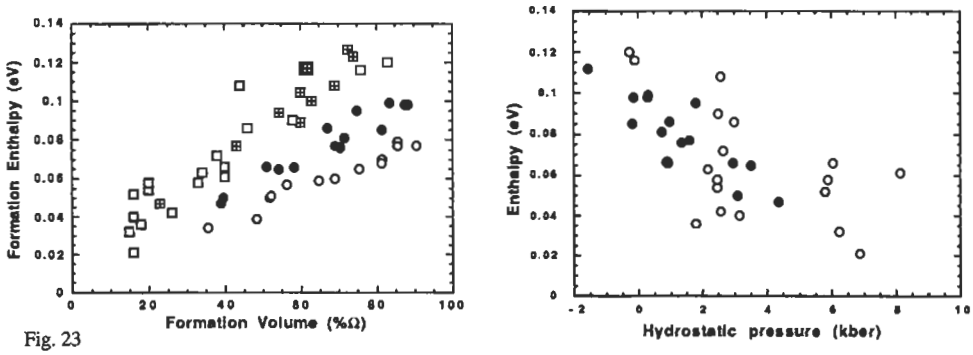

Fig. 23

a. Formation enthalpies, in eV, versus formation volumes, % of an atomic volume.
Rapidly quenched system: □ at 2.5 kbar.
Slowly quenched system: ⊙ at 0. kbar; ● at 0.8 kbar; ⊞ at 2.5 kbar.

b. Same formation enthalpies as in figure 8a but versus local pressure:
Rapidly quenched system: ⊙ at 2.5 kbar.
Slowly quenched system: ● at 0.8 kbar

are distributed. In our case the activation energies determined by local probes show a more or less broad spectrum (BALANZAT [1980], RETTENMEYER *et al.* [1986]), corresponding to a very large spreading of the jump frequencies. The site and the saddle point energies display such a distribution. However they have very different properties and effects upon diffusion, at least in a 3–D space: the saddle disorder tends to accelerate diffusion but the site one slows down a tracer particle. It has only recently be realized that the opposite effects of the two kinds of disorder should produce qualitatively new kinds of behaviour. A theory of the interstitial diffusion at low concentration, combining an analytical approach and Monte Carlo simulations, for the random walk on an energetically random lattice has been built (LIMOGE and BOCQUET [1988, 1989, 1990, 1993]. The main results are the following:

– with respect to long range diffusion, the two kinds of disorder *do not add but more or less compensate each other*. The diffusion coefficient of a tracer particle can be calculated in a mean field approximation as:

$$D^{\infty} = \exp\left(-\beta\left(\overline{\varepsilon_c} - \overline{\varepsilon_s}\right)\exp\left(\frac{1}{2}\beta^2\left(f\sigma_c^2 - \sigma_s^2\right)\right)\right) \tag{76}$$

for gaussian distributions of site and saddle point energies, described by their mean value, $\overline{\varepsilon_S}$ and $\overline{\varepsilon_C}$, and their variances, σ_s and σ_c; f is a slowly varying function of $\beta\sigma_c$ as well as of the nature of the underlying lattice, the high temperature limit of which is unity.

– for values of the σ's compatible with the experimental orders of magnitude, as deduced from the relaxation measurements, the non gaussian regime cannot be detected by *macroscopic diffusion* measurements since the dispersive regime lasts at most a few

jumps, but is accessible to local probes. Once more the two disorders do not add, but the saddle one appears to be dominant, with regard to the dispersive behaviour.

It is clear from the equation (76) that the residual term (exp $(\beta^2(f\sigma_c^2 - \sigma_s^2)/2)$ can be without proper judgement incorporated into an *apparent* D_0, thus appearing very much different from the true pre-exponential factor which is related to an activation entropy (in the above model D_0 equals 1); depending on the nature of the dominant disorder, very large or very low apparent D_0 are obtained. Using the experimental orders of magnitude, the expected deviations can amount to very large values, say of the order of $10^{\pm 3}$, even for undetectable residual curvatures of the Arrhenius plots. Finally, it is interesting to note that in a non perfectly compensated case, one can easily demonstrate that the result of this effect is a Zener-like correlation between the *apparent preexponential term and the apparent activation energy*, the order of magnitude of which is exactly what is found in the experimental results (LIMOGE [1992b]).

All the features of diffusion in amorphous metals can therefore be taken into account at the present day in the framework of the standard defect-mediated models. Of course, this cannot exclude that other mechanisms could compete and be even more efficient, for example the collective relaxation events mentioned above. The proper treatment of these other possibilities, collective or not, is a matter for years to come.

Note added in proof: A very recent work (OLIGSCHLEGER and SCHOBER [1995]) based on M. D. simulations in model glasses reported on the existence of collective relaxation events of low energy, which could partly answer our questions, if transposable to diffusion.

References

ABLITZER, D., 1977, Phil. Mag. **36**, 391.
ABLITZER, D., J. P. HAEUSSLER and K. V. SATHYARAJ, 1983, Philos. Mag. **A47**, 515
ABLITZER, D., and A. VIGNES, 1978, J. Nucl. Mater. **69–70**, 97.
*ABRAGAM, A., 1961, The Principles of Nuclear Magnetism (University Press, Oxford).
ACHAR, B. N. N., 1970, Phys. Rev. **B2**, 3848.
ADAM, P., 1971, Z. Naturf. **26a**, 40.
ADDA, Y., M. H. AMBROISE and F. BARBIER, 1994, Defect and Diffusion Forum **155–156**, 511.
ADDA, Y., M. BELEYER and G. BREBEC, 1975, Thin Solid Films **25**, 107.
ADDA Y., G. BREBEC, R. P. GUPTA and Y. LIMOGE, 1987, in ref. J), p.349.
ADDA. Y. and G. CICCOTTI, 1985, Rapport C. E. A. R-5328.
ADDA, Y. and A. KIRIANENKO , 1959, J. Nucl. Mater. **1**, 120
ADDA, Y. and A. KIRIANENKO, 1962, J. Nucl. Mater. **6**, 130
ADDA, Y., A. KIRIANENKO and C. MAIRY, 1959, J. Nucl. Mater. **3**, 300
*ADDA, Y. and J. PHILIBERT, 1966, La diffusion dans les solides (Presses Universitaires de France. Paris).
AGARWALA, R. P., 1984, Mat. Sc. Forum, **1**, 15.
AIFANTIS, E. C., 1979, Acta Metall. **27**, 683.
AIT SALEM, M., T. SPRINGER, A. HEIDEMANN and B. ALEFELD, 1979, Phil. Mag. **A39**, 797.
AKTHAR, D., B. CANTOR and R. W. CAHN, 1982, Acta Metall. Mater., **30**, 1571.
ALA-NISSILA, T. and S. C. YING, 1992, Progress in Surface Science **39**, 227.
ALEFELD, G., J. VÖLK and G. SCHAUMANN, 1970, Phys. Stat. Sol. **37**, 337.
ALLNATT, A. R., 1965, J. Chem. Phys. 43, 1855.
ALLNATT, A. R., 1981, J. Phys. **C14**, 5453.

ALLNATT, A.R., 1991, Phil. Mag. **A64**, 709.
ALLNATT, A.R. and E.L. ALLNATT, 1984, Phil. Mag. **A49**, 625.
ALLNATT, A.R. and E.L. ALLNATT, 1991, Phil. Mag. **A64**, 341.
ALLNATT, A.R. and E.L. ALLNATT, 1992, Phil. Mag. **A66**, 165.
ALLNATT, A.R., A. BARBU, A. D. FRANKLIN, A. B. LIDIARD, 1983, Acta Metall **31**, 1307.
ALLNATT, A.R. and A.B. LIDIARD, 1987a, Rep. Progr. Physics, 50, 373.
ALLNATT, A.R. and A.B. LIDIARD, 1987b, Acta Metal. **35**, 1555.
ALLNATT, A.R. and A.B. LIDIARD, 1987c, Phil. Mag. Letters **56**, 231.
ALLNATT, A.R. and Y. OKAMURA, 1984, Non-traditional Methods in Diffusion, ed. G.E. Murch, H.K. Birnbaum and J.R. Cost (N.Y.: Met. Soc. AIME), 237.
ANDERSEN H.C., 1980, J. Chem. Phys., **72**, 2384.
ANTHONY, T.R., 1971, Impurity Currents Generated by Vacancy Currents in metals, in: Proc. Conf. Atomic transport in Solids and Liquids, Marstrand (1970), eds. A. Lodding and T. Lagerwall (Zeitschrift für Naturforschung, Tübingen) p. 138.
ANTHONY, T.R., 1972, Solute Segregation and Stresses Generated around Growing Voids in Metals, in : Conf-71060, Proc. Conf. Radiation-induced Voids in Metals, Albany (1971), eds. J.W. Corbett and L.C. Ianniello (USAEC, Oak Ridge) p. 630.
ANTHONY, T.R., 1975, in ref. D), p. 353.
ANTHONY, L., J.K. OKAMOTO and B. FULTZ, 1993, Phys. Rev. Letters **70**, 1128.
AOKI, K. and O. IZUMI, 1975, Phys. Stat. Sol. **a82**, 657.
ARITA, M., M. KOIWA and S. ISHIOKA, 1989, Phil. Mag. **A60**, 563.
ARITA, M., H. NAKAJIMA, M. KOIWA and S. MIURA, 1991, Mat. Trans., JIM, **62**, 32.
Arkhipova, N.K., S.M. Klotsman, I.P. Polikarpova, A.N. Timofeev and P. Shepatkovskii, 1986, Fiz. Met. Metalloved **62**, 1882.
ARNAUD, B., LE HAZIF R. and MARTIN G., 1985, Acta Metall., **33**, 1105.
ARNHOLD, V., 1981, Inaugural dissertation, Münster.
ASKILL, J., 1971, Phys. Stat. Sol. **8**, 587.
AUDOUARD, A. and J.C. JOUSSET, 1979, Rad. Eff. Lett., **50**, 9.
AVERBACK, R.S., R. BENEDEK and K.L. MERKLE, 1978, Phys. Rev. B, **18**, 4156.
AVERBACK, R.S. and H. HAHN, 1988, Phys. Rev. B, **37**, 10833.
Averback, R.S. and H.J. Höfler, 1993, Def. Diff. Forum., **95–98**, 1131.
AVERBACK, R.S. and D.N. SEIDMAN, 1987, **15–18**, 963.
AYRAULT, G. and G. EHRLICH, 1974, J. Chem. Phys. **60**, 281.
BAIK, Y.-J. and D. N. YOON, 1990, Acta Metall. Mater. **38**, 1525.
BAKKER, H., 1971, Phys. Stat. Sol. **44**, 369.
BAKKER, H., 1979, Phil. Mag. **A40**, 525.
BAKKER, H., 1984, J. Less-Common Metals **99**, 257.
BAKKER, H., 1993, Defect and Diffusion Forum **95–98**, 803.
BALANZAT, M., 1980, Scr. Metall., **14**, 173.
BALANZAT, M., and J. HILLAIRET, 1980, The Zener relaxation: A Convenient Tool to Study Vacancy Sources and Sinks in a Metal Lattice, in: Proc. Conf. Internal Friction and Ultrasonic Attenuation in Solids, Manchester (1980), ed. C.C. Smith (Pergamon Press, New York) p. 123.
BALLUFFI, R.W., 1960, Acta Metall. **8**, 871.
BALLUFFI, R.W., and J.W. CAHN, 1981, Acta Metall. **29**, 493
BALLUFFI, R.W., T. KWOK, P.D. BRISTOWE, A. BROKMAN, P.S. HO and S. YIP, 1981, Scripta Metall. **15**, 951.
BALOGH, A.G., I. DESZI, J. PELLOTH, R.A. BRAND, W. KEUNE and W. PUFF, 1992, Materials Science Forum **105–110**, 897.
BARBU, A., 1978, Thèse, Univ. Nancy.
BARBU, A., 1980, Acta Metall. **28**, 499.
BARBU, A., DUNLOP A., LESUEUR D. and AVERBACK R.S., 1991, Europhys. Lett., **15**, 37
BARBU, A., and Y. LIMOGE, 1983, Acta Metall., **31**, 559.
BARBU, A., and G. MARTIN, 1977, Scripta Metall. **11**, 771.
BARCZ, A.J., B.H. PAINE and M.A. NICOLET, 1984, Appl. Phys. Lett., **44**, 45.

BARDEEN, J. and C. HERRING, 1951, Diffusion in Alloys and the Kirkendall Effect, in : Atom Movements, ed. J. H. Hollomon (ASM, Cleveland, OH) p. 87.
BARCZ, A. J., PAINE B. N. and NICOLET M. A., 1984, App. Phys. Lett., **44**, 45.
BARTDORFF, D., G. NEUMANN and P. REIMERS, 1978, Philos. Mag. **38**, 157.
BARTELS, A., 1987, Mat. Sci. Forum **15–18**, 1183.
BASSETT, D. W. and P. R. WEBBER, 1978, Surf. Sci. **70**, 520.
BEAMAN, D. R., and R. W. BALLUFFI, 1965, Phys. Rev. **137**, 917.
BEAMAN, D. R., R. W. BALLUFFI and R. O. SIMMONS, 1964, Phys. Rev. **A134**, 532.
BENNETT, C. H., 1975, in ref. D), 73.
BENNETT, C. H., P. CHAUDHARI, V. MORUZZI and P. STEINHARDT, 1979, Phil. Mag. **A40**, 485.
BENOIST, P., and G. MARTIN, 1975a, Thin Solid Films **25**, 181.
BENOIST, P., and G. MARTIN, 1975b, J. Physique. Colloq. **C4**, 213.
BENOIST, P., J. L. BOCQUET and P. LAFORE, 1977, Acta Metall. **25**, 265.
BERNARDINI, J. and G. MARTIN, 1976, Scripta Metall. **10**, 833.
BERRY, B. S., and J. L. OREHOTSKY, 1968, Acta Metall. **16**, 683.
BEYELER, M., and Y. ADDA, 1968, J. Physique **29**, 345.
BHARATI, S., and A. P. B. SINHA, 1977, Phys. Stat. Sol. (a) **44**, 391.
BLACK, J. E. and Z.-J. TIAN, 1993, Phys. Rev. Letters **71**, 2445.
BLOEMBERGEN, N., E. M. PURCELL and R. V. POUND, 1948, Phys. Rev. **73**, 679.
BOCQUET, J. L., 1972, Acta Metall. **20**, 1347.
BOCQUET, J. L., 1973, Thèse, Univ. Paris-Sud.
BOCQUET, J. L., 1974, Acta Metall. **22**, 1.
BOCQUET, J. L., 1981, C.E.A. (Saclay, France) Internal Report, R-5112.
BOCQUET, J. L., 1983a, J. Phys. **F13**, L33.
BOCQUET, J. L., 1983b, Phil. Mag. **A47**, 547.
BOCQUET, J. L., 1986, Acta Metall. **34**, 571.
BOCQUET, J. L., 1987, Res Mechanica **22**, 1.
BOCQUET, J. L., 1990a, in ref. G), p. 87.
BOCQUET, J. L., 1990b, CEA-Report-R-5531
BOCQUET, J. L., 1991, Phil. Mag. **A63**, 157.
BOCQUET, J. L. and G. MARTIN, 1979, J. Nucl. Mater. **83**, 186.
BONDY, A., P. REGNIER and V. LEVY, 1971, Scripta Metall. **5**, 345.
BONZEL, H. P., 1976, CRC Crit. Rev. Solid State Sci. **6**, 171.
BONZEL, H. P. and E. E. LATTA, 1978, Surf. Sci. **76**, 275.
BOSE, A., G. FROHBERG and H. WEVER, 1979, Phys. Stat. Sol. (a) **52**, 509.
BOSVIEUX, C. and J. FRIEDEL, 1962, J. Phys. Chem. Solids **23**, 12.
BOWKER, M. and D. A. KING, 1978a, Surf. Sci. **71**, 583.
BOWKER, M. and D. A. KING, 1978b, Surf. Sci. **72**, 208.
BRAGG, W. L. and E. J. WILLIAMS, 1934, Proc. Roy. Soc. **A145**, 699.
BRÄTTER, P. and H. GOBRECHT, 1970, Phys. Status Solidi **37**, 869
BREBEC, G., 1977, unpublished work.
BREBEC, G., 1978, Diffusion Atomique, in : Defauts Ponctuels dans les Solides (Les Editions de Physique, Orasy) p. 181.
BREBEC, G., 1990, in ref. G), p.339.
BREITLING, H. M., and R. F. HUMMEL, 1972, J. Phys. Chem. Solids **33**, 845.
BRINKMAN, J. A., 1954, Phys. Rev. **93**, 345.
BRÜNGER, G., O. KANERT and D. WOLF, 1980, Solid State Commun. **33**, 569.
BURTON, B., 1982, The Interaction of Oxidation with Creep Processes, in : Single Crystal Properties, vol. B1, ed. D. J. Fisher (Trans. Tech. S. A., Rockport) p. 1.
BURTON, M. K., N. CABRERA and F. C. FRANK, 1951, Phil. Trans. Roy. Soc. **A243**, 299.
BUTRYMOWICZ, D. B. and J. R. MANNING, 1978, Metallurg. Trans. **9A**, 947.
BUTZ, R. and H. WAGNER, 1979, Surf. Sci. **87**, 69 and 85.
CAHN, J. W., 1967, Trans. AIME **242**, 166.

CAHN, J. W. and R. W. BALLUFFI, 1979, Scripta Metall. **13**, 499.
CAHN, R. W., 1992, Ordered Intermetallics: Physical Metallurgy and Mechanical Behaviour, C. T. Liu, R. W. Cahn and G. Sauthoff Eds.,Kluwer Academic Publishers, 511.
CAPLAIN, A. and W. CHAMBRON, 1977, Acta Metall. **25**, 1001.
CARLSON, O. N. and F. A. SCHMIDT, 1981, J. Less-Common Met. **79**, 97.
CARLSON, P. T., 1976, Metallurg. Trans. **7A**, 199.
CARLSON, P. T., 1978, Metallurg. Trans. **9A**, 1287.
CAR R. and PARRINELLO M., 1985, Phys. Rev. Lett., **55**, 2471.
*CARSLAW, H. S. and J. C. JAEGER, 1959, Conduction of Heat in Solids (Clarendon Press; Oxford)
CAUVIN, R., 1981, C. E. A. report R-5105.
CAUVIN, R. and G. MARTIN, 1981, Phys. Rev. **B23**, 3322 and 3333.
CAUVIN, R. and G. MARTIN, 1982, Phys. Rev. **B25**, 3385.
CHABIK, St. and B. ROZENFELD, 1981, Appl. Phys. **25**, 143.
CHAMBRON, W., and A. CAPLAIN, 1974, Acta Metall. **22**, 357.
CHANDLER, D., 1978, J. Chem. Phys. **68**, 2959.
CHANDLER, D., 1986, J. Stat. Phys. **42**, 49.
CHANDLER, D., 1988, Faraday Discuss. Chem. Soc. **85**, 341.
CHATURVEDI, K. L., and A. R. ALLNATT, 1992, Phil. Mag. **A65**, 1169.
CHATURVEDI, K. L., and A. R. ALLNATT, 1994, Phil. Mag. **A70**, 657.
CHEN, C., and T. T. TSONG, 1994, Phys. Rev. Letters **72**, 498.
CHEN, L. Y., and S. C. YING, 1993, Phys. Rev. Letters **71**, 4361.
CHENG, Y. T., 1990, Mater. Sci. Rep., **5**, 45.
CHIRON, R., and G. FAIVRE, 1985, Philos. Mag. **A51**, 865.
CHOI, J. Y., and P. G. SHEWMON, 1962, Trans. Met. Soc. AIME **224**, 589.
CHU, W. K., J. W. MAYER and M. A. NICOLET, 1978, Backscattering Spectrometry (Academic, New York).
CICCOTTI G., 1991, in ref. R), p. 119.
CICCOTTI, G., M. GUILLOPE and V. PONTIKIS, 1982, in ref. I), p. 415.
* CICCOTTI G. and W. G. HOOVER, 1986, Molecular Dynamics simulations of Statistical Mechanical Systems, (North Holland, Amsterdam).
CLERI, F. and V. ROSATO, 1993, Phil. Mag. Letters **67**, 369.
COHEN M. H. and D. TURNBULL, 1961, J.Chem. Phys., **34**, 120.
COMBRONDE, J. and G. BRÉBEC, 1971, Acta. Metall. **19**, 1393.
COMPAAN, K. and Y. HAVEN, 1956, Trans. Farad. Soc. **52**, 786.
COMPAAN, K. and Y. HAVEN, 1958, Trans. Farad. Soc. **54**, 1498.
COOK, H. E. and J. E. HILLIARD, 1969, J. Appl. Phys. **40**, 2191.
CORDES, H., and K. Kim, 1966, J. Appl. Phys. **37**, 2181.
CORNET, J. A., 1971, J. Phys. Chem. Solids, **32**, 1489.
CORNET, J. F. and D. CALAIS, 1972, J. Phys. Chem. Solids **33**, 1675.
COSTE, V., P. BENOIST and G. MARTIN, 1976, Calcul de la Fréquence Moyenne de Saut des Atomes le long de Joints de Grains à Structure Périodique, in: Proc. 19ème Colloque Métall., La Diffusion dans les Milieux Condensés, Théories et Applications, Saclay 1976 (INSTN, Saclay, France) p. 507.
COUSTY, J., 1981, Thèse, Univ. Paris-Sud; Internal Report CEA-R-5143 (Saclay).
COUSTY, J., R. PEIX and B. PERRAILLON, 1981, Surf. Sci. **107**, 586.
COWAN, P., and T. T. TSONG, 1975, Phys. Lett. **53A**, 383.
COWLEY, J. M., 1950, Phys. Rev. **77**, 669.
*CRANK, J., 1956, The Mathematics of Diffusion (Clarendon Press, Oxford).
CROLET, J. L., 1971, Thèse, Univ. Paris-Sud.
DA FANO, A., and G. JACUCCI, 1977, Phys. Rev. Lett. **39**, 950.
DALLWITZ, M. J., 1972, Acta Metall. **20**, 1229.
DAMKÖHLER, R., and Th. HEUMANN, 1982, Phys. Stat. Sol. (a) **73**, 117.
DARIEL, M. P., D. DAYAN and A. LANGUILLE, 1971, Phys. Rev. **B4**, 4348.
DARIEL, M. P., G. EREZ and G. M. J. SCHMIDT, 1969, Philos. Mag. **19**, 1045.
DARKEN, L. S., 1948, Trans. AIME **175**, 184.

DAVIS, R.E., and W.D. MCMULLEN, 1972, Acta Metall. **20,** 593.
DAYANANDA, M.A., 1981, Acta Metall. **29**, 1151.
DAYANANDA, M.A., 1992, in 'Ordered Intermetallics: Physical Metallurgy and Mechanical Behaviour', Liu, C. T., CAHN R.W. and SAUTHOFF G. Eds, Kluwer Academic Publishers (Boston), 465.
DE BOER, F.R., R. BOOM, W.C.M. MATTENS, A.R. MIEDEMA and A. K. NIESSEN, 1988, Cohesion in Metals: Transition Metal Alloys (NorthHolland, Amsterdam).
DE BRUIN, H.J., A. BAKKER and L.P. VAN DER MEY, 1977, Phys. Stat. Sol. **b82**, 581.
DE BRUIN, H.J., G.E. MURCH, A. BAKKER and L.P. VAN DER MEY, 1975, Thin Solid Films **25**, 47.
DECKER, D.L., J.D. WEISS and H.B. VANFLEET, 1977, Phys. Rev. **B16**, 2392.
*DE GROOT, S.R., and P. MAZUR, 1969, Non-Equilibrium Thermodynamics (North-Holland, Amsterdam).
DELAYE, J.M., 1993, PhD Thesis, Univ. Paris VI.
DELAYE, J.M., and Y. LIMOGE, 1992, Europhys. Lett., **20,** 421.
DELAYE, J.M., and Y. LIMOGE, 1993a, J. Phys. I, **3,** 2063.
DELAYE, J.M., and Y. LIMOGE, 1993b, J. Phys. I, **3,** 2079.
DE LORENZI, G., and F. ERCOLESSI, 1992, Europhys. Let., **20**, 349.
DE LORENZI, G., G. JACUCCI and V. PONTIKIS, 1982, Surf. Sci. **166**, 391.
DESJONQUERES, M.C. and D. SPANJAARD, 1982, J. Phys. **C15**, 4007.
DETEMPLE, K., O. KANERT, K. LINGA MURTY and J. Th.M. DE HOSSON, 1991, Rad. Eff. Def. Sol., **119–121**, 771.
D'HEURLE, F.M., 1971, Proc. IEEE **59**, 1409.
D'HEURLE, F.M., and A. GANGULEE, 1972, Solute effects on Grain Boundaries, Electromigration and Diffusion, in: The Nature and Behaviour of Grain-Boundaries, ed. H. Hu (Plenum, New York).
DIAZ de la RUBIA, T., R.S. AVERBACK, R. BENEDEK and W.E. KING, 1987, Phys. Rev. Lett., **59**, 1930.
DIAZ de la RUBIA, T. and M.W. GUINAN, 1992, Mat. Sci. Forum, **97–99**, 23.
DICKEY, J.E., 1959, Acta Metall. **7,** 350.
DINHUT, J.F., T. BONOU and P. MOINE, 1976, Acta Metall. **24**, 445.
DIRKES, H. and Th. HEUMANN, 1982, J. Phys. **F12**, L 67.
DOAN, N.V., 1971, Thèse, Univ. Paris-Sud.
DOAN, N.V., 1972, J. Phys. Chem. Solids **33**, 2161.
DOAN, N.V., 1978, Dynamique Moléculaire, in: Défauts Ponctuels dans les Solides (Les Editions de Physique, Orsay) p. 285.
DOAN N.V., and Y. ADDA, 1987, Phil. Mag. A, **56**, 269.
DOAN, N.V., and J.L. BOCQUET, 1975, Thin Solid Films **25**, 15.
DOAN, N.V., and J.L. BOCQUET and Y. LIMOGE, 1976, Diffusion sous Champ Electrique et Gradient de Température, in: Proc. 19ème Colloque Métall., La Diffusion dans les Milieux Condensés, Théories et Applications, Saclay 1976 (INSTN, Saclay, France) p. 911.
DOMIAN, H.A., and H.I. AARONSON, 1965, Simultaneous Diffusion of Silver and Magnesium in Stoichiometric Monocrystalline b-AgMg, in: Diffusion in Body-Centered Cubic Metals (ASM, Cleveland, OH) p. 209.
DONALDSON, A.T., and R.D. RAWLINGS, 1976, Acta Metall. **24**, 285.
DORAN, D.G., 1970, Rad. Eff. **2**, 249.
DÖRNER W., and H. MEHRER, 1991, Phys. Rev. B, **44**, 101.
DOYAMA M., R. YAMAMOTO and H. SHIBUTA, 1981, Proc. Int. Conf. R.Q.4, Sendaï 1981, p. 781.
DRECHSLER, M., B.L. BLACKFORD, A.M. PUTNAM and M.H. JERICHO, 1989, Colloque de Physique **C8**, Supplt n°11, **50**, 223.
DUCASTELLE, F., 1978, Electronic Structure and Equilibrium Properties of Metals and Alloys, in: Solid State Phase Transformations in Metals and Alloys, Aussois, 1978, (Les Editions de Physique, Orsay) p. 51.
DUPOUY, J.M., J. MATHIE and Y. ADDA, 1966, Mem. Sci. Rev. Metall. **63,** 481.
DYMENT, F., 1980, in: Titanium 80, Proc. 46th Int. Conf. on titanium, Eds. H. Kimura and O. Izumi, Kyoto p. 519.
ECKSELER, H., and C. HERZIG, 1978, Phys. Stat. Sol. (b) **85**, 185.
EDELIN, G., 1979, Acta Metall. **27**, 455.
*EHRLICH, G., and K. STOLT, 1980, Ann. Rev. Phys. Chem. **31**, 603.
EHRLICH, G., 1994, Surface Science **299/300**, 628.

EINSTEIN, A., 1905, Ann. Phys. **17**, 549.
EINZIGER, R. E., J. N. MUNDY and H. A. HOFF, 1978, Phys. Rev B,**17**, 440.
ELCOCK, E. W., 1959, Proc. Roy. Soc. (London) **73A**, 250.
ELDRIDGE, J. and K. L. KOMAREK, 1964, Trans. AIME **230**, 226.
ELLIS, J., and J. P. TOENNIES, 1993, Phys. Rev. Letters **70**, 2118.
ENGELMANN, C., 1977, Analyse par Observation Directe des Réactions Nucléaires. Rétrodiffusion de Particles Chargées, in: Les Techniques de l'Ingénieur, ed. C. Engelmann, p. 2561.
ENGLISH, C. A., S. M. MURPHY and J. M. PERKS, 1990, J. Chem. Soc. Far. Trans., **86**, 1263.
ERCKMANN, V., and H. WIPF, 1976, Phys. Rev. **37**, 341.
ERMERT, U., W. RUPP and R. SIZMANN, 1968, Thermal and Radiation-Enhanced Self-Diffusion in Gold Single Crystals at low Temperature, in: Proc. Int. Conf. Vacancies and interstitials in metals, Jülich, 1968 (KFA Jülich) p. 30.
ESSMAN, U., and MUGHRABI H., 1979, Phil. Mag. A, **40**, 731.
FÄHNLE, M. 1982, J. Low Temp. Phys. **46**, 3.
FARRARO, R., and R. B. MCLELLAN, 1979, Mat. Sci. Eng. **39**, 47.
FAUPEL, F. and T. HEHENKAMP, 1987, Acta Metall. **35**, 771.
FEIBELMAN, P. J., 1990, Phys. Rev. Letters **65**, 729.
FEIT, M. D., 1972, Phys. Rev. **B45**, 2145.
FIKS, V. B., 1959, Fiz. Tverd. Tela **1**, 16.
FIKS, V. B., 1961, Sov. Phys. Solid. State. **3**, 724.
FIKS, V. B., 1973, Fiz. Metall. Metalloved. **36**, 253.
FILLON, J., and D. CALAIS, 1977, J. Phys. Chem. Solids **38**, 81.
FISHER, J. C., 1951, J. Appl. Phys. **22**, 74.
FLAHIVE, P. G., and W. R. GRAHAM, 1980a, Surf. Sci. **91**, 449.
FLAHIVE, P. G., and W. R. GRAHAM, 1980b, Surf. Sci. **91**, 463.
FLINN, P. A., 1980, Diffusion in Solids and Liquids, in: Application of Mössbauer Spectroscopy VII, ed. R. L. Cohen (Academic, New York) p. 393.
FLYNN, C. P., 1968, Phys. Rev. **171**, 682.
*FLYNN, C. P., 1972, Point Defects and Diffusion (Clarendon Press, Oxford) p. 306.
FLYNN, C. P., 1987, in ref. J), p. 281.
FOILES, S. M., and M. S. DAW, 1987, J. Mater. Res. **2**, 5.
FORT, D., 1987, J. Less. Com. Met., **134**, 45.
FOURNELLE, R. A., 1991, Materials Science and Engineering **A138**, 133.
FRADIN, F. Y., and T. J. ROWLAND, 1967, Appl. Phys. Lett. **11**, 207.
FRANK, F. C., and D. TURNBULL, 1956, Phys. Rev. **104**, 617.
FRANKLIN, A. D., and A. B. LIDIARD, 1983, Proc. R. Soc. Lond. **A389**, 405.
FRANKLIN, A. D., and A. B. LIDIARD, 1984, Proc. R. Soc. Lond. **A392**, 457.
FRENKEN, J. W. M., B. J. HINCH, J. P. TOENNIS and C. WÖLL, 1990, Phys. Rev. **B41**, 938.
FRIEDEL, J., 1964, Dislocations, (Pergamon, Oxford).
FROHBERG, G., 1971, Habilitationsschrift, Berlin, p. 132.
FROMONT, M., A. LANGUILLE and D. CALAIS, 1974, J. Phys. Chem. Solids, **35**, 1367.
FROMONT, F. and G. MARBACH, 1977, J. Phys. Chem. Solids **38**, 27.
GEISE, J., and Ch. Herzig, 1987, Z. Metallkd, 291.
GENDRE, P., Y. LIMOGE and J. L. BOCQUET, 1991, Rapport C.E.A. R-5548.
GERL, M., 1967, J. Phys. Chem. Solids **28**, 725.
GERL, M., 1968, Thèse, Orsay.
GERL, M., and M. LANNOO, 1978, Structure Electronique, in: Defauts Ponctuels dans les Solides (Les Editions de Physique, Orsay) p. 29.
GHALEB, D., 1983, Thèse, Univ. Paris-Sud.
GHILARDUCCI, A. and M. AHLERS, 1983, J. Phys. F: Met. Physics **13**, 1757.
GIBBS, G. B., D. GRAHAM and D. H. TOMLIN, 1963, Phil. Mag. **8**, 1269.
GIBSON J. B., A. N. GOLAND, M. MILGRAM and VINEYARD G., 1960, Phys. Rev., **120**, 1229.
GILDER, H. M., and D. LAZARUS, 1966, Phys. Rev. **145**, 507.

GILDER, M., and D. LAZARUS, 1975, Phys. Rev. **B11**, 4916.
GILLAN, M.J., 1977, J. Phys. C, **10**, 1641.
GILLAN, M.J., 1986, J. Phys. C, **19**, 6169.
GILLAN, M.J., 1989, J. Phys. Condens. Mater., **1**, 689.
GILLAN, M.J., J.H. HARDING and R.J. TARENTO, 1987, J. Phys. C, **20**, 2331.
GIRIFALCO, L.A., 1964, J. Phys. Chem. Solids **24**, 323.
GIRIFALCO, L.A. and H. HERMAN, 1965, Acta Metall. **13**, 583.
GISSLER, W., 1972, Ber. Bunsen Gesell. **76**, 770.
GONZALES, R., J. PIQUERAS and L.I. BRU, 1975a, Phys. Stat. Sol. **29**, 161.
GONZALES, R., J. PIQUERAS and L.I. BRU, 1975b, Mat. Sci. Eng. **20**, 95.
GORNY, D.S., and R.M. ALTOVSKII, 1970, Fiz. Met. Metalloved. **30**, 85.
GORSKY, W.S., 1935, Z. Phys. der Sowjetunion **8**, 457.
GRAF, H., G. BLAZER, E. RECKNAGEL, A. WEIDINGER and R.I. GRYNSZPAN, 1980, Phys. Rev. Lett. **44**, 1333.
GRAHAM, W.R., and G. EHRLICH, 1974, Surf. Sci. **45**, 530.
GRAHAM, W.R., and G. EHRLICH, 1975, Thin Solid Films **25**, 85.
GRANDJEAN, Y., P. BELLON and G. MARTIN, 1994, Phys. Rev. **B50**, 4228.
GREER, A.L., and F. SPAEPEN, in Synthetic modulated structures, 1985, ed. L.L. Chang and B.C. Giessen, (Academic Press. New York).
GUINIER, A., 1959, Adv. Solid State Phys. **9**, 293.
GUPTA, D., 1975, Thin Solid Films **25**, 231.
GUPTA, D., 1982, Phys. Rev., **25**, 5188.
GUPTA, D. and D.S. LIEBERMAN, 1971, Phys. Rev. **B4**, 1070.
GUPTA, D., D. LAZARUS and D.S. LIEBERMAN, 1967, Phys. Rev. **153**, 863.
GUPTA, R.P., 1982, Phys. Rev. **B25**, 5188.
GUPTA, R.P., 1986, Sol. Stat. Com., **59**, 219.
HAESSNER, F., S. HOFMANN and H. SECKEL, 1974, Scripta Metall. **8**, 299.
HAGENSCHULTE H., and Th. HEUMANN, 1989, Defect and Diffusion Forum, **66–69** (DIMETA-88), 459.
HAHN, H., and R.S. Averback, 1988, Phys. Rev. B, **37**, 6533.
HAHN, H., R.S. Averback and H.M. Shyu, 1988, J. Less Comm. Metals, **140**, 345.
HÄHNEL, R., W. MIEKELEY and H. WEVER, 1986, Phys. Stat. Sol. **a97**, 181.
HALBWACHS, M., 1977, PhD Thesis, Université de Grenoble.
HALBWACHS, M., and J. HILLAIRET, 1978, Phys. Rev. **B18**, 4927.
HALBWACHS, M., J. HILLAIRET and S.R. COST, 1978a, J. Nucl. Mater. **69–70**, 776.
HALBWACHS, M., J.T. STANLEY and J. HILLAIRET, 1978b, Phys. Rev. **B18**, 4938.
HALICIOGLU, T., and G.M. POUND, 1979, Thin Solid Films **57**, 241.
HANCOCK, G.F., and B.R. MCDONNELL, 1971, Phys. Stat. Sol. (a) **4**, 143.
HANSEN, L.B., P. STOLTZE, K.W. JACOBSEN and J.K. NÖRSKOV, 1993, Surface Science **289**, 68.
HARRISON, L.G., 1961, Trans. Farad. Soc. **57**, 1191.
HART, E.W., 1957, Acta Metall. **5**, 597.
HÄSSNER, A., and W. LANGE, 1965, Phys. Stat. Sol. **8**, 77.
HAUG, K., and H. METIU, 1991, J. Chem. Phys. **94**, 3251.
HEHENKAMP, T., 1981, Microchim. Acta Suppl. **9**, 15.
HEITJANS, P., A. KÖRBLEIN, H. ACKERMANN, D. DUBBERS, F. FUJIWARA and H.J. STÖCKMANN, 1985, J. Phys. F **15**, 41.
HERZIG, Ch., and H. ECKSELER, 1979, Z. Metallkd. **70**, 215.
HERZIG, Ch., H. ECKSCLER, W. BUSSMANN and D. CARDIS, 1978, J. Nucl. Mater. **69–70**, 61.
HERZIG, C., and Th. HEUMANN, 1972, Z. Naturforschung, **27a**, 1109.
HERZIG, C., and U. KÖHLER, 1987, in ref. J), p.301.
HERZIG, Ch., L. MANKE and W. BUSSMAN, 1982, in: Proc. of Yamada Vth Conf. on point defects and defect interactions in metals, Eds. J.I. Takamura, M. Doyama and M. Kiritani (Univ. of Tokyo Press), p. 578.
HERZIG, C., H.J. ROCKOSCH and R. HILGEDIECK, 1982, in ref I), p. 330.
HEUMANN, T., 1979, J. Phys. **F9**, 1997.
HEUMANN, Th., and R. IMM, 1968, J. Phys. Chem. Solids **29**, 1613.

HEUMANN, T., H. MEINERS and H. STÜER, 1970, Z. Naturforsch. **25a**, 1883.
HEUMANN, T., and Th. ROTTWINKEL, 1978, J. Nucl. Mater. **69–70**, 567.
HEUMANN, T., and H. STÜER, 1966, Phys. Stat. Sol. **15**, 95.
HILGEDIECK, R., 1981, Inaugural dissertation, Münster.
HILGEDIECK, R., and C. HERZIG, 1983, Zeit. Metallkunde **74**, 38.
HILL, J. M., 1979, Scripta Metall. **13**, 1027.
HIRANO, K., 1981, Jump Frequency on Impurity Diffusion in Cu Based on New Data, in: Proc. Yamada Conf. V. - Point Defects and Defect Interactions in Metals, Kyoto (Japan), eds. J. I. Takamura, M. Doyama and M. Kiritani (Univ. of Tokyo Press, 1982) p. 541.
HIRANO, K., R. P. AGARWALA, B. L. AVERBACH and M. COHEN, 1962, J. Appl. Phys. **33**, 3049.
HO, K., and R. A. DODD, 1978, Scripta Metall. **12**, 1055.
HO, K., M. A. QUADER, F. LIN and R. A. DODD, 1977, Scripta Metall. **11**, 1159.
HO, K. M., C. L. FU and B. N. HARMON, 1983, Phys. Rev. B, **28**, 6687.
HO, K. M., C. L. FU and B. N. HARMON, 1984, Phys. Rev. B, **29**, 1575.
HO, P. S., and T. KWOK, 1989, Rep. Prog. Phys., **52**, 301.
HÖFLER H. J., R. S. AVERBACK, G. RUMMEL and H. MEHRER, 1992, Phil. Mag. Lett., **66**, 301.
HOLCOMB, D. F., and R. E. NORBERG, 1955, Phys. Rev. **98**, 1074.
HOLDSWORTH, P. C. W., and R. J. ELLIOTT, 1986, Phil. Mag. **A54**, 601.
HOOD, G. M., 1978, J. Phys. F, **8**, 1677.
HOOD, G. M., 1993, in ref. K), p. 755.
HOOVER, W. G., 1985, Phys Rev A, **31**, 1695.
HORVATH, J., F. DYMENT and H. MEHRER, 1984, J. Nucl. Mater. **126**, 206.
HORVATH, J, J. OTT, K. PFAHLER and W. ULFERT, 1988, Mater. Sci. Eng., **97**, 409.
HORVATH J., K. PFAHLER, W. ULFERT, W. FRANK and H. MEHRER, 1985, J. de Phys., **46**, 645.
HOSHINO K., R. S. AVERBACK, H. HAHN and S. J. ROTHMAN, 1988, Def. Dif. Forum, **59**, 225.
HOSHINO, K., Y. IIJIMA and K. HIRANO, 1981a, Phil. Mag. **A44**, 961.
HOSHINO, K., Y. IIJIMA and K. HIRANO, 1981b, Isotope Effect and Diffusion of Cadmium in Copper, in: Proc. Yamada Conf. V. - Point Defects and Defect Interactions in Metals, Kyoto (Japan), eds. J. I. Takamura, M. Doyama and M. Kiritani (Univ. of Tokyo Press, 1982) p. 562.
HOSHINO, K., Y. IIJIMA and K. HIRANO, 1982, Acta Metall. **30**, 265.
HOWARD, R. E., 1966, Phys. Rev. **144**, 650.
HOWARD, R. E., and A. B. LIDIARD, 1963, J. Phys. Soc. Jap. **18**, Suppl. II, 197.
*HOWARD, R. E., and A. B. LIDIARD, 1964, Rep. Prog. Phys. **27**, 161.
HOWARD R. E., and J. R. MANNING, 1967, Phys. Rev. **154**, 561.
HUANG, F. M., and H. B. HUNTINGTON, 1974, Phys. Rev. **B9**, 1479.
HUANG, J., M. MEYER and V. PONTIKIS, 1991, Phil. Mag. **A63**, 1149.
HUNTINGTON, H. B., 1966, Bull. Am. Phys. Soc. **11**, 265.
HUNTINGTON, H. B., 1968, J. Phys. Chem. Solids. **29**, 1641.
HUNTINGTON, H. B., and A. R. GRÖNE, 1961, J. Phys. Chem. Solids **20**, 76.
HUNTINGTON, H. B., and S. C. HO, 1963, J. Phys. Soc. Jap. **18**, Suppl. II, 20.
HUNTINGTON, H. B., N. C. MILLER and V. NERSES, 1961, Acta Metall. **9**, 749.
HUNTLEY, F. A., 1974, Phil. Mag. **30**, 1075.
IIJIMA , Y., S. I. USHINO and K. I. HIRANO, 1985, Phil. Mag. Letters **A52**, L37.
IORIO, N. R., M. A. DAYANANDA and R. E. GRACE, 1973, Metallurg. Trans. **4**, 1339.
ISHIOKA, S., and M. KOIWA, 1978, Phil. Mag. **A37**, 517.
ISHIOKA, S., and M. KOIWA, 1980, Phil. Mag. **A41**, 385.
ISHIOKA, S., and M. KOIWA, 1984, Phil. Mag. **A50**, 505.
ITO, T., S. ISHIOKA and M. KOIWA, 1990, Phil. Mag. **A62**, 499.
ITOH, T., H. NAKAJIMA, Y. NAKAMURA, M. KOIWA and S. YAMAGUCHI, 1989, Defect and Diffusion Forum **66–69**, 509.
JAMES, D. W., and G. M. LEAK, 1966, Philos. Mag. **14**, 701.
JANOT, C., 1976, J. Physique **37**, 253.
JAUNET, J., C. WALDBURGER and J. PHILIBERT, 1982, Surface Science **121**, 452.

JOB, B., J. MATHIE and P. REGNIER, 1974, Acta Metall. **22**, 1197.
JOHNSON, R. A., and N. Q. LAM, 1976, Phys. Rev. **B13**, 4364.
JOHNSON, R. A., and J. R. BROWN, 1992, J. Mat. Res. **7**, 3213.
JOHNSON, W. L., Y. T. CHENG, M. VAN ROSSUM and M. A. NICOLLET, 1985, N.I.M. B, **7–8**, 657.
JONES, M. J., and A. D. LE CLAIRE, 1972, Phil. Mag. **26**, 1191.
JUVE-DUC, D., D. TREHEUX and P. GUIRALDENQ, 1980, Mat. Sci. Eng. **42**, 281.
KAUR, R., and S. PRAKASH, 1982, J. Phys. **F12**, 1383.
KAXIRAS, E., and J. ERLEBACHER, 1994, Phys. Rev. Letters **72**, 1714.
KEHR, K. W., 1978, Theory of the Diffusion of Hydrogen in Metals, in: Hydrogen in Metals, eds. G. Alefeld and J. Völkl (Springer, Berlin) vol. 1, p. 197.
KELLOG, G. L., 1994, Phys. Rev. Letters **72**, 1662.
KELLY, A., and C. CHIOU, 1958, Acta Metall. **6**, 565.
KIKUCHI, R., 1966, Progr. Theor. Phys. Suppt **35**, 1.
KIM, J. J., and D. A. STEVENSON, 1988, J. non Cryst. Sol., **101**, 187.
KIM, S. J., M. A. NICOLLET, R. S. AVERBACK and D. PEAK, 1988, Phys. Rev. B, **37**, 38.
KIM, S. M., 1991, J. Mat. Res. **6**, 1455.
KING, A. H., and G. DIXIT, 1990, J. de Physique (France), Colloque C1, **51**, 545.
KING, R. T., and W. W. MULLINS, 1962, Acta Metall. **10**, 601.
KIRCHHEIM, R., 1988, Prog. Mat. Sci., **32**, 261.
KIRCHHEIM, R., F. Sommer and G. Schluckebier, 1982, Acta. Metall. **30**, 1059.
*KIRKALDY, J. S., and D. J. YOUNG, 1987, Diffusion in the Condensed State (The Institute of Metals, London).
KNUTH, D. E., 1968, The Art of Computer Programming, (Addison Wesley, Reading).
KOCH, J. M., and C. KOENIG, 1986, Phil. Mag. **B54**, 177.
KÖGEL, G. 1992, Materials Science Forum **105–110**, 341.
KÖHLER, U., and Ch. HERZIG, 1987, Phys. Status Solidi (b) **144**, 243.
KOIWA, M., 1978, Phil. Mag. **45**, 1327.
KOIWA, M., and S. ISHIOKA,1983, Phil. Mag. **A47**, 927.
KOPONEN, I., 1991, Nuc. Instr. and Methods, **B61**, 394.
KÖPPERS, M., C. HERZIG, U. SÖDERVALL and A. LODDING, 1993, in ref. K), p. 783.
KRIVOGLAZ, M. A., 1969, Phys. Met. and Metallogr. **28**, 1.
KROLL, S., N. A. STOLWIJK, C. HERZIG and H. MEHRER, 1993, in ref. K), p. 865.
KRONMÜLLER, H., 1978, Magnetic After-Effects, in: Hydrogen in Metals, eds. C. Alefeld and J. Völkl (Springer, Berlin) vol. 1, p. 289.
KUMAR, P., and R. S. SORBELLO, 1975, Thin Solid Films **25**, 25.
KUO, M., and R. A. FOURNELLE, 1991, Acta Metall. Mater. **39**, 2835.
KUPER, A. B., D. LAZARUS, J. R. MANNING and C. T. TOMIZUKA, 1956, Phys. Rev. **104**, 1536.
KURTZ, A. D., B. L. AVERBACH and M. COHEN, 1955, Acta Metall. **3**, 442.
KUSUNOKI, K., K. TSUMURAYA and S. NISHIKAWA, 1981, Trans. Japan. Inst. Met. **22**, 501.
KWOK, J., P. S. HO, S. YIP, R. W. BALLUFFI, P. D. BRISTOWE and A. BROKMAN, 1981, Phys. Rev. Lett. **47**, 1148.
LAAKKONEN, J., and R. M. Nieminen, 1988, J. Phys. C, **21**, 3663.
LAAKKONEN, J., and R. M. Nieminen, 1990, Phys. Rev., B, **41**, 3978.
LAASONEN, K., 1994, Mater. Sci. Forum, **155–156**, 149.
LA VIA F., K. T. F. JANSSEN and A. H. READER, 1992, Appl. Phys. Lett., **60**, 701.
LAM, N. Q., N. V. DOAN, L. DAGENS and Y. ADDA, 1983, J. Phys. **F13**, 1369.
LANDAU L., and E. LIFSHITZ, 1984, Physique Statistique, 3rd edition, (ed. Mir, Moskow).
LANGUILLE, A., and D. CALAIS, 1974, J. Phys. Chem. Solids **35**, 1461.
LANGUILLE, A., M. P. DARIEL, D. CALAIS and B. COQBLIN, 1973, Mem. Sci. Rev. Metall. **70**, 241.
LANORE, J. M., 1974, Rad. Eff. **22**, 153.
LAPUJOULADE, J., 1994, Surf. Sci. Rep. **20**, 191.
LAZARUS, D., 1960, Solide State Phys. **10**, 71.
LEAMY, H. J., and G. H. GILMER, 1974, J. Cryst. Growth **24/25**, 499.
LE CLAIRE, A. D., 1951, Phil. Mag. **42**, 673.

LE CLAIRE, A. D., 1954, Phys. Rev. **93**, 344.
LE CLAIRE, A. D., 1958, Phil. Mag. **3**, 921.
LE CLAIRE, A. D., 1963, Brit. J. Appl. Phys. **14**, 351.
LE CLAIRE, A. D., 1966, Phil. Mag. **14**, 271.
LE CLAIRE, A. D., 1970a, Correlation Effects in Diffusion in Solids, in: Physical Chemistry, an Adavanced Treatise, eds. H. Eyring, D. Henderson and W. jost (Academic, New York) vol. 10, ch. 5.
LE CLAIRE, A. D., 1970b, Phil. Mag. **21**, 819.
LE CLAIRE, A. D., 1976, Le Point Actuel sur la Théorie de la Diffusion, Anomalies de Diffusion, in: Proc. 19ème Colloque Métall., La Diffusion dans les Milieux Condensés, Théories et Applications, Saclay, 1976 (INSTN, Saclay, France).
LE CLAIRE, A. D., 1978, J. Nucl. Mater. **69–70**, 70.
LE CLAIRE, A. D., 1983, in ref. I), p. 82.
LE CLAIRE, A. D., 1993, in ref. K), p. 19.
LE CLAIRE, A. D., and A. B. LIDIARD, 1956, Phil. Mag. **1**, 518.
LE CLAIRE, A. D., and W. M. LOMER, 1954, Acta Metall. **2**, 731.
LE CLAIRE, A. D., and A. RABINOVITCH, 1981, J. Phys. **C14**, 3863.
LE CLAIRE, A. D., and A. RABINOVITCH, 1982, J. Phys. **C15**, 3455.
LE CLAIRE, A. D., and A. RABINOVITCH, 1983, J. Phys. **C16**, 2087.
LEE, Ch. G., Y. IIJIAMA and K. HIRANO, 1988, The Ninth Japan Symposium Thermophysical properties, p. 1.
LEE Y. S., and D. A. STEVENSON, 1985, J. non Cryst. Sol., **72**, 249.
LEVASSEUR, J., and J. PHILIBERT, 1967, C. R. Acad. Sci. Paris **264**, Sér. C, 277.
LEVINE, H. S., and C. J. MACCALLUM, 1960, J. Appl. Phys. **31**, 595.
LEWIS T. G., and W. H. PAYNE, 1973, J. Ass. Comp. Mach., **20**, 456.
LIDIARD, A. D., 1985, Proc. R. Soc. Lond. **A398,** 203.
LIDIARD, A. D., 1986, Proc. R. Soc. Lond. **A406,** 107.
LIDIARD, A. D., 1987, Proc. R. Soc. Lond. **A413,** 429.
LIDIARD A. B., G. E. MURCH, Z. QUIN and L. ZHANG, 1990, Phil. Mag. A, **62**, 595.
LIMOGE, Y., 1976a, Thèse, Univ. Paris-Sud.
LIMOGE, Y., 1976b, Electromigration dans l'Aluminium, in: Proc. 19ème Colloque de Métall., La Diffusion dans les Milieux Condensés, Théories et Applications, Saclay, 1976 (INSTN, Saclay, France) p. 971.
LIMOGE, Y., 1987, Mat. Sci. Forum, **15–18**, 517.
LIMOGE, Y., 1990, Acta Metall., **38,** 1733.
LIMOGE, Y., 1992a, Scr. Metall., **26**, 809.
LIMOGE, Y., 1992b, Defect and Diffusion Forum, **83**, 145.
LIMOGE, Y., and J. L. BOCQUET, 1988, Acta Metall., **36**, 1717.
LIMOGE, Y., and J. L. BOCQUET, 1989, Diff. Def. Data, **66–69**, 269.
LIMOGE, Y., and J. L. BOCQUET, 1990, Phys. Rev. Lett., **65**, 60.
LIMOGE, Y., and G. BREBEC, 1988, Acta Metall., **36,** 665.
LIMOGE, Y., G. BREBEC and Y. ADDA, 1982, in ref. I), p. 285.
LIMOGE, Y., J. M. DELAYE and J. L. BOCQUET, 1994, Proc. of the 1993 A.S.M./T.M.S. Meeting, Pittsburg, October 1993, ed. H. Jain, D. Gupta, The Min. Met. Mat. Soc., Warrendale, P.A., 79.
LIMOGE, Y., J. L. SERAN and R. SEGUIN, 1977, in Proc. 8th Int. Conf. on X-Ray Optics and Microanalysis, (Boston, MA., U.S.A.).
LITTMARK, U., and W. O. HOFFER, 1980, N.I.M., **168**, 329.
LIU, C. L., and J. B. ADAMS, 1992, Surface Science **265**, 262.
LIU, C. L., J. M. COHEN, J. B. ADAMS and A. F. VOTER, 1991, Surface Science **253**, 334.
LIU, C. T., R. W. CAHN and G. SAUTHOFF, 1992, Ordered Intermetallics: Physical Metallurgy and Mechanical Behaviour, Kluwer Academic Publishers (Boston).
LIU, D., W. A. MILLER and K. T. AUST, 1989, Acta Metall. **37**, 3367.
LO CASCIO, D. M., 1992, Thesis (Amsterdam).
LO CASCIO, D. M. R., P. I. LOEFF and H. BAKKER, 1992, J. Phys.: Condensed Matter **4,** 7441.
LODDER, A., Sol. Stat. Com., 1991, **79**, 143.
LOMER, W. M., 1954, AERE Report T/R 1540.

LORMAND, G., 1970, Thèse, Lyon.
LLOYD J.R., 1990, App. Phys. Let., **57**, 1167.
LUNDY, T.S., and J.F. MURDOCK, 1962, J. Appl. Phys. **33**, 1671.
LUTSKO, J.F., D. WOLF and S.J. YIP, 1988, J. Chem. Phys., **88**, 6525.
LYNN, K.G., and D.O. WELCH, 1980, Phys. Rev. **B22**, 99.
MA, Q., and R.W. BALLUFFI, 1993, Acta Metall. Mater. **41**, 133.
MA, Q., and R.W. BALLUFFI, 1994, Acta Metall. Mater. **42**, 1.
MA, Q., C.L. LIU, J.B. ADAMS and R.W. BALLUFFI, 1993, Acta Metall. Mater. **41**, 143.
MAIER, K., H. MEHRER, E. LESSMANN and W. SCHÜLE, 1976, Phys. Status Solidi (b) **78**, 689.
MAIER, K., H. MEHRER and G. REIN, 1979, Z. Metallkd **70**, 271.
MALLARD, W.C., A.B. GARDNER, R.F. BASS and L.M. SLIFKIN, 1963, Phys. Rev. **129**, 617.
MANNING, J.R., 1964, Phys. Rev. **136**, A 1758.
*MANNING, J.R., 1968, Diffusion Kinetics for Atoms in Crystals (Van Nostrand, Princeton).
MANNING, J.R., 1971, Phys. Rev. **B4**, 111.
MANNING, J.R., 1978, Bull. Am. Phys. Soc., **23**, 287.
MAO, C., 1972, Phys. Rev. **B5**, 4693.
MARECHE, J.F., J.C. RAT and H. HEROLD, 1979, Z. Phys. Chem. Neue Folge **115**, 137.
MARTIN, G., 1972, Phys. Stat. Sol. **14**, 183.
MARTIN, G., and A. BARBU, 1993, in ref. Z), p. 179.
MARTIN, G., and P. BENOIST, 1977, Scripta Metall. **11**, 503.
MARTIN, G., D.A. BLACKBURN and Y. ADDA, 1967, Phys. Stat. Sol. **23**, 223.
MARTIN, G., and P. PERRAILLON, 1979, Measurements of Grain Boundaries Diffusion, in: Grain Boundary Structure and Kinetics, ASM Materials Science Seminar 1979 (ASM, Metals Park, OH) p. 239.
MATANO, C., 1933, Jap. J. Phys. **8**, 109.
MATHUNI, J., O.N. CARLSON, E. FROMM and R. KIRCHHEIM, 1976, Metallurg. Trans. **7A**, 977.
MATHUNI, J., R. KIRCHHEIM and E. FROMM, 1979, Acta Metall. **27**, 1665.
MATLOCK, J.H., and J.P. STARK, 1971, Acta Metall. **19**, 923.
MAYDET, S.I., and K.C. RUSSELL, 1977, J. Mater. Nuc., **64**, 101.
MCCOMBIE, C.W., and E.W. ELCOCK, 1958, Phys. Rev. **B2**, 1451.
MCCREA, W.H., and F.J.W. WHIPPLE, 1940, Proc. Roy. Soc. Edinb. **60**, 281.
MCKEE, R.A., and J.P. STARK, 1975, Acta Metall. **23**, 1145.
MCVAY, G.L., and A.R. DUCHARME, 1974, Phys. Rev. **B9**, 627.
MEHRER H., and W. DÖRNER, 1989, Defect and Diffusion Forum, **66–69**, 189.
MELIUS, C.F., and W.D. WILSON, 1980, Rad. Eff. **53**, 111.
MEYER, R.O., 1969, Phys. Rev. **181**, 1086.
MILITZER, M., W.P. SUN and J.J. JONAS, 1994, Acta Metall. Mater., **42**, 133.
MILLER, J.W., 1969, Phys. Rev. **181**, 1095.
MILLION, B., and J. KUCERA, 1969, Acta Metall. **17**, 339.
MILLION, B., and J. KUCERA, 1971, Czech. J. Phys. **B21**, 161.
MILLION, B., J. RUZICKOVA, J. VELISEK and J. VRESTAL, 1981, Mat. Sc. Eng. **50**, 43.
MIYAGAWA, H., Y. HIWATARI, B. BERNU and J.P. HANSEN, 1998, J. Chem. Phys., **88**, 3879.
MONMA, K., H. SUTO and H. OIKAWA, 1964, J. Japan. Inst. Met. **128**, 192.
MONTET, G.L., 1973, Phys. Rev. **B7**, 650.
MONTY, C., 1972, Thèse, Univ. Paris-Sud.
MULLEN, J.G., 1961, Phys. Rev. **124**, 1723.
MÜLLER A., V. NAUNDORF and M.P. MACHT, 1988, J. Appl. Phys., **64**, 3445.
MULLINS, W.W., and P.G. SHEWMON, 1959, Acta Metall. **7**, 163.
MUNDY, J.N., 1971, Phys. Rev **B3**, 2431.
MUNDY, J.N., 1992, in ref. E), p. 1.
MUNDY, J.N., H.A. HOFF, J. PELLEY, S.J. ROTHMAN, L.J. NOWICKI and F.A. SCHMIDT, 1981, Phys. Rev. **B24**, 658.
MUNDY, J.N., and W.D. MCFALL, 1973, Phys. Rev. **B7**, 4363.
MUNDY, J.N., T.E. MILLER and R.J. PORTE, 1971, Phys. Rev **B3**, 2445.

MUNDY, J. N., S. J. ROTHMAN, N. Q. LAN, H. A. HOFF and L. J. NOWICKI, 1978, Phys. Rev. **B18,** 6566.
*MÜNSTER, A., 1966, Thermodynamique des Processus Irréversibles (Presses Universitaires de France, Paris).
MURCH, G. E., 1982a, Phil. Mag. **A45**, 941; 1982b, Phil. Mag. **A46**, 565; 1982c, Phil. Mag. **A46**, 575.
MURCH G. E., and L. ZHANG, 1990, in ref. G), p. 251.
NACHTRIEB, N. H., and G. S. HANDLER, 1954, Acta Metall. **2**, 797.
NAKAJIMA, H., M. YOSHIOKA and M. KOIWA, 1987, Trans. Jap. Inst. Metals, **28**. 949.
NAKAJIMA, H., and M. KOIWA, 1993, in ref. K), p. 775.
NEEL, L., 1951, J. Phys. Rad. **12**, 339.
NEEL, L., 1952, J. Phys. Rad. **13**, 249.
NEEL, L., 1954, J. Phys. Rad. **14**, 225.
NEUMAN, G., and W. HIRSCHWALD, 1972, Z. Phys. Chem. Neue Folge **Bd.8**, 515.
NEUMANN, C. H., D. LAZARUS and D. B. FITCHEN, 1961, J. Phys. Chem. Solids **20**, 170.
NEUMANN, J. P., 1980, Acta Metall. **28**, 1165.
NICHOLS, F. A., and W. W. MULLINS, 1965a, J. Appl. Phys. **36**, 1826.
NICHOLS, F. A., and W. W. MULLINS, 1965b, Trans. AIME **233**, 1840.
NIELSEN, O. H., J. P. SETHNA, P. STOLTZE, K. W. JACOBSEN and J. K. NØRSKOV, 1994, Europhys. Letters **26**, 51.
NOIMANN, Kh., G. KLOZE and I. L. SOKOL'SKAYA, 1964, Sov. Phys. Solid State **6,** 1369.
NOSE S., 1984, Mol. Phys., **52**, 255.
NOWICK, A. S., 1952, Phys. Rev. **88**, 925.
*NOWICK, A. S., and B. S. BERRY, 1972, Anelastic Relaxation in Crystalline Solids (Academic, New York).
OKAMOTO, P. R., and H. WIEDERSICH, 1974, J. Nucl. Mater. **53**, 336.
OKAMURA, Y., and A. R. ALLNATT, 1983a, J. Phys. **C16**, 1841.
OKAMURA, Y., and A. R. ALLNATT, 1983b, Phil. Mag. **A48**, 387.
OKAMURA, Y., and A. R. ALLNATT, 1984, Phil. Mag. **A50**, 603.
OKAMURA, Y., and A. R. ALLNATT, 1986, Acta Metall. **34**, 189.
OLIGSCHLEGER, C., and H. R. SCHOBER, 1995, Sol. State Comm. **93,** 1035.
ORIANI, R. A., 1969, J. Phys. Chem. Solids **30**, 339.
PANDEY, K. C., 1986, Phys. Rev. Letters **57**, 2287.
PARIS, D., and P. LESBATS, 1975, Scripta Metall. **9**, 1373.
PARIS, D., and P. LESBATS, 1978, J. Nucl. Mater. **69–70**, 628.
PARRINELLO M., and A. RAHMAN, 1981, J. App. Phys., **52**, 7182.
PAVLINOV, L. V., A. M. GLADYSHEV and V. N. BYKOV, 1968, Fiz. Met. Metalloved. **26,** 823.
PERINET, F., 1975, Rapport CEA-4657, Saclay.
PENISSON, J. M., and A. BOURRET, 1975, Mise en Odre de l'Alliage Fe–Ni, in: Proc. 4th Int. Conf. on High-Voltage Electron Microscopy, Toulouse (1975), eds. B. Jouffrey and P. Favard (Sté Française de Microscopie Electronique, Paris) p. 205.
PERRAILLON, B., I. M. TORRENS and V. LEVY, 1972, Scripta Metall. **6**, 611.
PETERSON, D. T., 1977, Electromigration as a Purification Process, in: Electro- and Thermotransport in Alloys, eds. R. E. Hummel and H. B. Huntington (AIME, New York) p. 54.
PETERSON, D. T., and M. F. SMITH, 1982, Metallurg. Trans. **13A**, 821.
PETERSON, N. L., 1964, Phys. Rev. **A136**, 568.
PETERSON, N. L., 1975, in ref. D), p. 115.
PETERSON, N. L., 1978, J. Nucl. Mater. **69–70**, 3: Proc. Int. Conf. on the Properties of Atomic Defects in Metals, Argonne (1976), eds. N. L. Peterson and R. W. Siegel.
PETERSON, N. L., and S. J. ROTHMAN, 1967, Phys. Rev. **163**, 645.
PETERSON, N. L., and S. J. ROTHMAN, 1970, Phys. Rev. **B1**, 3264.
PETERSON, N. L., and S. J. ROTHMAN, 1971, Diffusion and Correlation Effects in Copper-Zinc Alloys, in: Proc. Conf. Atomic Transport in Solids and Liquids, Marstrand (1970), eds. A. Lodding and T. Lagerwall (Zeitschrift für Naturforschung, Tübingen) p. 248.
PETRY W., A. HEIMING, C. HERZIG, and J. TRAMPENAU, 1991, Def. Diff. Forum, **75**, 211.
PETTIFOR, D. G., 1992, in: Ordered Intermetallics: Physical Metallurgy and Mechanical Behaviour, C. T. Liu, R. W. CAHN and G. SAUTHOFF, eds., Kluwer Academic Publishers (Boston), 47.
PIKE, G. E., W. J. CAMP, C. H. SEAGER and G. L. MCVAY, 1974, Phys. Rev. **B10**, 4909.

PONTAU, A. E., and D. LAZARUS, 1979, Phys. Rev. **B19**, 4027.
*PRATT, J. N., and R. G. R. SELLORS, 1973, Electrotransport in Metals and Alloys, in: Diffusion and Defect Monograph Series, ed. F. H. Wöhlbier (Trans. Tech. Publications, Aedermannsdorf, Switzerland).
*PRIGOGINE, I., 1947, Etude Thermodynamique des Phénomènes Irréversibles (Desoer, Liège).
PRINZ, N., and H. WEVER, 1980, Phys. Stat. Sol. **a61**, 505.
QIN, Z., and G. E. MURCH, 1993a, Phil. Mag. **A67**, 757.
QIN, Z., and G. E. MURCH, 1993b, Phil. Mag. **A67**, 369.
QIN, Z., and G. E. MURCH, 1993c, Phil. Mag. **A67**, 381.
RADELAAR, S., 1966, J. Phys. Chem. Solids **27**, 1375.
RADELAAR, S., 1968, Phys. Stat. Sol. **27**, K23.
RADELAAR, S., 1970, J. Phys. Chem. Solids **31**, 219.
RAHMAN, A., 1964, Phys. Rev., **136**, 405.
RÄTZKE K., and F. FAUPEL, 1992, Phys. Rev. B, **45**, 7459.
RÄTZKE K., P. W. HÜPPE and F. FAUPEL, 1992, Phys. Rev. Lett., **68**, 2347.
REGNIER, P., and M. HALBWACHS, 1980, Electron Micros. **4**, 204.
REHN, L. E., and P. R. OKAMOTO, 1989, N.I.M. B, **39**, 104.
REIN, G., and H. MEHRER, 1982, Phil. Mag. A, **45**, 467.
REIN, G., H. MEHRER and K. MAIER, 1978, Phys. Status Solidi (a) **45**, 253.
REINHOLD, U., A. NEIDHARDT, G. KRAUTHEIM and A. ZEHE, 1980, Phys. Stat. Sol (a) **61**, K13.
RESING, H. A., and N. H. NACHTRIEB, 1961, J. Phys. Chem. Solids **21**, 40.
RETTENMEYER, F., E. KISDI-KOSZO and H. KRONMÜLLER, 1986, Phys. Stat. Sol. A, **93**, 597.
REY-LOSADA, C., M. HAYOUN and V. PONTIKIS, 1993, Mat. Res. Soc. Symp. Proc. **291**, 549.
REYNOLDS, J. E., B. L. AVERBACH and M. COHEN, 1957, Acta Metall. **5**, 29.
RHEAD, G. E., 1975, Surf. Sci. **47**, 207.
RICE, S. A., 1958, Phys. Rev., **112**, 804.
RIMBEY, P. R., and R. S. SORBELLO, 1980, Phys. Rev. **B21**, 2150.
RIVIERE, J. P., and J. GRILHE, 1974, Phys. Stat. Sol. (a) **25**, 429.
ROBINSON, J. T., and N. L. PETERSON, 1972, Surf. Sci. **31**, 586.
ROBROCK, K. H., 1981, Mechanical Relaxation Studies of Point Defects in Metals, in: Internal Friction and Ultrasonic Attenuation in Solids, Lausanne (1981), J. Physique **C15**, 709.
ROCKOSCH H. J., and C. HERZIG, 1983, Zeit. Metall., **74**, 94.
ROSENBLUM, M. P., F. SPAEPEN and D. TURNBULL, 1980, Appl. Phys. Lett. **37**, 184.
ROTHMAN, S. J., 1981, in ref. V), p. 189.
ROTHMAN, S. J., and N. L. PETERSON, 1967, Phys. Rev. **154**, 552.
ROULET, C., 1973, Surf. Sci. **36**, 295.
RUOFF, A. L., 1967, J. Appl. Phys. **38**, 3999.
RUOFF, A. L., and R. W. BALLUFFI, 1963, J. Appl. Phys. **34**, 2862.
RUSH, J. J., T. J. UDOVIC, R. HEMPELMANN, D. RICHTER and G. DRIESEN, 1989, J. Phys., **1**, 1061.
RUSSELL, K. C., 1985, Prog. Mater. Sci., **28**, 229.
SANCHEZ, J. M., and D. DE FONTAINE, 1975, Phys. Rev. Lett. **35**, 227.
SANDERS, D. E., and A. E. DEPRISTO, 1992, Surface Science **260**, 116.
SATO, H., 1984, in: Non-Traditional Methods in Diffusion, TMS Conf. Proc., 283.
SCHAEFER, H.-E., R. WÜRSCHUM, M. SOB, T. ZAK, W. Z. YU and W. ECKERT, 1990, Phys. Rev. **B41**, 11869.
SCHAICH, W. L., 1976, Phys. Rev. **B13**, 3350.
SHARMA, S. K., and P. MUKHOPADHYAY, 1990, Acta Metall., **38**, 129.
SCHILLING, W., 1978, J. Nucl. Mater. **69–70**, 465.
SCHILLING, W., 1981, Diffusion of Helium in Metals, in: Proc. Yamada Conf. V: Point Defects and Defect Interactions in Metals, Kyoto (Japan, 1981), Eds. J. I. Takamura, M. Doyama and M. Kiritani (Tokyo) p. 303.
SCHMALZRIED, H., 1974, Solid State Reactions (Academic, New York) ch. 7.
SCHMATZ, D. J., H. A. DOMIAN and H. I. AARONSON, 1966, J. Appl. Phys. **37**, 1741.
SCHMIDT, H., G. FROHBERG and H. WEVER, 1992a, Acta Metall. Mater. **40**, 3105.
SCHMIDT, H., G. FROHBERG, W. MIEKELEY and H. WEVER, 1992b, Phys. Stat. Sol. **b171**, 29.

SCHMITZ, F., and M. FOCK, 1967, J. Nucl. Mater. **21,** 317.
SCHOBER H. R., PETRY W. and TRAMPENAU J., 1992, J. Phys. Condens. Mater., **4,** 9321.
SCHOTTKY, G., 1965, Phys. Stat. Sol. **8,** 357.
SCHULTZ, H., 1991, Mat. Sci. Eng., **A 141,** 149.
SEEGER, A., 1976, The Interpretation of Radiation Damage in Metals, in: Proc. Conf. Fundamental Aspects of Radiation Damage in Metals, Gatlinburg, USA (1975), eds. M. T. Robinson and F. W. Young Jr. (ERDA Report CONF-751006, Oak Ridge) vol. 1, p. 493.
SEEGER, A., 1993, in ref. K), p. 147.
SEEGER, A., and H. MEHRER, 1970, Analysis of Self-Diffusion and Equilibrium Measurements, in: Vacancies and Interstitials in Metals, eds. A. Seeger, D. Schumacher, W. Schilling and J. Diehl (North-Holland, Amsterdam) p. 1.
SEEGER, A., D. WOLF and H. MEHRER, 1971, Phys. Stat. Sol. (b) **48,** 481.
SEPIOL, B., and G. VOGL, 1993a, Phys. Rev. Letters **71,** 731.
SEPIOL, B., and G. VOGL, 1993b, Defect and Diffusion Forum **95–98,** 831.
SEPIOL, B., O. G. RANDL, C. KARNER, A. HEIMING and G. VOGL, 1994, J. Phys.: Condens. Matter **6,** L43.
SERAN, J. L., and Y. LIMOGE, 1981, Surf. Sci., **107,** 176.
SERRUYS, Y., and G. BREBEC, 1982a, Phil. Mag. **A45,** 563.
SERRUYS, Y., and G. BREBEC, 1982b, Phil. Mag. **A46,** 661.
SEYMOUR, E. W. F., 1953, Proc. Phys. Soc. (Lond.) **A66,** 85.
SHALAYEV, V. I., I. B. TKACHENKO, V. A. PAVLOV, N. I. TIMOFEYEV and A. V. GUSHCHINA, 1970, Fiz. Metal. Metalloved **39,** 1061.
SHANKAR, S., and L. L. SEIGLE, 1978, Metallurg. Trans. **9A,** 1467.
SHARMA, S. K., S. BANERJEE, K. JAIN and A. K. JAIN, 1989, J. Mater. Res., **4,** 603.
SHARMA, S. K., M. P. MACHT and V. NAUNDORF, 1993, Def. Dif. Forum, **95–98,** 1145.
SHIANG, K.-D., and T. TSONG, 1994, Phys. Rev. **B49,** 7670.
SHIH, S., and J. P. STARK, 1978, Phys. Rev. **B18,** 711.
SHIRAI, Y., K. MATSUMOTO, M. YAMAGUCHI, K. FUKUDA, R. TANIGUCHI and S. TSUKUI, 1992, Materials Science Forum **105–110,** 1229.
SHIRN, G. A., 1955, Acta Metall. **3,** 87.
SHOLL, C. A., 1981, J. Phys. C., **14,** 2723.
SINGH, R., and D. K. CHATURVEDI, 1993, Phys. Rev. **B48,** 16366.
SINGWI, K. S., and A. SJÖLANDER, 1960a, Phys. Rev. **120,** 1093.
SINGWI, K. S., and A. SJÖLANDER, 1960b, Phys. Rev. **119,** 863.
SIZMANN, R., 1978, J. Nucl. Mater. **69–70,** 386.
SLATE N. B., 1959, The theory of unimolecular reactions, (Cornell Univ. Press).
SMALL, M. B., and D. A. SMITH, 1992, Appl. Phys. Lett., **60,** 3235.
SMIGELKAS, A. D. and E. O. KIRKENDALL, 1947, Trans. AIME **171,** 130.
SNOEK, J. L., 1939, Physica **6,** 591.
SOMENKOV, V. A., and S. S. SHIL'STEIN, 1979, Prog. Mater. Sci. **24,** 267.
SORBELLO, R. S., 1972, Phys. Rev. **B6,** 4757.
SORBELLO, R. S., 1975, Comm. Solid. State Phys. **6,** 117.
SPAEPEN, F., 1981, in Les Houches Lectures XXV, eds. M. Kléman and J. P. Poirier, (North Holland), p. 136.
SPEDDING, F. H., and K. Shiba, 1972, J. Chem. Phys. **57,** 612.
SPOKAS, J. J., and C. P. Slichter, 1959, Phys. Rev. **113,** 1462.
*SPRINGER, T., 1972, Quasi-elestic Neutron Scattering for the Investigation of Diffusive Motion in Solids and Liquids (Springer, Berlin).
STELTER, E., and D. LAZARUS, 1987, Phys. Rev. B, **36,** 18, 9545.
STEPHENSON, B., 1988, Acta Metall. **36,** 2663.
STEINDL, R., G. KÖGEL, P. SPERR, P. WILLUTZKI, D. T. BRITTON and W. TRIFTSHAUSER, 1992, Mater. Sc. Forum, **105–110,** 1455.
STOLWIJK, N. A., 1981, Phys. Stat. Sol. (b) **105,** 223.
STOLWIJK, N. A., BRACHT H., HETTWER H. G., LERCH W., MEHRER H., RUCKI A. and JÄGER W., 1994, Mater. Sci. Forum, **155–156,** 475.

STOLWIJK, N. A., M. VAN GEND and H. BAKKER, 1980, Phil. Mag. **A42**, 783.
STONEHAM, A. M., 1979, Hyperfine Interactions **6**, 211.
STUMP, R., and M. SCHEFFLER, 1994, Phys. Rev. Letters **72**, 254.
SUZUOKA, T., 1961a, Trans. Japan Inst. Met. **2**, 25.
SUZUOKA, T., 1961b, Trans. Japan Inst. Met. **2**, 176.
SUZUOKA, T., 1964, J. Phys. Soc. Jap. **18**, 839.
SZABO, I. A., M. KOIWA and S. ISHIOKA, 1991, Phil. Mag. **A63**, 1137.
SZABO, I. A., I. DARUKA and D. L. BEKE, 1994, Defect and Diffusion Forum **155–156**, 289.
TANIGUCHI, S., 1955, Sci. Rep. Res. Inst. Tohoku Univ. **A7**, 269.
TARCZON, J. C., W. HALPERIN, S. C. CHEN and J. O. BRITTAIN, 1988, Mat. Sc. Eng. **A101**, 99.
TEICHLER, H., 1979, Hyperfine Interactions **6**, 251.
THOMPSON, M. D., and H. B. HUNTINGTON, 1982, Surf. Sci. **116**, 522.
THOMPSON, M. S., and J. E. MORRAL, 1986, Acta Metall. **34**, 339.
TOKUHIRO, T., S. SUSMAN, T. O. BRUN and K. J. VOLIN, 1989, J. Phys. Soc. Jap. **58**, 2553.
TOLLER, M., G. JACUCCI, G. DE LORENZI and C. P. FLYNN, 1985, Phys. Rev. B, **32**, 2082.
TORRENS, I. M., and M. T. ROBINSON, 1972, Computer Simulation of Atomic Displacement Cascades in Metals, in: Proc. Conf. Radiation-Induced Voids in Metals, Albany (1971), eds. J. W. Corbett and L. C. Ianello (USAEC, Oak Ridge) p. 739.
TORREY, H. C., 1954, Phys. Rev. **96**, 690.
TRIFTSHÄUSER, W., and G. KÖGEL, 1987, in ref. DD), p. 218.
TRINGIDES, M. C., and R. GOMER, 1992, Surf. Sci. **265**, 283.
TSOU, J. C., and D. J. QUESNEL, 1983, Mat. Sci. Eng., **59**, 99.
TULLY, J. C., G. H. GILMER and M. SHUGARD, 1979, J. Chem. Phys. **71**, 1630.
TUNG, R. T., and W. R. GRAHAM, 1980, Surf. Sci. **97**, 73.
TURBAN, L., P. NOZIERES and M. GERL, 1976, J. Physique **37**, 159.
TYAGI, A. K., M. P. MACHT and V. NAUNDORF, 1991a, J. Mater. Nucl., **179–181**, 1026.
TYAGI, A. K., M. P. MACHT and V. NAUNDORF, 1991b, Acta Metall. Mater., **39**, 609.
UEBING, C., and R. GOMER, 1991, J. Chem. Phys. **95**, 7626.
UZ, M., and O. N. CARLSON, 1986, J. Less. Com. Met., **116**, 317.
VALENTA, P., K. MAIER, H. KRONMULLER and K. FREITAG, 1981, Phys. Stat. Sol., **105**, 537, and **106**, 129.
VALLEAU, J. P., and S. G. WHITTINGTON, 1977, in ref. O), 137.
VAN DER EERDEN, J. P., P. BENNEMA and T. A. CHEREPANOVA, 1978, Prog. Cryst. Growth Charact. **1**, 219.
VANFLEET, H. B., 1980, Phys. Rev. **B21**, 4340.
VAN EK, J., and A. LODDER, 1991, J. Phys., **3**, 7307 and 7331.
VAN HOVE, L., 1954, Phys. Rev. **95**, 249.
VAN OMNEN, A. H., and J. DE MIRANDA, 1981, Phil. Mag. **A43**, 387.
VAN WINKEL, A., A. W. WEEBER and H. BAKKER, 1984, J. Phys. F: Met. Phys. **14**, 2631.
VAN WINKEL, A., and H. BAKKER, 1985, J. Phys. F: Met. Phys. **15**, 1565.
VAROTSOS, P. A., 1978, J. Phys. **F8**, 1373.
*VAROTSOS P. A., and K. D. ALEXOPOULOS, 1986, Thermodynamics of point defects and their relation with bulk properties, (North Holland).
VERBRUGGEN, A. H., 1988, IBM J. Res. Dev., **32**, 93.
VILLEMAIN, P., 1970, 3rd Cycle Thesis, Grenoble University.
VINEYARD, G. H., 1957, J. Phys. Chem. Sol., **3**, 121.
VOGL, G., C. H. KARNER, O. RANDL, B. SEPIOL and D. TUPPINGER, 1992, Ordered Intermetallics: Physical Metallurgy and Mechanical Behaviour, C. T. Liu, R. W. Cahn and G. Sauthoff Eds., Kluwer Academic Publishers, 497.
VOGL, G., W. PETRY, T. FLOTTMANN and A. HEIMING, 1989, Phys. Rev. B, **39**, 5025.
VOGL, G., O. G. RANDAL, W. PETRY and J. HÜNECKE, 1993, J. Phys.: Condensed Matter **5**, 7215.
VÖLKL, J., 1972, Ber. Bunsen Gesell. **76**, 797.
VÖLKL, J., and G. ALEFELD, 1978, Diffusion of Hydrogen in Metals, eds. G. Alefeld and J. Völkl (Springer, Berlin) vol.1, p. 231.
VOTER, A. F., and J. DOLL, 1985, J. Chem. Phys. **82**, 80.

WADE, W. Z., D. W. SHORT, J. C. WALDEN and J. W. MAGANA, 1978, Metall. Trans. **9A**, 965.
WAEGEMAEKERS, A. A. H. J., Thesis (Amstersdam 1990).
WAHNSTROM, G. H., 1991, Phys. Rev., **A44**, 3752.
WARBURTON, W. K., 1975, Phys. Rev. **B11**, 4945.
WARBURTON, W. K., and D. TURNBULL, 1975, in ref. D), p. 171.
WEILER, D., H. MEHRER and N. A. STOLWIJK, 1984, Phil. Mag. **A50**, 559.
WELCH, D. O., G. J. DIENES and O. W. LAZARETH, 1984, J. Phys. Chem. Solids **45**, 1225.
WELCH, D. O., and A. D. LE CLAIRE, 1967, Phil. Mag. **16**, 981.
WERNER, M., H. MEHRER and H. SIETHOFF, 1983, J. Phys. C: Solid State Phys. **16**, 6185.
WERT, C. A., and C. ZENER, 1949, Phys. Rev., **76**, 1169.
WEVER, H., 1983, Zeit. Metall., **74**, 1.
WEVER, H., 1992, Defect and Diffusion Forum, **83**, 55.
WHIPPLE, R. T. P., 1954, Phil. Mag. **45**, 1225.
WIEDERSICH, H., 1990, Rad. Eff. Deff. Solids, **113**, 97.
WIEDERSICH, H., P. R. OKAMOTO and N. Q. LAM, 1979, J. Mater. Nuc., **83**, 98.
WILLAIME, F., and C. MASSOBRIO, 1990, in Atomic Scale Calculations of Structure in Materials, eds. M. S. Daw and M. A. Schluter, (MRS Soc., Pittsburgh), p. 295.
WILLAIME, F., 1991, to be published.
WILLAIME, F., and M. NASTAR, 1994, private communication.
WILLIAM, M. L., R. F. LANDEL and J. D. FERRY, 1955, J. Am. Chem. Soc., **77**, 3701.
WILSON, W. D., and C. L. BISSON, 1973, Rad. Eff. **19**, 53.
WINTENBERGER, M., 1959, Acta Metall. **7**, 549.
WIRTZ, K., 1943, Z. Phys. **44**, 231.
WOLF, D., 1979, Spin Temperature and Nuclear Spin Relaxation in Matter (Clarendon Press, Oxford).
WOLF, D., 1980, J. Phys. Chem. Solids **41**, 1053.
WOLF, D., 1983, Phil. Mag. A, **47**, 147.
WOLF, D., 1990a, J. Mater. Res. **5**, 1708.
WOLF, D., 1990b, J. Appl. Phys. **69**, 185.
WOLF, D., 1991, Phil. Mag. **A63**, 1117.
WOLLENBERGER, H., V. NAUNDORF and M. P. MACHT, in ref. L), p. 201.
WONNELL, S. K., J. M. DELAYE, M. BIBOLE and Y. LIMOGE, 1992, J. Appl. Phys., **72**, 5195.
WU, H. M., 1991, Effect of Atomic Size on Diffusion in Metallic Glasses, Ph. D. thesis, Illinois Univ.
WYNBLATT, P., and N. A. GJOSTEIN, 1968, Surf. Sci. **12**, 109.
XIE, Z.-Y., and D. FARKAS, 1994, J. Mat. Res. **9**, 875.
YANG, M. H., and C. P. FLYNN, 1989, Phys. Rev. Letters **62**, 2476.
YASUDA, H., H. NAKAJIMA and M. KOIWA, 1993, Defect and Diffusion Forum **95–98**, 823.
YASUNAGA, H., 1991, Surf. Sci. **242**, 171.
YOSHIDA, Y., 1989, Hyper. Int., **47**, 95.
YU, G., and K. LÜCKE, 1992, Acta Metall. Mater. **40**, 2523.
ZEE, R. P., 1989, J. Phys., **1**, 5631.
ZENER, C., 1943, Trans. AIME **152**, 122.
ZENER, C., 1947, Phys. Rev. **71**, 34.
ZENER, C., 1951, J. Appl. Phys. **22**, 372.
ZHANG, L., W. A. OATES and G. E. MURCH, 1989a, Phil. Mag. **B60**, 277.
ZHANG, L., W. A. OATES and G. E. MURCH, 1989b, Phil. Mag. **A59**, 171.
ZHANG, Z., K. HAUG and H. METIU, 1990, J. Chem. Phys. **93**, 3614.
ZIERLER, N., 1959, J. Soc. Ind. Appl. Math., **7**, 31.

Further reading

The references in the preceding list marked with an asterisk can also be used for general reading.

Diffusion data

A) All numerical results concerning diffusion are gathered in: Diffusion and Defect Data (DDD), eds. F. H. Wohlbier and D. J. Fisher (Trans. Tech. Publications, Aedermannsdorf, Switzerland), a review which appears three times a year.

B) A comprehensive issue of the Landolt–Börnstein New Series (vol. 26), Ed. O. Madelung (Springer-Verlag, 1990) is devoted to "Diffusion in Solid Metals and Alloys".

General references

C) PHILIBERT, J., 1991, Atom movements, diffusion and mass transport in solids, (Editions de Physique, Les Ulis, France).

D) Diffusion in Solids - Recent Developments, 1975, eds. A. S. Nowick and J. J. Burton, (Academic, New York).

E) Diffusion in Solids: unsolved Problems, 1992, Ed. G. E. Murch, (Trans. Tech. Pub., Aedermansdorf).

F) Atomic Transport in Solids, A. R. Allnatt and A. B. Lidiard, 1993, (Cambridge Univ. Press).

G) Diffusion in Materials, 1990, NATO ASI Series n° E 179, eds. A. L. Laskar, J. L. Bocquet, G. Brebec and C. Monty, (Kluwer, Dordrecht).

H) Proc. Int. Conf. on Atomic Defects in Metals, Argonne (1976), eds. N. L. Peterson and R. W. Siegel, J. Nucl. Mater. **69–70** (1978).

I) Proc. Int. Conf. on Diffusion in Metals and Alloys, 1982, Tihany (Hungary), eds. F. J. Kedves and D. L. Beke, 1983, Diff. and Defect Monograph, n° **7**.

J) Proc. Int. Conf. on Vac. and Int. in Metals and Alloys, 1986, Berlin, 1987, Mater. Sci. Forum, **15–18**.

K) Proc. Int. Conf. on Diffusion in Materials, 1992, Kyoto (Japan), 1993, Def. Diff. Forum, **95–98**.

L) Diffusion Processes in Nuclear Materials, 1992, ed. R. P. Agarwala, (North Holland, Amsterdam).

Spectroscopic measurement methods

M) Petry, W., and G. Vogl, 1987, Mater. Sci. Forum, **15–18**, 323.

N) Vogl, G., 1990, Hyper. Int., **53**, 197.

Molecular Dynamics and Monte Carlo simulations

O) Berne B. J., 1977, Statistical Mechanics, part A and B, modern Theoretical Chemistry 5 and 6, (Plenum, New York).

P) Hansen, J. P., and I. R. McDonald, 1986, Theory of Simple Liquids, 2nd ed., (Academic, London).

Q) Allen M. P., and D. J. Tildesley, 1987, Computer Simulation of Liquids, (Clarendon, Oxford).

R) Meyer, M., and V. Pontikis, 1991, Computer Simulation in Materials Science, (Kluwer).

S) Binder, K., 1992, The Monte Carlo Method in Condensed Matter Physics, (Springer, Berlin).

Diffusion under stresses and stress gradients

T) Larché, F. C., and J. W. Cahn, 1982, Acta Metall. **30**, 1835, and references therein.

Diffusion in thin films

U) Balluffi, R. W., and J. M. Blakely, 1975, Thin Solid Films **25**, 363.

V) Martin, G., and B. Perraillon, 1976, Diffusion dans les milieux limités, in: Proc. 19ème Colloque de Métall., La Diffusion dans les Milieux Condensés, Théories et Applications, Saclay 1976 (INSTN, Saclay, France) p. 367.

Precipitation under irradiation

W) Phase Stability under Irradiation, Proc. of the Fall Meeting of AIME, Pittsburgh (1980), eds. J. R. Holland, L. K. Mansur and D. I. Potter (The Metallurgical Society of AIME, Warrendale, 1981).

X) Phase transformations and Solute Redistribution in Alloys during Irradiation, ed. F. V. Nolfi, Jr. (Applied Science Publishers, Barking, UK).

Y) Phase Stability under Irradiation, K. C. Russell, Prog. Mater. Sci., 1984, **28**, 229.

Z) Materials under Irradiation, Solid State Phenomena, 1993, **30** & **31**.

Alloys under irradiation as dynamical systems

AA) Non Linear Phenomena in Materials Science, ed. L. Kubin and G. Martin, Vol. 1, 1988, Vol. 2, 1992, Vol. 3, 1995 (Trans. Tech. Pub., Aedermansdorf, Switzerland).

Amorphous metallic Alloys

There are two famillies of conferences devoted to A.M.A.:

BB) the "LIQUID and AMORPHOUS METALS" serie the last of which have been published as follows: L.A.M. VI, 1988, Zeits. Phys. Chem. Neue Folge, **156–157**; L.A.M. VII, 1990, J. non Cryst. Sol., **117–118**; L.A.M. VIII, 1993, J. non Cryst. Sol., **156–158.**

CC) the "RAPIDLY QUENCHED METALS", series which have been published as: **R.Q.5**" Rapidly Quenched Metals", 1985, eds. S. Steeb and H. Warlimont, (North Holland, Amsterdam); **R.Q.6**, 1988, Mater. Sci. Eng., **97–99**; R.Q.7, 1991, Mater. Sci. Eng., **A133–134**; **R.Q.8**, 1994, Mater. Sci. Eng., **A179–180.**

DD) Amorphous and Liquid Materials, 1987, ed. E. Luscher, G. Fitsch and G. Jacucci, NATO ASI Series E n° 118, (Martinus Nijhoff Pub.).

Diffusion in Grain Boundaries

EE) Fundamentals of Grain and Interphase Boundary Diffusion, 1989, eds. I. Kaur and W. Gust, (Ziegler Press, Stuttgart).

FF) Handbook of Grain and Interphase Boundary Diffusion, 1989, eds. I. Kaur, W. Gust and L. Kozma, (Ziegler Press, Stuttgart).

CHAPTER 8

SOLIDIFICATION

H. BILONI

Laboratorio de Entrenamiento Multidisciplinario
para la Investigación Tecnológica (LEMIT-CIC)
1900 La Plata
Argentina

and W. J. BOETTINGER

National Institute of Standards & Technology
Gaithersburg
MD 20899-0001
USA

R. W. Cahn and P. Haasen†, eds.
Physical Metallurgy; fourth, revised and enhanced edition

1. Introduction

In this chapter, we give a general view of the formation of the solid from its melt. This process is generally driven by the extraction of heat from the melt and the first section deals with heat flow during conventional casting, directional solidification, and rapid solidification processing. Next, the fundamentals of the freezing process are treated under the headings: i) Thermodynamics of solidification, ii) Nucleation, iii) Interface attachment kinetics, iv) Solute distribution for planar and nearly planar solid–liquid (S–L) interfaces, v) Cellular and dendritic growth and vi) Polyphase solidification. Subsequently, fluid flow and associated phenomena are discussed. The last portion of the chapter deals with the application of these fundamentals to conventional and continuous casting, welding processes, manipulation of structure and new and emerging solidification processes. Rapid solidification is not treated separately, but is included in the headings above in an attempt to provide a general understanding of the solidification process as the solidification rate is increased.

2. Heat flow in solidification

When hot metal is poured into a mould, the rate at which it can lose heat is controlled by a number of thermal resistances. Figure 1 shows schematically the thermal conditions for a simple geometry of solidifying metal. In different parts of the metal-mould system heat transfer may occur by conduction, convection or radiation. The formal treatment of this problem involves considerable complexity as a consequence of the continuous generation of latent heat at the moving S–L interface, the nature of the S–L interface geometry which can be cellular or dendritic for alloys, and the variation of the physical properties of the metal-mould system with temperature. The major impediments to the removal of the latent heat are the solidifying metal itself, the metal-mould interface, and the mould. For these, the solidification process is primarily controlled by heat diffusion and Newtonian heat transfer across the mould-metal interface. Many numerical software packages are now available to solve the heat flow problem and are becoming more widely used to treat the complex shapes involved in industrial foundry applications.

In the following sections we describe heat transfer inside the solid/liquid metal system, heat transfer to the mould, examples of heat flow analysis in 1-D and more complex geometries, as well as software developments and the use of controlled solidification geometries for research purposes.

2.1. Heat transfer within the solid/liquid metal system

If the system under consideration involves an interface between solid and liquid that has a relatively smooth shape, as in the case of solidification of pure substances or dilute alloys, it is convenient to treat the phases as two different media. For pure conduction heat diffusion equations are applied separately to the solid and liquid.

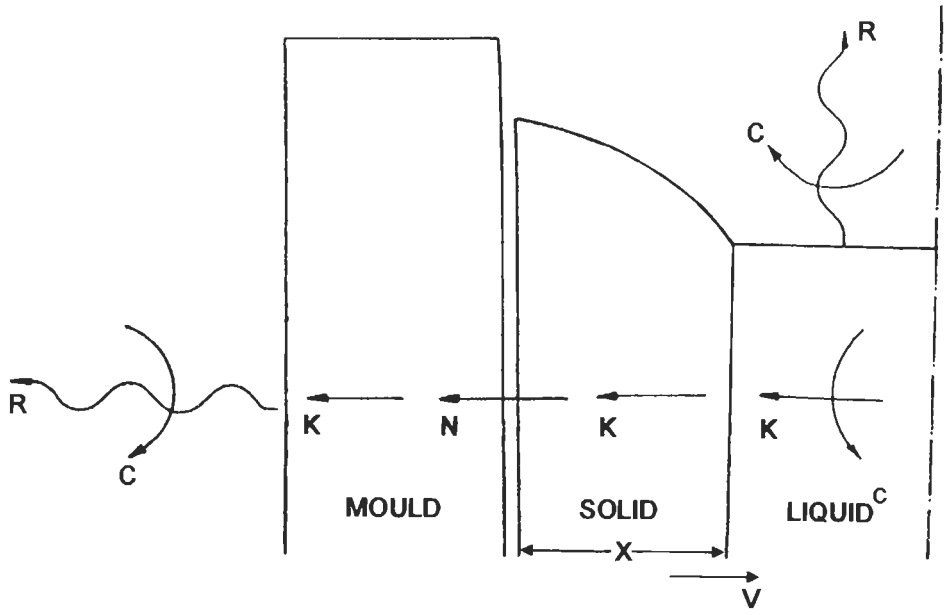

Fig. 1. Thermal conditions for solidification of a simple geometry of a pure superheated liquid metal. In the figure, K corresponds to heat transfer by conduction, N to Newtonian heat transfer across the mould–metal interface, C to convective heat transfer, and R to heat transfer by radiation.

$$div\left[K_S\, grad\, T_S(\vec{x},t)\right] = C_p^S \frac{\partial T_s(\vec{x},t)}{\partial t}, \tag{1}$$

$$div\left[K_L\, grad\, T_L(\vec{x},t)\right] = C_p^L \frac{\partial T_L(\vec{x},t)}{\partial t}, \tag{2}$$

and the heat flux and temperatures are matched at the S–L interface using

$$K_S G_S - K_L G_L = LV, \tag{3}$$

$$T_L = T_S = T_i \tag{4}$$

where K_S = solid thermal conductivity, K_L = liquid thermal conductivity, G_S = normal component of the thermal gradient in solid, G_L = normal component of the thermal gradient in the liquid, V = normal velocity of the S–L interface, T_i = interface temperature which may depend on curvature and V (see § 5), T_L = liquid temperature, T_S = solid temperature, C_p^L = volumetric liquid specific heat, C_p^S = volumetric solid specific heat, and L = volumetric latent heat.

Convection within the melt can also be important and influences solidification at both the macroscopic and microscopic levels. At the macroscopic level it can change the shape of the isotherms and reduce the thermal gradients within the liquid region. Also the

References: p. 830.

local solidification conditions, macrosegregation, and microstructure can be affected by convection. In particular the orientation of columnar dendritic structure, the occurrence of the columnar-to-equiaxed (CET) transition and nucleation initiated by dendrite arm detachment are all influenced by convection (see § 9).

When solidification of alloys that exhibit a large solidification range are treated, a *mushy zone* (see § 7) is usually present. In this case the solid and liquid phases are often treated as a single domain (RAPPAZ and STEFANESCU [1988] and RAPPAZ [1989]). The heat diffusion equation to be solved is

$$div\left[K(T)\,grad\,T(\vec{x},t)\right] + \dot{Q} = C_P(T)\frac{\partial T(\vec{x},t)}{\partial t}, \tag{5}$$

where $K(T)$ is the thermal conductivity, $C_p(T)$ is the volumetric specific heat and $\dot{Q}$ is the heat source term associated with the phase change.

$$\dot{Q} = L\frac{\partial f_S(\vec{x},t)}{\partial t}, \tag{6}$$

with $f_S(\vec{x},t)$ being the solid fraction. To solve eq. (5) a relationship for $f_S(\vec{x},t)$ must be known.

The simplest and most widely used method assumes that f_S depends only on T. Then eqs. (5) and (6) can be combined as

$$div\left[K(T)\,grad\,T(\vec{x},t)\right] = \left[C_P(T) - L\frac{df_S}{dT}\right]\frac{\partial T(\vec{x},t)}{\partial t}. \tag{7}$$

This equation can be rewritten according to two different numerical techniques. When the *specific heat method* is considered the equation is

$$div\left[K(T)\,grad\,T(\vec{x},t)\right] = C_P^e(T)\frac{\partial T(\vec{x},t)}{\partial t}, \tag{8}$$

where C_P^e is an altered specific heat

$$C_P^e(T) = \left(C_P(T) - L\frac{df_S}{dT}\right), \tag{9}$$

that includes the latent heat. When the *enthalpy method* is used, instead of treating the temperature as a variable, the volumetric enthalpy H is adjusted and equation (7) becomes

$$div\left[K(T)\,grad\,T(\vec{x},t)\right] = \frac{\partial H(\vec{x},t)}{\partial t} \tag{10}$$

where

$$H(T) = \int_0^T C_P(T')dT' + L\left[1 - f_S(T)\right]. \tag{11}$$

RAPPAZ [1989] discussed the advantages and disadvantages of using the equivalent

specific heat method (eq. (8)) and the latent heat method (eq. (10)). In standard macroscopic modeling of solidification the relationship $f_S(T)$, C_p^e (T), or $H(T)$ can either be deduced from DTA-type measurements or from a simple solute model as that of SCHEIL [1942] to be discussed in § 6.

More complex methods, where f_S is not simple a function of T, must be considered if the details of nucleation and growth or solid diffusion (BRODY and FLEMINGS [1966]) are to be coupled to the macroscopic heat flow (RAPPAZ [1989]). For example, for columnar dendritic growth, f_S depends on the local isotherm velocity and temperature gradient, as well as the temperature.

2.2. Heat transfer at the metal-mould interface

The heat flow from the solidifying metal is often limited by the metal-mould thermal resistance. This resistance is quantified by the value of the heat transfer coefficient, h_i, defined by

$$q = h_i(T_{iS} - T_{iM}), \tag{12}$$

corresponding to a Newtonian heat transfer model where q is the heat flux across the interface, T_{iS} is the metal temperature and T_{iM} the mould temperature, both at the metal-mould interface. When the melt first enters into contact with the mould wall, the mould surface is at a low temperature and the liquid is at the melting point plus the superheat. The thermal contact is not perfect and the h_i value depends on the complex nature of the contact between metal and mould as shown in fig. 2a. Also important are the thermal resistance imposed by any coating present on the mould surface (BILONI [1977]) and the "air gap" that often develops between the mould surface and the solidifying metal due to metal shrinkage (DAS and PAUL [1993]). Consequently, the physical nature of the thermal contact can change with time and from point to point and may also depend on the wetting capacity of the melt, existence of oxides, grease, etc.

HO and PEHLKE [1984], [1985] and CAMPBELL [1991a], [1991b] give a clear picture of the heat flow at the metal-mould interface including the origin, development, and nature of the so called "*air gap*". The following facts must be considered:
1) When the metal enters the mould, good contact exists between the molten metal and the mould surface as PRATES and BILONI [1972] and MORALES *et al.* [1979] proved through the analysis of the casting surface structure. Contact occurs at the peaks of the mold surface roughness where large supercooling creates *predendritic nuclei* (BILONI and CHALMERS [1965]). The application of pressure enhances the contact and the h_i value can be increased dramatically (CAMPBELL [1991a]). 2) After the creation of a solidified layer with sufficient strength, the casting and mould both deform due to thermal contraction and the contact is reduced to isolated points at greater separations than that determined by the surface roughness. The interface gap starts to open and the conduction across the interface decreases drastically. Consequently, the h_i value falls by more than one order of magnitude. When radiation is neglected, the important mechanism becomes the conduction of heat through the gas phase in the gap. In this case $h_i = K_f/e$, where e is the equivalent thickness averaged over the metal-mould interface and K_i an effective thermal

References: p. 830.

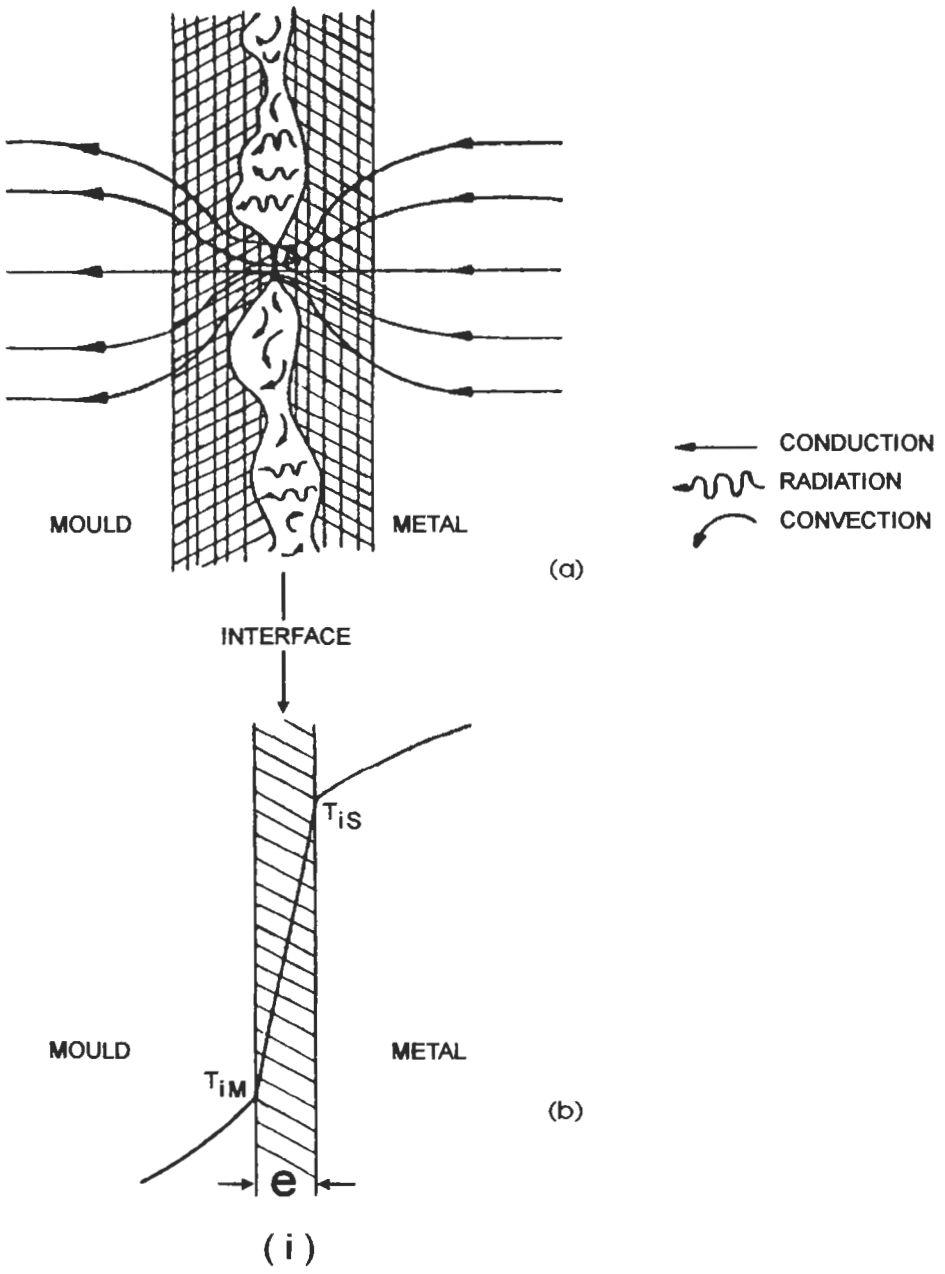

Fig. 2. Nature of the thermal contact between the metal and the mould and equivalent Newtonian model of the metal–mould interface. (a) The complex nature of the contact and different types of heat transfer occurring at the interface are shown schematically. At point A good local contact assures a higher heat conduction. As a consequence, h_i will locally be higher than at the rest of the metal–mould interface. (b) The equivalent Newtonian model is based on an effective value of the gap, e, to yield an average value of h_i.

conductivity of the gas. Then, h_i corresponds to an *average value* represented by the equivalent model of fig. 2b but local values can be considerably different. The important aspects for modelling h_i are the identity of the gas in the gap and the gap thickness.

HO and PEHLKE [1984] and CAMPBELL [1991a], [1991b] discuss the nature of the gas in the gap. For iron and steel castings in sand moulds, the gas present is likely to be hydrogen. This is significant, because of the high thermal conductivity of hydrogen, which is of the order of seven times greater than for air. For metallic moulds the lower H content in the gap will result in a lower thermal conductivity, but the h_i value may still be twice that of air (CAMPBELL [1991b]). These conclusions must be considered seriously when h_i values are estimated for heat transfer calculations.

The width of the gap is treated as a thermal expansion effect of the casting and the mould. If the mould expansion is considered homogeneous, transient heat flow consideration yields (CAMPBELL [1991a]) that e/D is proportional to

$$a_c(T_m - T) + a_M(T_{Mi} - T_o), \tag{13}$$

where e = gap size, D = casting diameter, T_m = freezing point, T_{Mi} = temperature of the mould interface, T_o = original temperature of the mould, a_c = casting thermal diffusivity, a_M = mould thermal diffusivity.

However, in general, there will be powerful geometrical effects and the gap thickness can change differently in various parts of the mould. Therefore, the situation in shaped casting is complicated as CAMPBELL [1991b] affirms and has yet to be tackled successfully by theoretical models. Indeed HO and PELKE [1984] and [1985] demonstrate the difference in h_i value obtained for chilling surfaces located at the top or bottom of a cylindrical Al casting.

MEHRABIAN [1982] reported the measurement of h_i in splat cooling, in pressurized aluminium against a steel mould and in liquid die casting against a steel mould. He estimates that an upper limit exists for practically achievable heat transfer between liquid and substrates of about $h_i = 10^5$–10^6 J/m^{2}Ks. Table 1 gives the order of magnitude of h_i for different conditions of a metal in contact with a mould.

Careful measurements and analysis are necessary to obtain accurate heat transfer coefficients. Using thermocouple measurements and numerical solution of the *inverse heat conduction problem*, HO and PEHLKE [1985] have obtained h_i values that show the onset of gap formation, and its time evolution.

More recently HAO *et al.* [1987] performed experiments with ductile iron and discussed the effect on h_i of the expansion of graphite precipitated during the solidification period. SHARMA and KRISHMAN [1991] discussed the effect of the microgeometry of moulds considering several combinations of V grooves upon the mould or chill surface. DAS and PAUL [1993] determined h_i in castings and quenching using a solution technique for inverse problems based on the Boundary Element Method (BEM).

2.3. Heat flow in one dimensional solidification geometries

Two examples of the analysis of one dimensional heat flow during solidification are given here. The first is often applicable in ordinary casting processes, while the second applies to rapid solidification.

References: p. 830.

2.3.1. Freezing at mould wall

The pioneering work by PIRES *et al.* [1974] analytically treated the case where the effects of a finite heat transfer coefficient at the metal-mould interface and conduction in the both metal and mould are important. Later, GARCIA and PRATES [1978] and GARCIA *et al.* [1979] obtained similar results. CLYNE and GARCIA [1980] reviewed the analytical solutions, known now as the "Virtual Adjunct Method" (VAM), and described various limiting cases. The basic assumptions are: i) Conductive heat flow is unidirectional with semi-infinite metal and mould regions. ii) The Newtonian interface resistance is represented by a heat transfer coefficient, h_i, which remains constant throughout the process. The important case of variable h_i is not treatable by exact analytical methods. iii) The metal solidifies with a planar S–L interface that remains at the equilibrium melting point. iv) The metal solidifies with zero superheat in the liquid. v) Convection currents and radiation losses are assumed to be small. vi) The thermal properties of the metal and mould do not change with temperature. The analytical solution for the solidification time, t_S, as a function of the distance solidified, X, has the form:

$$t_S(X) = AX^2 + BX \tag{14}$$

where

$$A = \frac{1}{4\phi^2 a_S}, \tag{15}$$

$$B = \frac{L\rho_S}{h_i(T_m - T_o)} \tag{16}$$

with ϕ evaluated numerically from the equation

$$\phi \exp(\phi^2)[M + \operatorname{erf}\phi] = \frac{1}{\sqrt{\pi}L^+}. \tag{17}$$

Here, a_S is the thermal diffusivity of the solid metal, $M = (K_S C_p^S / K_M C_p^M)^{1/2}$ = mould constant, subscripts or superscripts S and M refer to solidified metal and mould,

Table 1
Order of magnitude of heat-transfer coefficient, h_i, for different processes. MEHRABIAN [1982].

Process	h_i (J/m^{2}Ks)
Massive mould, polished	4×10^3
Massive mould, coated	7.5×10^2
Cooled mould, polished	5×10^3
Cooled mould, coated	10^3
Pressure-Cast	3×10^3–3×10^4
Die-cast	5×10^4
Drop-smash	10^4–10^5
Splat-cooling	10^5–10^6

respectively, C_p is the volumetric specific heat, and L^+ is the dimensionless latent heat given by $L/C_S(T_m-T_0)$. The two terms in eq. (14) describe respectively: (i) the time necessary to solidify a metal of specified thickness if h_i were infinite, that is, if the thermal contact between metal and mould were perfect and (ii) the time necessary to solidify a metal of specified thickness if the thermal conductivity of the mould and metal were large and $h_i \neq \infty$, that is, the second term only considers the effect of the Newtonian thermal resistance at the metal-mould interface. PIRES *et al.* [1974] and GARCIA and PRATES [1978] successfully checked eq. (14) for the particular case of efficient refrigeration of the chill mould in unidirectional solidification of Sn, Pb, Zn and Al. In this case, $M \cong 0$ giving a more simplified form of the general solution. GARCIA *et al.* [1979] extended the experiments to moulds where $M \neq 0$. These authors calculated the h_i value from the experimental curves, $X=f(t_S)$, through eq. (16).

GARCIA and CLYNE [1983] consider that in the case of Al–Cu alloys, having an appreciable temperature range of solidification, this method can be used without major modification. An analytical treatment that takes account of the mushy zone has been developed by LIPTON *et al.* [1982]. In addition, the VAM method has been extended to freezing processes involved in certain types of splat cooling (CLYNE and GARCIA [1981]). When the effects of superheat are considered, numerical methods are necessary, as shown for example by HILLS *et al.* [1975].

2.3.2. Rapid freezing in contact with a cold substrate with initial melt supercooling

Rapid cooling of a melt often causes the liquid phase to be cooled below the melting point. The interplay of liquid volume to be frozen, melt supercooling and external heat transfer to a cold substrate controls the solidification speed as in splat cooling. Theoretical details of this process have been examined numerically by CLYNE [1984]. A major complication occurs for heat flow analysis when high solidification velocities are involved even for pure materials. The temperature of the S–L interface T_i, cannot be treated as a constant, equal to the melting point, T_m, but rather it is a function of the interface velocity. As a result, the heat flow analysis depends on the details of this function, which are even more complicated for dendritic growth and for alloys (see § 5 and 7). CLYNE [1984] treats the case of a pure metal freezing with a smooth (non-dendritic) S–L interface governed by a kinetic law for the interface velocity given by $V=\mu(T_m-T_i)$ where μ is the linear interface attachment coefficient taken as 4 cm s^{-1} K^{-1} (see § 5).

Calculations show the importance of the initial supercooling ΔT on the development of high solidification velocities. Large values of ΔT can develop if nucleation on the substrate is difficult. Figure 3 (from CLYNE [1984]) shows temperature-time plots at two positions inside a 50 μm thick layer of an Al melt cooling in contact with a substrate with $h_i = 10^6$ Wm^{-2} K^{-1}. For example, at a position 5 μm from the substrate, the temperature in the liquid drops until nucleation occurs near the substrate at a dimensionless supercooling $\Delta\theta = \Delta T/(L/C_p^L) \cong 0.4$, which he assumes to be predicted from homogeneous nucleation theory (see § 4). The temperature at this position then rises rapidly as the S–L interface proceeds from the substrate towards the 5 μm position. After the

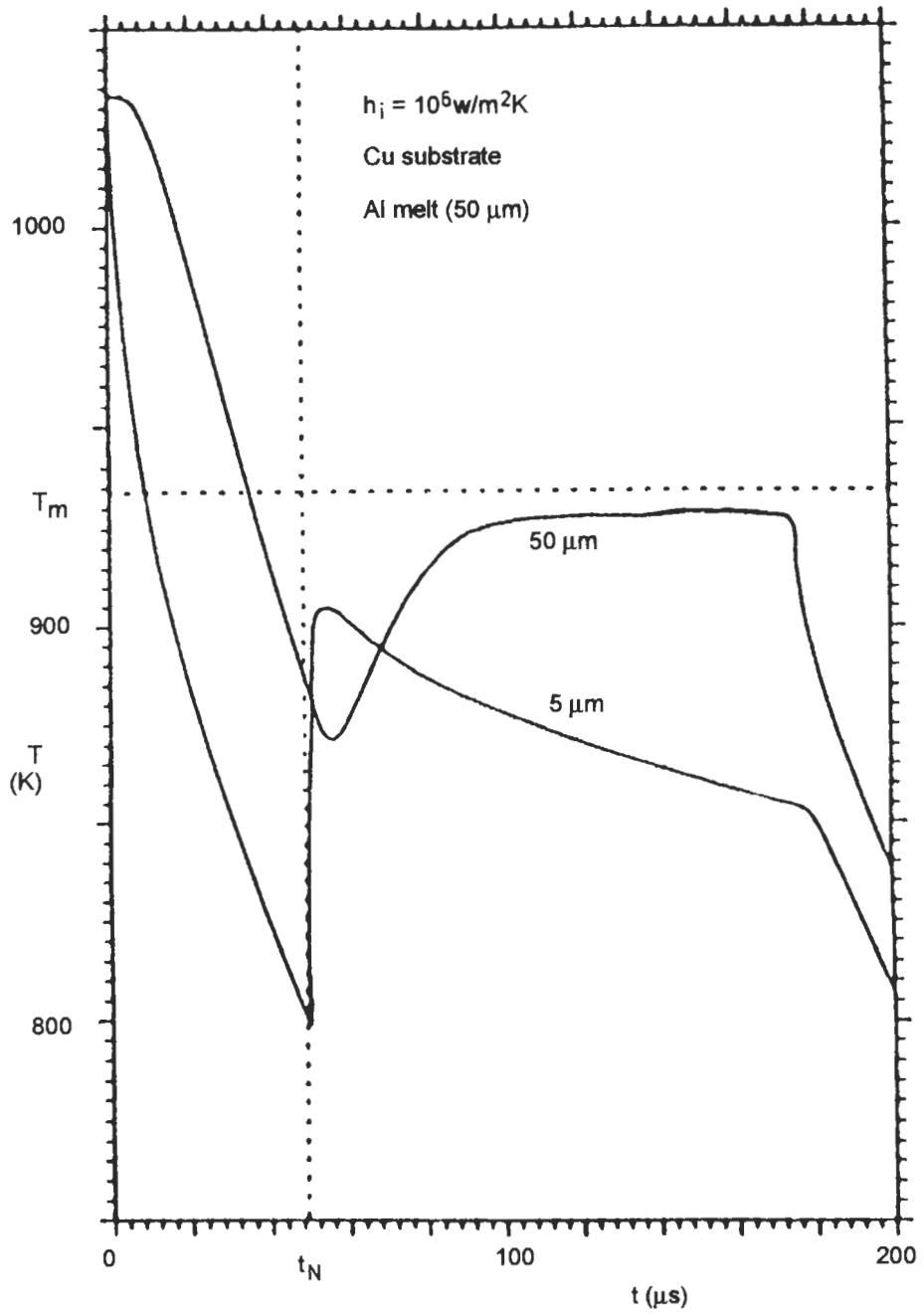

Fig. 3. Calculated temperature–time histories for two positions within a liquid layer 5 and 50 μm from a chilling substrate. Nucleation occurs at the substrate surface at time, t_N, at an undercooling of $-0.4\,L/C_p^L$. The recalescence after the passing of the liquid–solid interface is evident at both positions. CLYNE [1984].

interface passes the 5 μm position, the temperature falls slowly. A plot for the temperature at the 50 μm position shows a smaller initial drop in temperature followed by a gradual rise as the interface approaches. The supercooling of the interface when it passes the 5 and 50 μm position is approximately 25 and 5 K respectively which correspond to interface velocities of 100 cm s^{-1} and 20 cm s^{-1}. Thus, the initial supercooling produces a much higher solidification rate close to the chill than would be possible without initial supercooling.

2.4. Heat flow in more complex solidification geometries

In general the analysis given above is useful for one-dimensional heat flow. In more complicated geometries there are several aspects that lead to difficulties, including the nonlinearity of the heat transfer problem due to the latent heat of fusion, the geometric complexity of shaped castings, the disparities in thermal properties between the metal and mould. Also the treatment of temperature dependent properties and heat transfer coefficient. In this framework, the techniques of *numerical modeling* are necessary.

From the pioneering work of HENZEL and KEVERIAN [1965], applying successfully the Transient Heat Program (THP) to heavy steel cast production, an explosive growth of computer modeling techniques have arisen, especially in the last 15 years (BERRY and PEHLKE [1988]). As a result macroscopic modeling of solidification processes are well developed and different processes can be treated. We shall present here the application of these methods in two cases: controlled directional solidification and rapid solidification of atomized metal droplets into powder. In § 10 we discuss the application of numerical modeling of heat flow to welding and continuous casting processes.

2.4.1. Heat flow in controlled directional solidification of metals

Although a number of variations in the construction of DS equipment has been described in the literature, in many cases the process used is the Bridgman technique where a cylindrical crucible is moved through at a fixed temperature gradient, G_L, with a constant translation velocity V^*. It is often assumed that the interface will remain stationary with respect to the furnace during most of the growth period and that the growth velocity of the interface, V, is equal to that of the crucible or the moving furnace (V^*). However, CLYNE [1980a], [1980b] combined experimental investigation of commercial purity Al with mathematical modeling to determine the relationship between the interface and the traverse speed. He used a finite difference model to investigate a number of facets of the process. It was calculated that V can differ from V^* by 50% or more over a significant distance in some cases. The difference between V and V^* was found to increase as the thermal diffusivity of the metal increases. The model was used to examine the conditions under which the departure from ideal behavior would be significant and some practical steps were suggested to eliminate this problem.

2.4.2. Powder solidification

LEVI and MEHRABIAN [1982] examined theoretically the heat flow during rapid cooling of metal droplets. Relationships were established between atomization paramet-

ers, growth kinetics, and interface velocity. They developed a numerical solution based on the enthalpy method for simulating the solidification process from a single nucleation event occurring at the powder surface and their results are compared with the trends predicted from a Newtonian cooling model. They also discuss the implications of single vs. multiple nucleation events. Their results stressed the importance of the initial supercooling, ΔT, when nucleation occurs, on the development of high solidification velocities. Figure 4 adapted by BOETTINGER and PEREPEZKO [1985] from LEVI and MEHRABIAN [1982] shows the interface temperature and interface velocity as solidification proceeds from one side of the droplet to the other, increasing the fraction solid. The curves shows the case of an initial supercooling of $\Delta\theta = 0.5$ (~182 K for Al) for various values of h_i. The velocity starts at a high value (>3 m/s) and slows as the interface moves across the droplet. This decrease in velocity is due to the evolution of the latent heat at the S–L interface and the resultant reduction in the interface supercooling. The effect of changing the heat transfer coefficient by two orders of magnitude is primarily to alter the velocity after the fraction solid exceeds the dimensionless initial supercooling (0.5 in this case). Growth at small fraction solid is controlled primarily by heat flow inside the powder particle, while growth at large fraction solid is controlled by external heat flow. If no initial supercooling were present, the growth velocities across the entire particle would be near those seen at large fraction solid (fig. 4), which are typically less than 10 cm/s.

2.5. Software packages

Different numerical methods have been used to treat solidification. RAPPAZ [1989] discusses five main computational techniques: i) The finite difference method (FDM) with or without the alternative implicit direction (ADI) time stepping scheme, ii) The finite element method (FEM), iii) The boundary element method (BEM), iv) The direct finite difference method (DFDM), v) The control volume element method (VEM). He discussed the basic advantages and/or inconveniences of these methods using schematic 2-dimensional enmeshments that are associated with the five main computational techniques. OHNAKA [1991] analyzed solidification for a thermal conduction model and reviewed critically these computational techniques. BERRY and PEHLKE [1988] give a comprehensive view of the steps to be taken when solidification modeling is used, stressing the fact that the thermophysical properties and details about mould material are often poorly known. Indeed, conditions such as moisture, property dependence on temperature, etc., would require an almost limitless data base. Software packages permit, through suitable interactions, the generation of maps displaying the variation of specific criteria functions that affect casting soundness, such as local temperature gradient, freezing time, front speed or cooling rate.

DANTZIG and WIESE [1986] and WIESE and DANTZIG [1988] have focused on a technique to reduce the computation time involved in FEM methods for sand castings. Considering that the number of nodes located within the mold is far greater than those within the casting, the authors replace the sand mold by a set of boundary conditions applied at each element on the surface of the casting. This method was initially proposed by NIYAMA [1977] and later by WEI and BERRY [1980] and is known as the *Q-Dot*

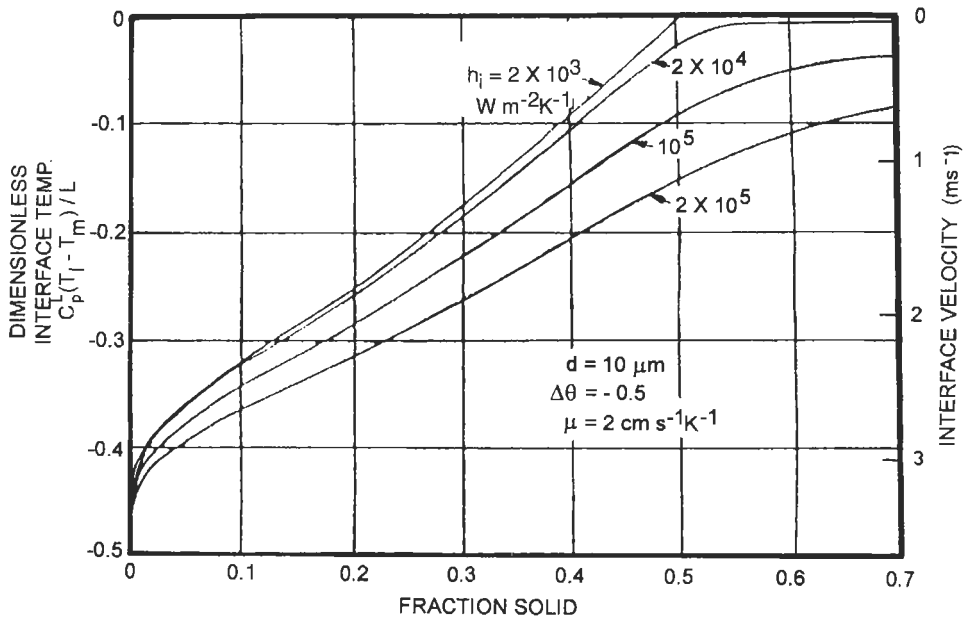

Fig. 4. Calculated interface temperature (LEVI and MEHRABIAN [1982]) for the solidification of a powder particle initially undercooled by $1/2\ L/C_p^L$. The temperature rises and the velocity falls as growth proceeds from the point of nucleation on the powder surface across the powder particle. The effect of various values of the heat transfer coefficient h_i is also shown. The velocity scale on the right was added by BOETTINGER and PEREPEZKO [1985].

method. More recently DANTZIG and LU [1985] and DANTZIG and WIESE [1985] developed the Boundary Curvature Method (BCM). In both techniques the heat flow from the surface of the casting is treated using a library of special functions, related to the local geometry, which contain the information about heat flow from that shape into a mould material. The BCM method seems to adapt better to arbitrary shapes in three dimensions than the *Q-Dot method.* DANTZIG and WIESE [1986] present an example of a complex casting (a cylinder block section) stressing the fact that this problem would have required much greater computation time without the BCM.

2.6. Experimental methods involving controlled solidification

The difficulties associated with predicting external heat transfer in casting has lead to the development of two research techniques of controlled solidification: unidirectional solidification and solidification with prescribed bulk supercooling. Much of the understanding of solidification laws comes from unidirectional solidification experiments based on the simple principle that the extraction of latent heat must be achieved without allowing the melt to supercool sufficiently to permit the nucleation of crystals ahead of the solidification front. In practice this requires a heat sink that removes heat from the

solid and a heat source that supplies heat to the melt. The extensive use of such techniques by CHALMERS and his school (CHALMERS [1964], [1971]) produced the basis of modern understanding in solidification. The basic heat flow objectives are to obtain a unidirectional thermal gradient across the interface and to move it so that the interface moves at a controlled rate. For a planar S–L interface the gradients are related by eq. (3). Based on this idea different techniques have also been developed to obtain single crystals employed for research purposes. FLEMINGS [1974] gives details of the different techniques used. Heat flow in controlled directional solidification (DS) is treated in § 2.4.1.

Another directional controlled process corresponds to the extraction of heat via a botton chill. Growth occurs in a direction parallel and opposite to the heat flux direction. In this situation a better control of microstructure and properties is obtained in comparison with conventional casting. However the microstructure is not uniform as in the Bridgman method, because V and G decrease with the distance from the chill. It is possible to improve the microstructure uniformly by programmed furnace temperature and withdrawal rates.

The above examples of controlled solidification do not involve bulk liquid supercooling. However, when a crystal is nucleated at a specified temperature and grows freely into the liquid, the bulk supercooling ΔT plays a major role in determining the structure observed during the solidification process. This type of study has been performed with both low and high supercooling and important structural information has been obtained in organic material analogues (GLICKSMAN [1981]) and metallic alloys (FLEMINGS and SHIOHARA [1984], WILLNECKER *et al.* [1989], [1990]). More details will be given in § 11.

3. *Thermodynamics of solidification*

3.1. Hierarchy of equilibrium

The process of solidification cannot occur at equilibrium. However it is clear that different degrees of departure from full equilibrium occur and constitute a hierarchy which is followed with increasing solidification rate. This hierarchy is shown in Table 2 (BOETTINGER and PEREPEZKO [1985]).

The conditions required for global equilibrium, (i), are usually obtained only after long term annealing. Chemical potentials and temperature are uniform throughout the system. Under such conditions no changes occur with time. Global equilibrium is invoked for descriptions of solidification that apply the lever rule at each temperature during cooling to give the fraction of the system that are liquid and solid as well as the compositions of the (uniform) liquid and solid phases. This situation is only realized during solidification taking place over geological times.

During most solidification processes, gradients of temperature and composition must exist within the phases. However one can often accurately describe the overall kinetics using diffusion equations to describe the changes in temperature and composition within

Table 2
Hierarchy of Equilibrium.

i.	Full Diffusional (Global) Equilibrium
	a. No chemical potential gradients (composition of phases are uniform)
	b. No temperature gradients
	c. Lever rule applicable
ii.	Local Interfacial Equilibrium
	a. Chemical potential for each component continuous across the interface
	b. Phase diagram gives compositions and temperatures only at Solid–Liquid interface
	c. Correction made for interface curvature (Gibbs–Thomson Effect)
iii.	Metastable Local Interfacial Equilibrium
	a. Important when stable phase cannot nucleate or grow fast enough
	b. Metastable phase diagram (a true thermodynamic phase diagram missing the stable phase or phases) gives the interface conditions
iv.	Interfacial Non-Equilibrium
	a. Phase diagram fails to give temperature and compositions at interface
	b. Chemical potentials are not equal at interface
	c. Free energy functions of phases still lead to criteria for the "impossible" (Baker and Cahn [1971])

each phase and using the equilibrium phase diagram to give the possible temperatures and compositions for boundaries between the phases, e.g., at the solidification interface. The Gibbs–Thomson effect is included to determine shifts in equilibrium due to the curvature of the liquid–solid interface. This condition is called the local equilibrium condition, (ii) in table 2.

For a dilute alloy the liquidus and solidus of the phase diagram can often be represented as straight lines (fig. 5). The local equilibrium condition for a curved interface is given in this case by

$$T_i = T_m + m_L C_L^* - T_m \Gamma K_m \tag{18}$$

and

$$C_S^* = k_o C_L^*, \tag{19}$$

where T_i and T_m are the interface temperature and pure solvent melting temperature, m_L is the liquidus slope, C_L^* and C_S^* are the compositions at the interface of the liquid and solid, Γ is the ratio of the liquid–solid surface energy to the latent heat per unit volume, K_m is the mean curvature of the interface (defined as positive when the center of curvature is in the solid), and k_o is the equilibrium partition coefficient.

Local equilibrium is never strictly valid, but it is based on the notion that interfaces will equilibrate much more quickly than will bulk phases. The conditions described in (ii) of Table 2 are widely used to model the majority of solidification processes that occur in castings. For example, under the assumptions of fast diffusion in the liquid phase, negligible diffusion in the solid phase, and local equilibrium at the interface, the Scheil Equat-

References: p. 830.

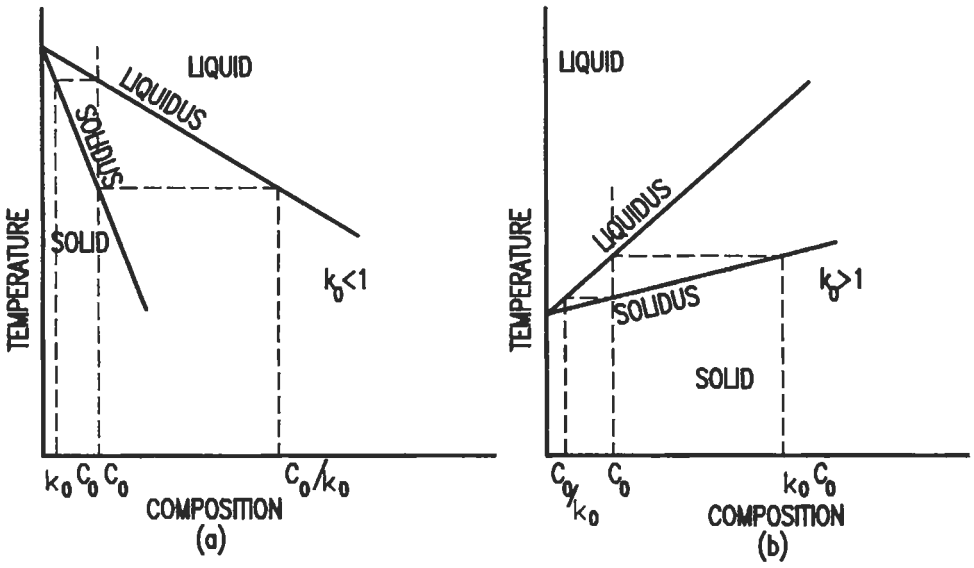

Fig. 5. Solidus–liquidus relationships for dilute binary alloys. For a liquid composition of C_0 the equilibrium solid composition is k_0C_0. For a solid of composition, C_0, the equilibrium liquid composition is C_0/k_0.

ion (see § 7.3) gives a reasonable first approximation to the "nonequilibrium" dendritic coring or microsegregation in conventional castings. Clearly phase diagrams constitute an essential part of the data base for the modeling and analysis of solidification problems.

Metastable equilibrium, (iii) in Table 2, can also be used locally at interfaces and is important in ordinary metallurgical practice. For example, one can understand the microstructural change of cast iron from the stable gray form (austenite and graphite) to the metastable white form (austenite and cementite) with increasing solidification rate (and interface supercooling) using information from the stable and the metastable phase diagrams combined with a kinetic analysis (JONES and KURZ [1980]). The eutectic temperature and composition for white cast iron are well defined thermodynamic quantities just as they are for gray cast iron. Metastable equilibrium is represented by a common tangent construction to the molar free energy vs. composition curves for the liquid, austenite, and cementite phases and thus minimizes the free energy as long as graphite is absent. When solidification is complete, a two phase mixture of austenite and cementite can exist in a global metastable equilibrium. The concept of local metastable equilibrium is especially important during rapid solidification (PEREPEZKO and BOETTINGER [1983], PEREPEZKO [1988]) because some equilibrium phases, especially those with complex crystal structures, have sluggish nucleation and/or growth kinetics and are absent in rapidly solidified microstructures.

An example of a metastable phase diagram superimposed on a stable phase diagram is given in fig. 6 for the Al–Fe system. If Al_3Fe is absent, phase boundaries involving a metastable phase, Al_6Fe, which is isomorphous with Al_6Mn, are obtained. In particular a metastable eutectic, $L \rightarrow Al + Al_6Fe$ occurs. Transitions of microstructures involving

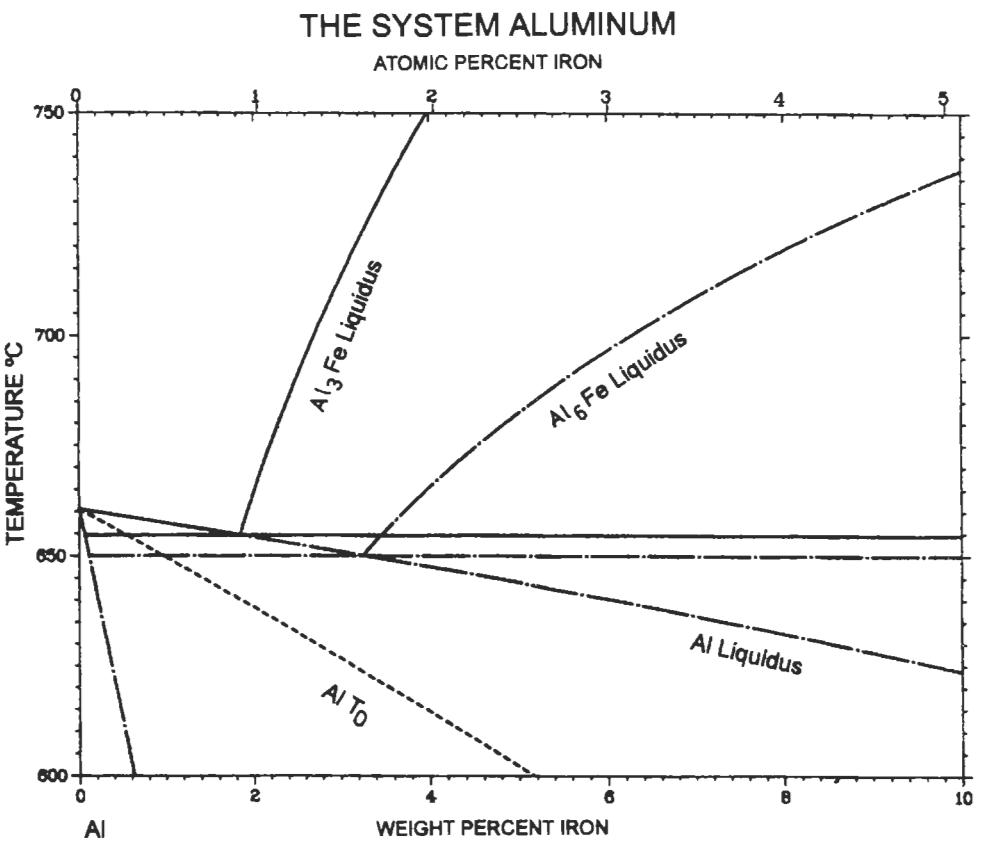

Fig. 6. Calculated Al-rich portion of the stable Al–Fe phase diagram is shown by solid lines. If Al_3Fe is absent, a metastable phase diagram (dot-dashed lines) involves a eutectic L→Al+Al_6Fe. The T_0 for the solidification of Al solid solution is shown dashed. The solvus curves are omitted for clarity. MURRAY [1983a].

Al_3Fe to those involving Al_6Fe have been observed with increasing solidification speed by ADAM and HOGAN [1972] and by HUGHES and JONES [1976]. The competitive growth kinetics of the two can also be analyzed using the stable and metastable phase diagrams.

For local equilibrium, whether stable or metastable, the chemical potentials of the components for the liquid and solid are equal across the interface. In Table 2, however, another situation is described in (iv), and relates to a situation where chemical potentials can not be approximated as being equal across an interface growing at a high rate and large supercooling. These rapid growth rates can trap the solute into the freezing solid at levels exceeding the equilibrium value for the corresponding liquid composition present at the interface. Thus the chemical potential of the solute increases upon being incorporated in the freezing solid in a process called *solute trapping*. This increase in chemical potential of the solute across the interface must be balanced by a decrease in chemical potential of the solvent in order for crystallization to occur; i.e., to yield a net decrease

in free energy (BAKER and CAHN [1971]). The free energy change during solidification, ΔG, is given by

$$\Delta G = \left[\left(\mu_S^A - \mu_L^A\right)\left(1 - C_S^*\right) - \left(\mu_S^B - \mu_L^B\right)C_S^*\right], \tag{20}$$

where μ_S^A and μ_S^B are the chemical potentials for species A and B in the solid, and μ_L^A and μ_L^B are the chemical potentials in the liquid. These potentials are functions of the temperature and solid or liquid composition (C_S^* or C_L^*) at the interface during solidification. Despite the loss of interface equilibrium during rapid solidification, the free energy functions of the solid and liquid phases and their associated chemical potentials can be used to define the possible range of compositions that can exist at the interface at various temperatures. This restriction is obtained by the requirement that ΔG be negative. Figure 7 shows the region of allowable solid compositions at the interface for a fixed liquid composition, C_L^*, at the interface as a function of interface temperature (BOETTINGER [1982]). Such allowable regions can be calculated from a thermodynamic model of the system of interest.

3.2. T_0 curves

For any selected pair of liquid and solid compositions, a thermodynamic temperature can be described that is the highest temperature where crystallization can occur as shown in fig. 7. However one often considers a limiting case, called *partitionless solidification*, which is favored at very high solidification rate, where the composition of the solid formed at the interface, C_S^*, equals the composition of the liquid at the interface, C_L^*. The T_0 temperature is the highest temperature where this can occur (APTEKAR and KAMENETSKAYA [1962]), (BILONI and CHALMERS [1965]). This is the temperature where the molar free energies of the liquid and solid phases are equal for the composition of interest; i.e., the temperature where $\Delta G = 0$ for $C_S^* = C_L^*$ in Equation (20). As illustrated in fig. 7, a T_0 curve represents only part of the thermodynamic information available, when solidification occurs without local equilibrium.

T_0 curves exist for the liquid with stable or metastable phases, and lie between the liquidus and solidus for those phases. In fact for dilute alloys the slope of the T_0 curve is $m_L\,[(\ln k_0)/(k_0 - 1)]$. Figure 8 shows schematically, possible T_0 curves for three eutectic phase diagrams (BOETTINGER [1982]). An important use of these curves is to determine whether a bound exists for the extension of solubility by rapid melt quenching. If the T_0 curves plunge to very low temperatures as in fig. 8a, single phase α or crystals with composition beyond their respective T_0 curves cannot be formed from the melt. In fact, for phases with a retrograde solidus, the T_0 curve plunges to absolute zero at a composition no greater than the liquidus composition at the retrograde temperature, thus placing a bound on solubility extension (CAHN *et al.* [1980]). Experiments on laser-melted doped Si alloys seem to confirm this bound (WHITE *et al.* [1983]). Eutectic systems with plunging T_0 curves are good candidates for easy metallic glass formation. An alloy in the center of such a phase diagram can only crystallize into a mixture of solid phases with different compositions regardless of the departure from equilibrium. The diffusional kinetics of this separation from the liquid phase frequently depresses the

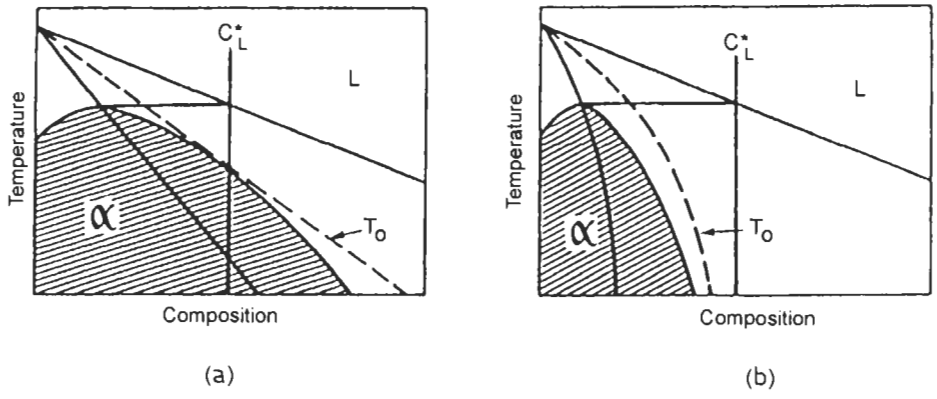

Fig. 7. The shaded regions indicate thermodynamically allowed solid compositions that may be formed from liquid of composition at various temperatures. The T_0 curve gives the highest temperature at which partitionless solidification ($C_L^* = C_S^*$) can occur. In (b) the T_0 temperature plunges and partitionless solidification is impossible for liquid of composition C_L^*. BOETTINGER [1982].

solidification temperature to near the glass transition, T_g, where an increased liquid viscosity effectively halts crystallization.

In contrast, alloys with T_0 curves which are only slightly depressed below the stable liquidus curves, as in fig. 8b, c, make good candidates for solubility extension and unlikely ones for glass formation. In fig. 8b the crystal structures of α and β are different and the T_0 curve cross, whereas in fig. 8c the crystal structures are the same and the T_0 curve is continuous across the diagram. At temperatures and liquid compositions below the T_0 curves, partitionless solidification is thermodynamically possible. Ni–Cr and Ag–Cu are examples of the behavior in fig. 8b and c.

4. *Nucleation*

4.1. Nucleation in pure liquids

Nucleation during solidification can be defined as the formation of a small crystal from the melt that is capable of continued growth. From a thermodynamic point of view the establishment of a S–L interface is not very easy. Although the solid phase has a lower free energy than the liquid phase below T_m, a small solid particle is not necessarily stable because of the free energy associated with the S–L interface. The change in free energy corresponding to the liquid–solid transition must therefore include not only the change in free energy between the two phases but also the free energy of the S–L interface. From a kinetic point of view it is possible to arrive at the same result on the basis that the atoms at the surface of a very small crystal have a higher energy than the surface atoms of a larger crystal (CHALMERS [1964]). Therefore, the equilibrium temperature at which atoms arrive and leave at the same rate is lower for a very small

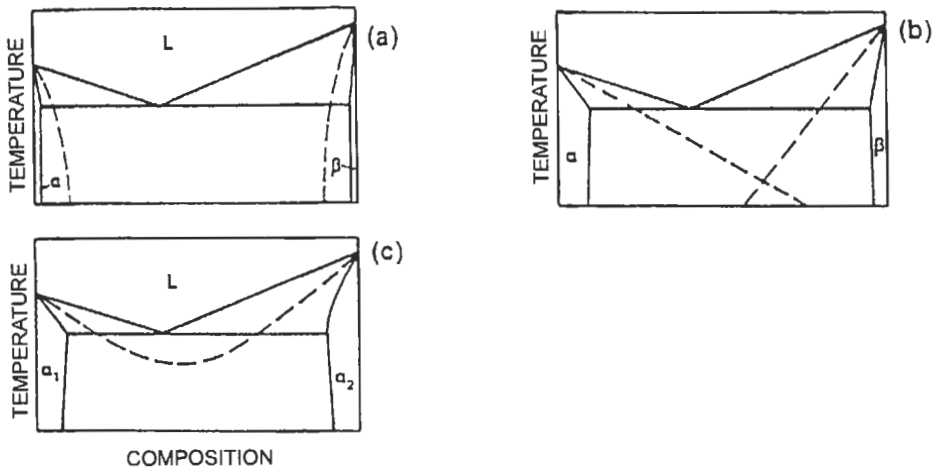

Fig. 8. Schematic representation of T_0 curves for liquid to crystal transformations in three types of eutectic systems. BOETTINGER [1982].

crystal than for a larger one. Consequently for each temperature below T_m, a solid particle can be in equilibrium with the liquid when its radius of curvature has a particular value, known as the *critical radius*. Because at higher supercooling there is more bulk free energy to compensate for the surface free energy, the critical radius decreases with increasing supercooling.

On the other hand, at any supercooling, there exists within the melt a statistical distribution of atom clusters or embryos of different sizes having the character of the solid phase. The probability of finding an *embryo* of a given size increases as the temperature decreases. *Nucleation* occurs when the supercooling is such that there are sufficient embryos with a radius larger than the *critical radius* (HOLLOMON and TURNBULL [1953]).

4.1.1. Calculation of the critical radius and energy barrier

The change in the free energy per unit volume, ΔG, to form a solid embryo of spherical shape of radius, r, from liquid of a pure material involves the variation of the volume free energy and the surface free energy associated with the S–L interface and is given by

$$\Delta G = \Delta G_v + \Delta G_i = -\frac{4}{3}\pi r^3 \frac{L\Delta T}{T_m} + 4\pi\gamma_{SL} r^2, \tag{21}$$

where ΔG_v is the change in free energy on solidification associated with the volume and ΔG_i is the free energy associated with the interface, γ_{SL} is the S–L interfacial free energy, L is the latent heat per unit volume and ΔT is the supercooling. The critical radius, r^*, occurs when ΔG has a maximum given by the condition, $d(\Delta G)/dr = 0$, as

$$r^* = \frac{2\gamma_{SL}T_m}{L\Delta T}. \tag{22}$$

Figure 9, due to KURZ and FISHER [1989], gives a comprehensive picture of the variation of the free energy of an embryo as a function of its radius and ΔT: (a) At temperatures T greater than T_m both ΔG_v and ΔG_i increase with r. Therefore the sum ΔG, increases monotonically with r. (b) At the melting point, $\Delta G_v = 0$ but ΔG_i still increases monotonically. (c) Below the equilibrium temperature the sign of ΔG_v is negative because the liquid is metastable while the behavior of ΔG_i is the same as in (a) and (b). At large values of r, the cubic dependence of ΔG_v dominates over ΔG_i and ΔG passes through a maximum at the critical radius, r^*. When a thermal fluctuation causes an embryo to become larger than r^*, growth will occur as a result of the decrease in the total free energy. Nucleation in a homogeneous melt is called *homogeneous nucleation* and from eq. (21) the *critical energy of activation* for an embryo of radius r^* is given by

$$\Delta G^* = \frac{16}{3}\pi \frac{\gamma_{SL}^3 T_m^2}{L^2 \Delta T^2}. \tag{23}$$

The unlikelihood that statistical fluctuations in the melt can create crystals with a large radius is the reason why nucleation is so difficult at small values of the supercooling. Thus, homogeneous nucleation is only possible for high supercooling (on the order of 0.25 T_m) according to the HOLLOMON and TURNBULL [1953] theory. However small contamination particles in the melt, oxides on the melt surface or contact with the walls of a mould may catalyze nucleation at a much smaller supercooling and with fewer atoms required to form the critical nucleus. This is known as *heterogeneous nucleation*.

In fig. 10, homogeneous and heterogeneous nucleation are compared for a flat catalytic surface and isotropic surface energies. For this simple case, the embryo is a spherical cap that makes an angle θ with the substrate given by

$$\gamma_{cL} - \gamma_{cS} = \gamma_{SL} \cos\theta, \tag{24}$$

where γ_{cL} is the catalyst–liquid interfacial free energy and γ_{cS} the catalyst–solid interfacial free energy. At a supercooling, ΔT, the critical radius of the spherical cap is again given by eq. (22), but the number of atoms in the critical nucleus is smaller than that for homogeneous nucleation as a consequence of the catalytic substrate. Indeed the thermodynamic barrier to nucleation ΔG^* is reduced by a factor $f(\theta)$ to

$$\Delta G^* = \frac{16}{3}\pi \frac{\gamma_{SL}^3 T_m^2}{L^2 \Delta T^2} f(\theta) \tag{25}$$

where

$$f(\theta) = \frac{(2 + \cos\theta)(1 - \cos\theta)^2}{4}. \tag{26}$$

If nucleation occurs in a scratch or a cavity of the catalytic substrate, the number of atoms in a critical nucleus and the value of ΔG^* can be reduced even more. For a planar catalytic surface, the reduction in the free energy barrier compared to that for homo-

References: p. 830.

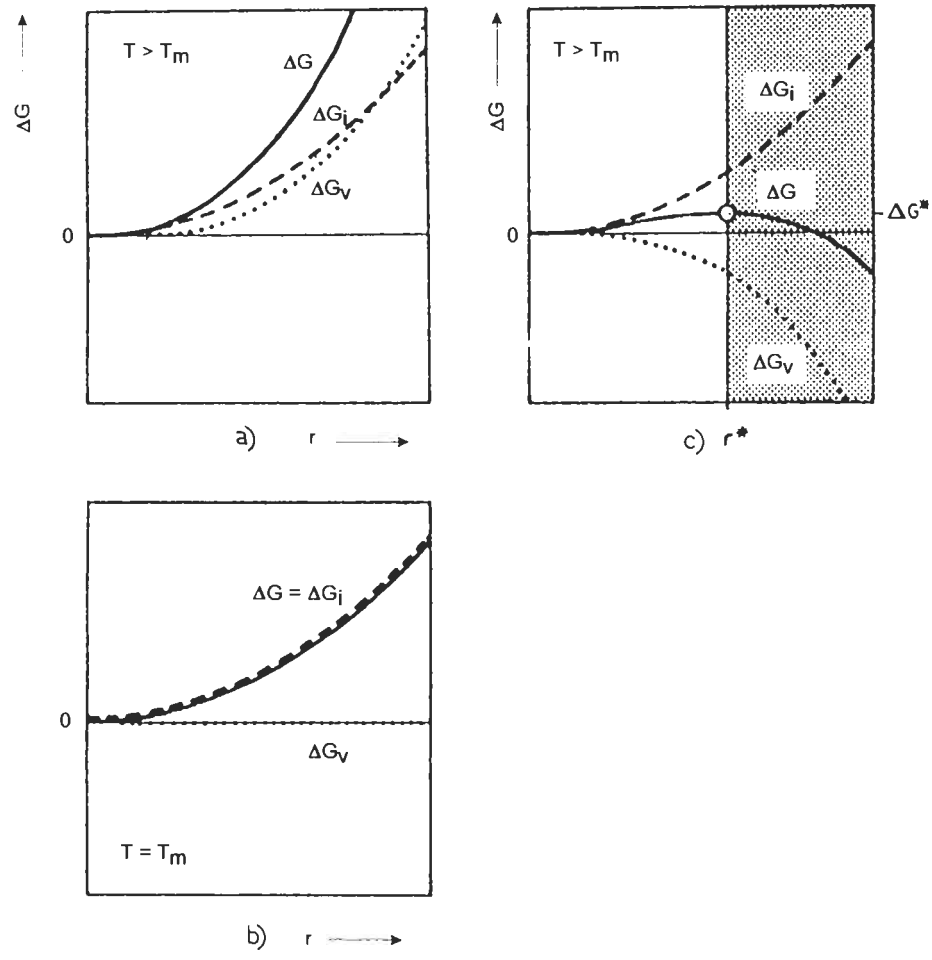

Fig. 9. Volume, surface and total values of the free energy of a crystal cluster as a function of radius, r, at three temperatures: (a) $T > T_m$, (b) $T = T_m$, and (c) $T < T_m$. KURZ and FISHER [1989].

geneous nucleation depends on the contact angle. Any value of θ between 0° and 180° corresponds to a stable angle. When $\theta = 180°$, the solid does not interact with the substrate, $f(\theta) = 1$ and the homogeneous nucleation result is obtained. When $\theta = 0°$, the solid "wets" the substrate, $f(\theta) = 0$, and $\Delta G^* = 0$. As a result, solidification can begin immediately when the liquid cools to the freezing point. From the classical heterogeneous nucleation point of view, a good nucleant corresponds to a small contact angle between the nucleating particle and the growing solid. According to eq. (24) this implies that γ_{cS} must be much lower than γ_{cL}. However, in general, the values of γ_{cS} and γ_{cL} are not known and, therefore it is rather difficult to predict the potential catalytic effectiveness of a nucleant. TILLER [1970] pointed out that there is no clear insight into what deter-

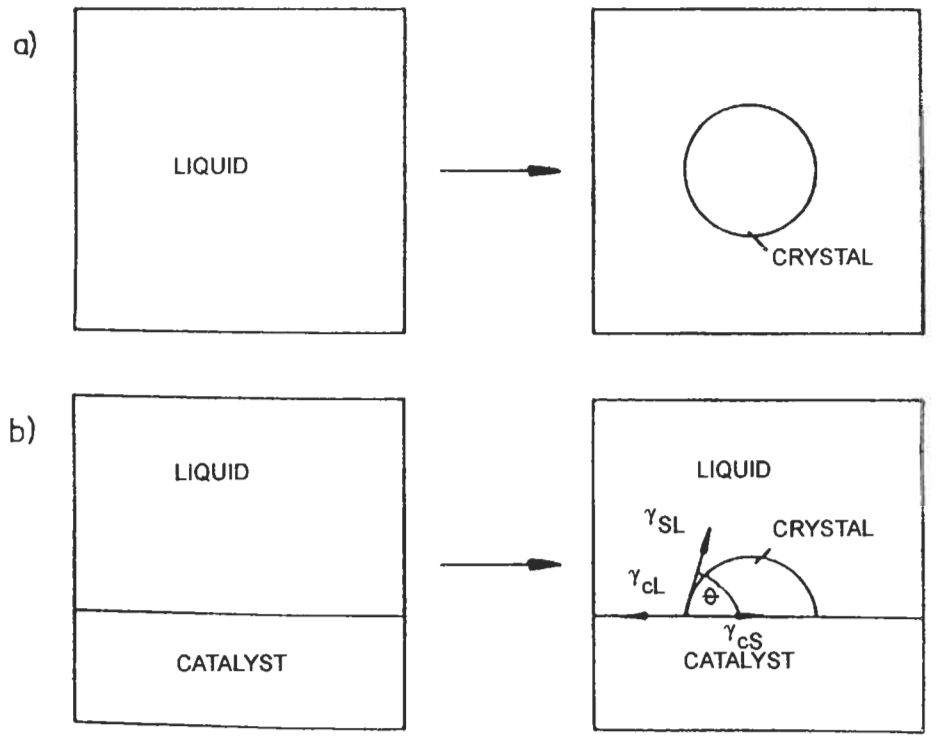

Fig. 10. Schematic comparison of (a) homogeneous and (b) heterogeneous nucleation of a crystal in a supercooled liquid. The interface energies are assumed to be isotropic and in (b) the catalytic surface is assumed to be flat.

mines θ and how it varies with (i) lattice disregistry between substrate and the stable phase, (ii) topography of the catalytic substrate surface, (iii) chemical nature of the catalytic surface and, (iv) absorbed films on the catalytic substrate surface.

4.1.2. Nucleation rate

The rate of homogeneous nucleation, I, is the number of embryos formed with a size that just exceeds the critical value per unit time per unit volume of liquid. Similarly, the heterogeneous nucleation rate is considered per unit area of active catalytic site. To determine the rate of nucleation, it is necessary to find expressions for the number of embryos that have critical size and the rate at which atoms or molecules attach to the critical nucleus.

By considering the entropy of mixing between a small number, N_n, of crystalline clusters, each of which contains n atoms, and N_L atoms of the liquid, an expression for the equilibrium number of clusters with n atoms can be obtained as,

$$\frac{N_n}{N_L} = \exp\left(-\frac{\Delta G_n}{k_B T}\right), \tag{27}$$

where k_B is Boltzmann's constant, ΔG_n is the value of ΔG, obtained from eq. (21) for a cluster of radius, r, containing n atoms. In particular, the number, N_n^*, of clusters of critical radius, r^*, is given by

$$\frac{N_n^*}{N_L} = \exp\left(-\frac{\Delta G_n^*}{k_B T}\right), \tag{28}$$

where ΔG_n^* corresponds to the critical size cluster.

If one can assume that an equilibrium number of critical nuclei can be maintained in the melt during the nucleation process, the homogeneous nucleation rate (#nuclei/time/volume) is then given by

$$I = K_1 \nu \frac{N_n^*}{N_L}, \tag{29}$$

where K_1 is a constant involving the product of the number of atoms per unit volume and the number of atoms on a nucleus surface, and where ν is the rate at which atoms can attach to the critical embryos. This is called the steady state nucleation rate. The value for ν is usually thought to scale with D_L/a_0^2, where D_L is the diffusion coefficient in the liquid and a_0 is the atomic jump distance. For metals, this attachment rate is fairly independent of temperature and so

$$I = K_2 \exp\left(-\frac{K_3}{T\Delta T^2}\right), \tag{30}$$

K_2 typically has a value of $10^{42}/\mathrm{m}^3\mathrm{s}$. For nonmetallic melts, where the diffusion coefficient in the liquid can depend strongly on temperature,

$$I = K_4 \exp\left(\frac{\Delta G_n^* + \Delta G_d}{k_B T}\right), \tag{31}$$

where K_4 includes the pre-exponential factor for diffusion, and ΔG_d is the activation energy for diffusion. For heterogeneous nucleation, similar expressions can be developed but is described per unit area of catalytic surface.

An evaluation of eq. (30) shows that as the supercooling is increased, I increases very rapidly at a critical supercooling in the range of 0.2 T_m to 0.4 T_m. Changes in the pre-exponential term in eq. (30) by orders of magnitude do not appreciably affect the calculated supercooling for sensible nucleation rates. This rapid rise in nucleation rate with temperature effectively defines a *nucleation temperature*.

During rapid cooling of the melt especially to large supercoolings in glass forming alloys, atomic transport may be too slow to maintain an equilibrium number of clusters. This requires the examination of transient nucleation theory and effectively introduces a

delay time into nucleation kinetics that can be important during glass formation or during devitrification as described by THOMPSON *et al.* [1983].

One of the major assumptions of the classical nucleation theory is that the free energy per unit volume and free energy per unit surface area are independent of the size of the embryo. Since the interface between solid and liquid is usually considered to be diffuse on the level of a few atomic dimensions (see § 5), embryo that are a few atomic dimensions in radius cannot be described classically. This leads to a radius (or temperature) dependence of the surface energy as shown by LARSON and GARSIDE [1986] and SPAEPEN [1994]. PEREPEZKO [1988] has pointed out that if θ approaches zero for a heterogeneous nucleation process, the thickness of the spherical cap can approach atomic dimensions, even when the cap radius is much larger, a fact that would also necessitate a nonclassical approach to heterogeneous nucleation.

4.2. Effect of melt subdivision

When a volume of liquid metal is converted to an array of liquid droplets, large supercoolings prior to solidification are often obtained in many of the droplets. This fact leads to a method for the study of nucleation and to understand the supercooling often obtained in metal droplets created by atomization. For the study of nucleation this method was pioneered by TURNBULL and CECH [1950] and continued most notably by PEREPEZKO and ANDERSON [1980]. An example of the effect of supercooling on microstructure development is given for atomized Al–8%Fe alloys by BOETTINGER *et al.* [1986].

If the nucleating sites contained within a given liquid volume are distributed randomly, the arrangement of nucleants among the droplets may be described by a Poisson distribution. For this case the nucleant free droplet fraction, X, is represented by $X = \exp(-mv)$ where m is the average number of nucleants per volume in the melt and v is the droplet volume. Based on experience with droplet emulsion samples (PEREPEZKO and ANDERSON [1980]), supercooling effects become measurable for size refinement below about 100 μm diameter and can become appreciable for powder sizes less than about 10 μm. This suggests that typical values for nucleant densities within the volume of a melt must be in the range from about 10^6–10^9 cm^{-3}. The relatively sharp selection of a given X value (e.g., $X = 0.9$) with the droplet volume indicates the important role of size refinement in achieving large supercooling. Similar relationships can be developed for surface nucleant distributions.

4.3. Experiments on nucleation in pure metals

PEREPEZKO and ANDERSON [1980] have summarized the principal techniques for nucleation experiments conducted at slow cooling rates as shown in fig. 11. The most common corresponds to the dispersion of a pure metal into droplets within a suitable medium. For metals that melt below 500°C, organic fluids with added surfactants are used to form the droplet dispersion. In addition to the isolation of nucleants discussed above, the surfactant probably plays a role in rendering some nucleates inactive. For systems with high melting points, molten salts and glasses have been employed. In both

References: p. 830.

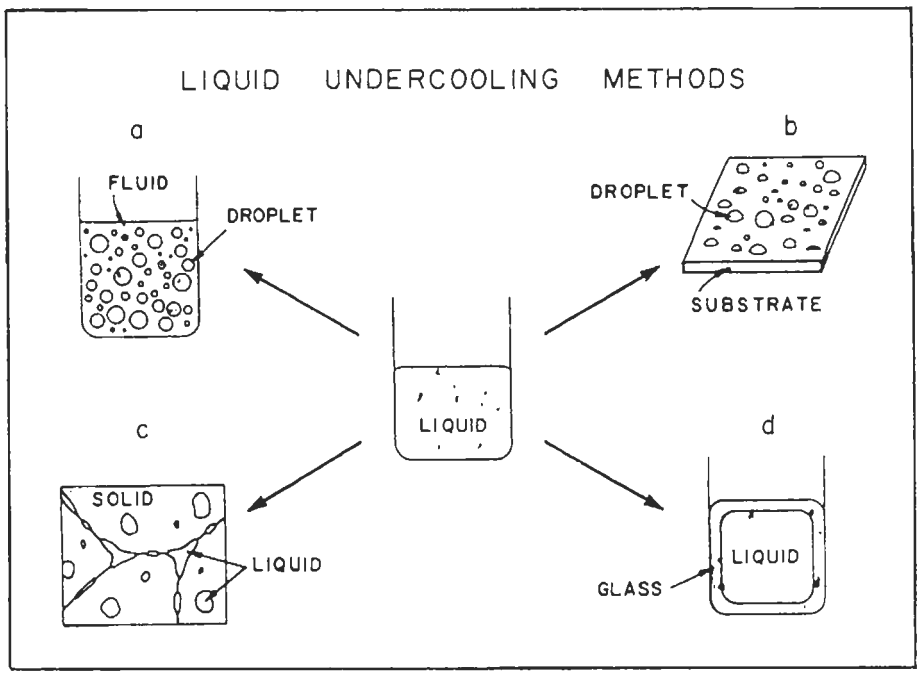

Fig. 11. Sample configuration for different supercooling methods. (after PEREPEZKO and ANDERSON [1980]).

cases, independence and separation of droplets are maintained by a thin inert coating which must be non-catalytic to nucleation. Such dispersions of droplets can be thermally cycled in a DTA or DSC to determine the supercooling of the majority of droplets prior to nucleation. PEREPEZKO [1984] summarizes the maximum supercoolings obtained by his coworkers and by previous work. Maximum supercoolings in the range of 0.3–0.4 T_m are typically obtained. Often maximum supercoolings are used to compute the liquid–solid surface energy using the homogeneous nucleation temperature. Such procedures can provide only a lower bound on the value of the surface energy, unless it is known that the nucleation is indeed homogeneous. It may be that heterogeneities still limit the observed maximum supercoolings in most metals.

In practice the predictive capability of nucleation theory is limited by the unavailability of data for liquid–solid surface energy, which appears in the nucleation rate expression as γ_{SL}^3, and by a lack of knowledge about the catalytic sites present in liquid metals and alloys. Improvements in the independent experimental determination of γ_{SL} for metals would be invaluable in allowing a clearer evaluation of theoretical interface models and more reliable nucleation and growth rate calculations. While the measurements of surface energy using techniques such as grain boundary grove experiments (for example GUNDUZ and HUNT [1985] and HARDY *et al.* [1991]) is preferable, the difficulty of these measurements has led to the development of theoretical models. SPAEPEN [1975] and SPAEPEN and MEYER [1976] estimate the surface energy based on

the configurational entropy of a structural transition that enforces polyhedral atomic packing in the interfacial region. Their result is equivalent to the expression

$$\gamma_{SL} = \frac{\alpha(T/T_m)L}{\left(\frac{V_m}{N_a}\right)^{1/3}}, \tag{32}$$

where N_a is Avogadro's number, V_m is the molar volume and α is a numerical factor related to the atomic packing (0.866 for fcc and hcp and 0.71 for bcc metals). KIM *et al.* [1988a], [1988b] have used this model to calculate homogeneous nucleation rates for the fcc and bcc phases for all compositions in Fe–Ni alloys. Due primarily to the higher α values for fcc as described above, nucleation of fcc phase is predicted to dominate in these alloys even for compositions where bcc has a higher liquidus. Indeed this is confirmed in their own experiments in 3–30 μm size powders as well as in the earlier work of CECH [1956].

4.4. Alloy nucleation

For a binary alloy, ΔG_v in eq. (21) depends not only on the temperature but also on the composition of the liquid and of the solid nuclei. Thus for a given liquid composition, critical values of nucleus composition as well as size are required to determine ΔG^*. If the surface energy and $f(\theta)$ are constants independent of cluster composition, the smallest value of r^* (hence easiest nucleation) is obtained if the composition of the critical cluster maximizes ΔG_v. For alloy nucleation the appropriate expression for ΔG_v is obtained by dividing the expression given in eq. (20) by the molar volume of the solid. It is apparent from eq. (20) that ΔG_v would be maximized for a composition of the solid where $\mu_S^A - \mu_L^A = \mu_S^B - \mu_L^B$; i.e., by a parallel tangent construction as shown in fig. 12. This maximum driving force condition has been proposed (HILLERT [1953], THOMPSON and SPAEPEN [1983]) to find the favoured nucleus composition for a given temperature and liquid composition. In order to use this condition, one must have a thermodynamic model for the alloy of interest; i.e., the free energy functions for the liquid and solid phases must be known. For simple analysis, regular solution models are often employed for the liquid and solid phases. More precise models that fit the measured phase diagram and other thermodynamic data are often available in the literature. In contrast, by including a simple model of the composition dependence of the surface energy, ISHIHARA *et al.* [1986] have shown that the critical nucleus composition can approach the bulk liquid composition at large supercoolings.

Experience with alloy supercooling indicates that the composition dependence of the nucleation temperature, T_N, reflects the composition dependence of liquidus temperature T_L. For example in the Pb–Sb system, the supercooling results shown in fig. 13 reveal that T_N follows a similar trend to T_L even for different T_N levels resulting from catalytic sites of different potency, i.e., different surface coatings (RICHMOND *et al.* [1983]). The maximum ΔG_v condition to determine nucleus composition has been used to successfully predict the composition dependence of measured values of T_N in various alloy systems (THOMPSON and SPAEPEN [1983]).

References: p. 830.

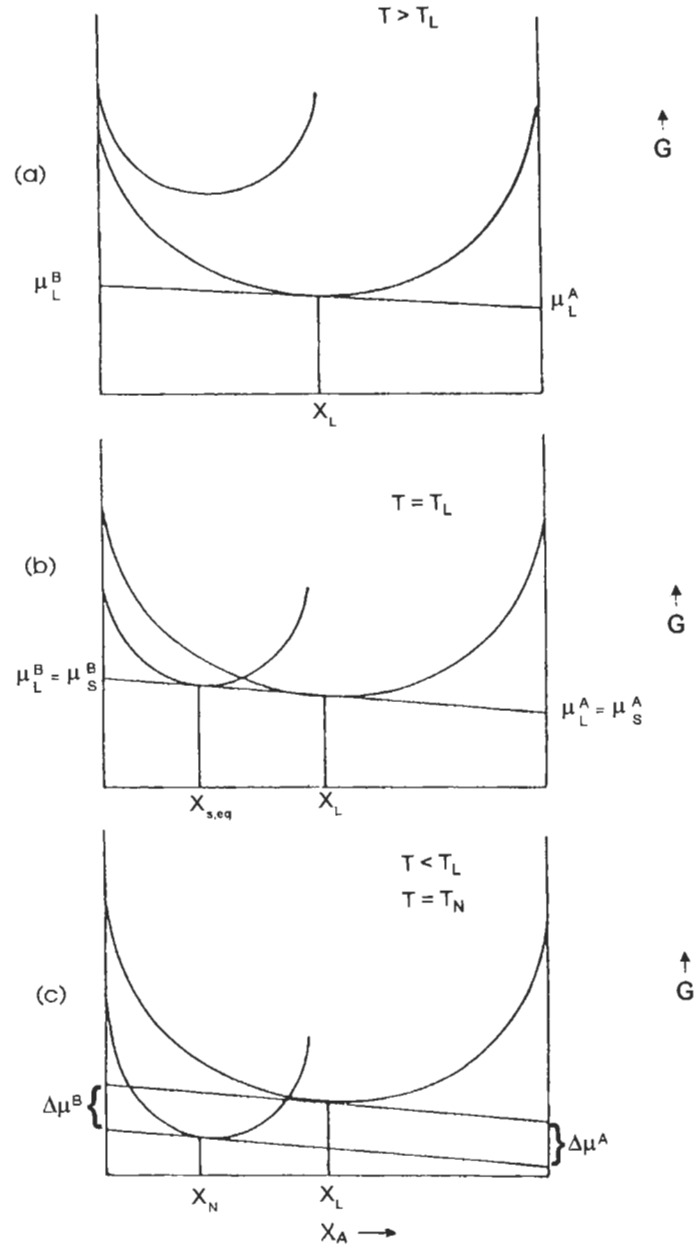

Fig. 12. Schematic free energy versus composition curves for liquid and solid at three temperatures: (a) above the liquidus for composition x_L, (b) at the liquidus, and (c) below the liquidus at an arbitrary nucleation temperature. The composition of a nucleus, x_N, that maximizes the free energy change at the temperature given in (c) is given by the parallel tangent construction. THOMPSON and SPAEPEN [1983]).

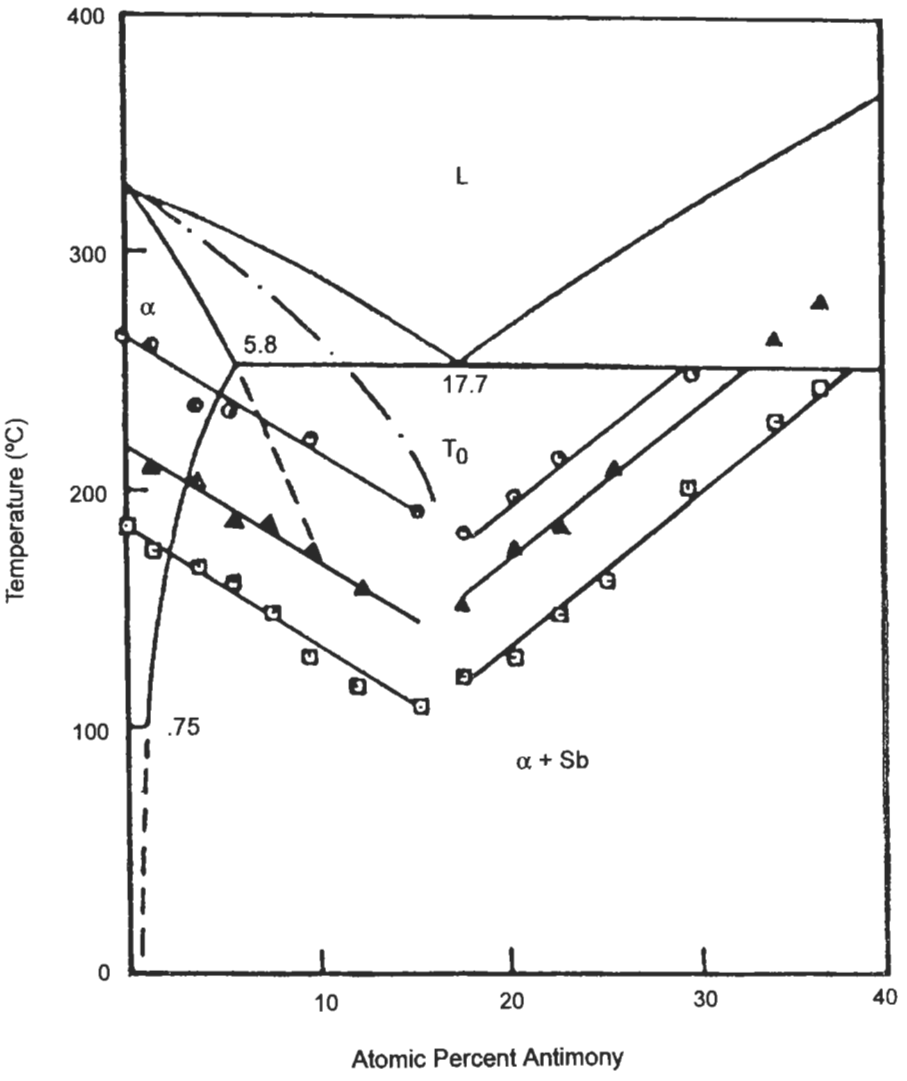

Fig. 13. Summary of nucleation temperatures for Pb–Sb alloys which generally follow the liquidus slope (RICHMOND *et al.* [1983]). Supercooling trends at different levels are produced by different droplet surface coating treatments.

4.5. Experiments on heterogeneous nucleation

While it is clear that most nucleation processes are heterogenous, and the formalism of embryo/substrate interaction is useful, rarely have the heterogeneities been identified

with any certainty. The most common way to control the catalytic substrate is to use binary alloys, typically of the simple eutectic type, and to determine the nucleation temperature of each solid phase in the presence of the other. These experiments can be performed using entrained droplets (SOUTHIN and CHADWICK [1978], with analysis by CANTOR and DOHERTY [1979], MOORE *et al.* [1990], KIM and CANTOR [1991]) or the droplet emulsion technique used extensively by PEREPEZKO and coworkers. A typical thermal cycle for a collection of droplets employed for this purpose is shown in fig. 14. A composition on one side of the eutectic is first melted to determine the characteristic double peaked endotherm corresponding to eutectic ($\alpha+\beta$) and primary phase (β) melting. The sample is then cooled to form solid at T_N and then reheated. After eutectic melting, heating is halted and the sample is equilibrated in the (liquid $+\beta$) two phase field. During subsequent cooling, the nucleation peak observed at T_{het} is then the nucleation temperature of α on β. In Perepezko's work great care was taken to confirm that β was indeed the catalytic surface and that α formed rather than a metastable phase. A summary of such measurements is given in Table 3 where ΔT_{het} is taken as the difference between the eutectic temperature and T_{het}.

One simple idea put forward originally by SUNDQUIST and MONDOLFO [1961] was that of a nonreciprocal potency; i.e., that if α is an effective nucleant for β, then β was an ineffective nucleant for α. Writing two expressions as in eq. (24), one for the contact angle, $\theta_{\alpha\beta}$, of α on a β substrate and one for the contact angle, $\theta_{\beta\alpha}$, of β on an α substrate and eliminating $\gamma_{\alpha\beta}$, it is easy to show that

$$\frac{1+\cos\theta_{\alpha\beta}}{1+\cos\theta_{\beta\alpha}}=\frac{\gamma_{\beta L}}{\gamma_{\alpha L}}. \tag{33}$$

Thus if $\gamma_{\beta L}>\gamma_{\alpha L}$, $\theta_{\alpha\beta}<\theta_{\beta\alpha}$, and β is a more effective substrate for the nucleation of α than α is for β. For example, values of liquid solid surface energy for both Pb and Sn phases in contact with eutectic liquid have been measured by GUNDUZ and HUNT [1985] using the grain boundary groove technique. They find that $\gamma_{SnL}>\gamma_{PbL}$ (132 and 56 erg/cm^2, respectively). Thus the contact angle for nucleation of Pb on a Sn substrate is smaller than the contact angle for Sn on a Pb substrate. Thus both factors in the product, $\gamma^3_{SL}f(\theta)$ in eq. (25), contribute to a lower activation energy for nucleation for Pb on Sn. This is consistent with the results in Table 3 for Pb–Sn.

Recently HOFFMEYER and PEREPEZKO [1988] have intentionally added heterogeneous sites to pure Sn. Using the droplet emulsion technique and by carefully changing the

Table 3
Heterogeneous Nucleation in the Presence of the Primary Phase (PEREPEZKO [1994])

System	Pb–Sn	Pb–Cd	Pb–Sb	Pb–Ag	Bi–Cd	Bi–Ag
Substrate	Pb	Pb	Pb	Pb	Bi	Bi
ΔT_{het}(°C)	80	69	43	27	61	28
Substrate	Sn	Cd	Sb	Ag	Cd	Ag
ΔT_{het}(°C)	22	39	23	40	94	160

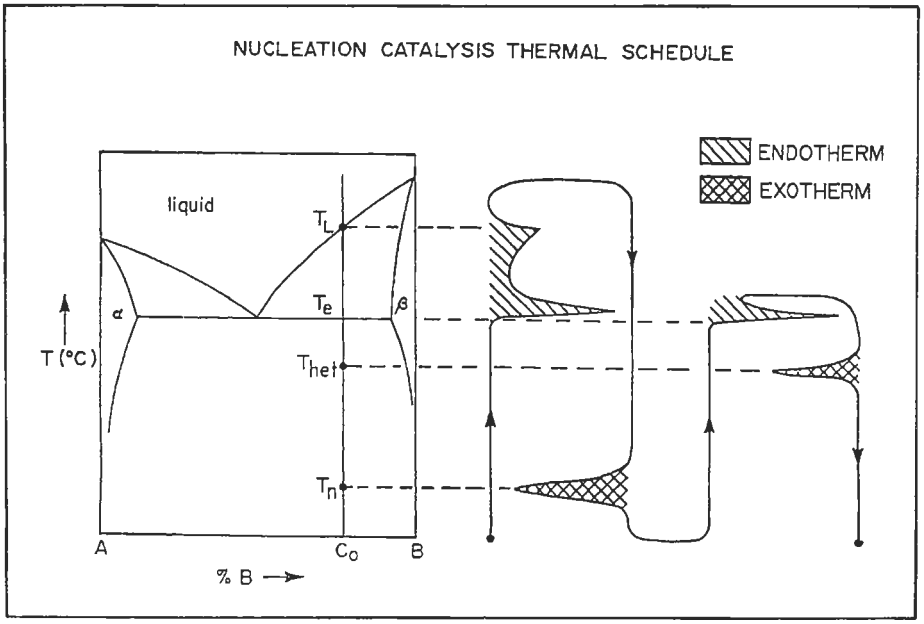

Fig. 14. Example of the interrupted thermal cycle using the droplet emulsion technique that can be used to measure the heterogeneous nucleation temperature, T_{het}, of α phase on a β substrate. PEREPEZKO [1992].

droplet coatings to prove that spurious nucleation by the coating was unimportant, they measured the nucleation temperature of Sn in the presence of various stable oxides, sulphides, and tellurides. The supercooling response of each class was identical even though the lattice disregistry within each class varied. This result indicates that a common surface reaction product may form in each class and catalyze the nucleation process. More details about heterogeneous nucleation and grain refining will be given in § 11.

4.6. Formation of metastable phases by supercooling

One of the most dramatic effects of large supercoolings prior to solidification is the possibility of forming metastable phases. An elegant yet simple example occurs for pure Bi (YOON *et al.* [1986]). A dispersion of Bi droplets was cooled from above the Bi melting temperature of 271°C to approximately 50°C where nucleation took place. Upon reheating the dispersion, melting of a metastable phase occurred at 174°C. If one examines the pressure–temperature diagram for Bi and extrapolates the melting curve for the high pressure Bi(II) phase to atmospheric pressure, one obtains a metastable melting point for Bi(II) very close to 174°C. In addition performing the supercooling experiment with an increase in ambient pressure modified the melting point of the metastable phase in a manner consistent with it being Bi(II). Thus the formation of metastable Bi(II) occured rather than the stable Bi(I) phase at large supercooling.

The bulk free energy change for solidification, ΔG_v (eq. 21) is always largest for the

stable phase. However in the context of the heterogeneous nucleation theory described above, a metastable phase may make a smaller contact angle with a particular catalytic site than does the stable phase. Thus the barrier for nucleation of a metastable phase may be smaller than the barrier for the stable phase. Of course one must always supercool below the melting point of the metastable phase in order for ΔG_v for the metastable phase to be negative. Similarly metastable phases have been formed in alloy systems. In fact in the Pb–Sn system, by avoiding the nucleation of the stable Sn phase, the metastable Pb liquidus and solidus curves have been measured more than 80K below the Pb–Sn eutectic temperature as shown in fig. 15 (FECHT and PEREPEZKO [1989]). When nucleation did occur in this supercooled state, a metastable phase was formed.

4.7. Grain size predictions in castings

Perhaps one of the most elusive problems in the prediction of cast microstructure involves the grain size. THEVOS *et al.* [1989] and STEFANESCU *et al.* [1990] have found it necessary to postulate respectively the existence of a distribution of catalytic sites or a cooling rate dependence for the number of sites to predict accurately the grain size of castings. This subject will be discussed in more detail in § 9 and 11.

5. *Interface kinetics*

As mentioned in § 3, local equilibrium is often a good approximation for interface conditions during growth of metals and alloys under casting conditions. Here we quantify the degree of nonequilibrium (interface supercooling) required to move an interface between a crystal and a melt at a given velocity. First we describe pure materials and then describe alloy effects focussing on the nonequilibrium incorporation of solute into a growing crystal at high solidification velocity.

5.1. Pure materials

The nature of the S–L interface and the rate at which atoms attempt to join the crystal can have a decisive influence on the kinetics and morphology of crystal growth. For solidification of a pure material, the parameter which governs the atomic or molecular attachment kinetics is the interface supercooling, ΔT_k, which is the difference between the thermodynamic melting point and the interface temperature. The dependence of ΔT_k on growth velocity is the subject of this section. The discussion of bulk supercooling and supersaturation and their effect on transport of heat and solute will be addressed in later sections on dendritic and polyphase growth.

An interface can advance by two basic processes depending on the nature of the S–L interface. (i) Non-uniform (or lateral growth) advances the interface by lateral motion of steps that are typically interplanar distances in height. An atom or molecule can attach itself to the solid only at the edge of a step and as a result the crystal only grows by the passage of steps. The relationship between the lateral spreading rate and the effective growth rate normal to the interface is very sensitive to the number and formation

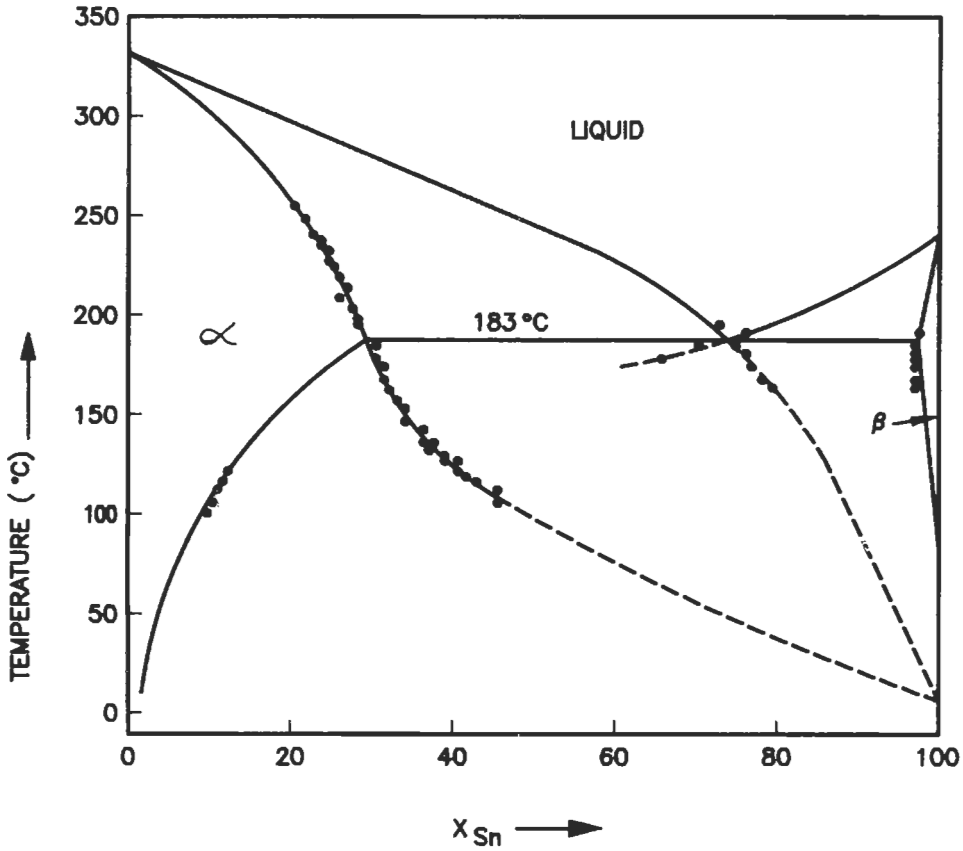

Fig. 15. The stable Pb–Sn phase diagram (solid line), including measured and calculated metastable extensions (dashed line) of liquidus and solidus curves. FECHT and PEREPEZKO [1989].

mechanism of new steps. (ii) Uniform or continuous growth advances the interface without needing steps, that is, growth can equally well proceed from any point. For a given material and supercooling, it is important to determine which type of growth occurs. The supercooling required for lateral growth at a given interface velocity, is typically much larger than that for continuous growth. Moreover, an interface that advances by continuous growth can propagate with a smoothly curved interface on a microscopic scale while lateral growth leads to facets. Whereas growth from the vapor or growth from supersaturated aqueous solutions is easily observed and usually occurs by lateral growth, such atomic scale observations are not usually possible for melt growth. Thus the nature of the S–L interface for metals is the subject of various models. In fact there is strong evidence that most metals freeze by continuous growth.

References: p. 830.

5.1.1. Interface structure

There are two approaches involved in the description of the transition in order from a liquid to a crystal across an interface. In the first, atoms are considered to belong to either the crystal or the liquid and the interface is considered to be sharp. The geometry of the surface that separates the two types of atoms may be smooth or meandering on an atomic scale. The former is called a facetted interface while the later is called a rough interface. In either case the atomic position of atoms in the crystal at the interface are considered to be in perfect crystallographic positions. The second approach includes the additional possibility of a gradual transition in atomic position from the randomness associated with a liquid to the perfect registry of the crystal. This later is called a *diffuse interface*. Indeed if the thickness of the transition layer is of the same order as the roughness, the distinction between rough and diffuse is lost. A facetted interface provides the most difficult situation for growth while a diffuse/rough interface moves most easily. First we describe sharp interface structure models and later describe models based on diffuse interfaces.

JACKSON [1958] has considered a sharp interface model and estimates the conditions when a facetted or a rough interface will occur between liquid and solid. Using a near-neighbor bond model and assuming that a random arrangement of atoms are added to an atomically planar crystal surface, he obtained an expression for the change in free energy as a function of the fraction, x, of the N possible sites occupied by "solid atoms" as

$$\frac{\Delta G}{RT_m} = \alpha^* x(1-x) + x\ln x + (1-x)\ln(1-x), \tag{34}$$

where

$$\alpha^* = \left\{\frac{L_m}{RT_m}\right\}\xi, \tag{35}$$

R is the gas constant, L_m the molar latent heat and ξ is a factor depending on the crystallography of the interface. This factor is always less than 1 and is usually greater than 0.5 and is largest for close-packed planes. This theory has been successfully used to classify and categorize growth morphologies (JACKSON [1971]). Figure 16 shows plots of eq. (34) for different values of α^*. When $\alpha^* < 2$, the minimum value of ΔG occurs at $x = 1/2$; i.e., when half the sites are full. This represents a rough interface. Solidification will then occur by continuous growth because there are so many sites for easy attachment. In these circumstances, from a macroscopic point of view the S–L interface is, in general, non-faceted and may exhibit curvature on a scale much larger than atomic dimensions. When $\alpha^* > 2$, minima in x occur at small and large values of x indicating a interfacial layer with only a few filled (or empty) sites. This represents a smooth (facetted) interface. Solidification must then occur by layer or lateral growth. Planes that are not close-packed have smaller values of ξ and thus for some materials, can exhibit roughness while close-packed planes may be facetted. Planes that are rough will grow faster than the close-packed planes leading to a crystal growth shape composed only of slowly growing close-packed interfaces.

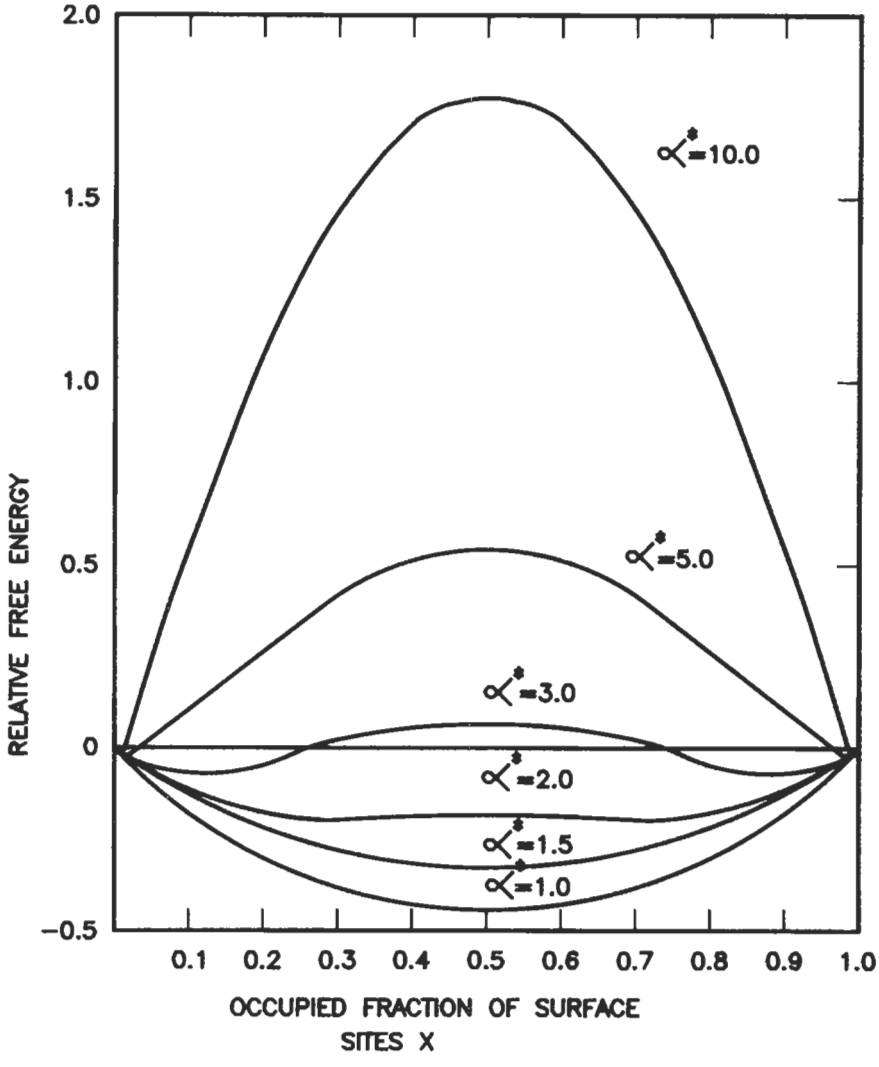

Fig. 16. Change in free energy of a monolayer at the liquid–solid interface as a function of the fraction, x, of sites that are occupied. The value of α^* depends most strongly on the entropy of fusion and to a lesser extent on the crystallographic orientation of the face. JACKSON [1958].

Another approach to interface roughness comes from the consideration of how thermal vibrations affect the surface energy of a step on an otherwise facetted interface (CHERNOV [1984]). It is found that the step energy vanishes when L_m/RT_m falls below a critical value of order unity. When the step energy goes to zero there is no barrier to surface roughening. This analysis gives the same qualitative result as Jackson's approach. Various statistical multilevel models of interface structure and Monte Carlo simulations (TEMKIN

References: p. 830.

[1964, 1969], LEAMY and JACKSON [1971], JACKSON [1974]) also indicate the importance of the ratio L_m/RT_m presented in eq. (35). A common feature of all these models is that the roughness of the interface increases with decreasing L_m/RT_m. Figure 17 shows simulations of an interface at several values of L_m/RT_m (LEAMY and GILMER [1974]).

Molecular dynamics simulations have also been used to model interface structure. Because the position of each atom is computed as a function of time, the approach allows an interface to be diffuse. Indeed simulations show that the transition between liquid and solid for a material with a Lennard–Jones interatomic potential takes place over several atomic layers (BROUGHTON *et al.* [1981]). Such potentials are thought to approximate nondirectional metallic-like bonding. Figure 18 shows the calculated structure of successive (111) layers between the liquid and crystal. In another technique, density functional theory, superposition of ordering waves are employed to represent the local atomic density (OXTOBY and HAYMET [1982]). This method also shows the interface to be several atom layers thick. The expansion relating the free energy to the local density uses order parameters that describe the amplitude of the ordering waves through the interfacial region. This is in fact a generalization of the gradient energy approach of CAHN [1960] except that liquid structure factor data are used to determine the interface thickness and gradient energy coefficient.

5.1.2. Continuous growth

The growth of a rough, sharp interface is called continuous or normal growth because the interface can propagate normal to itself in a continuous manner due to the large number of sites for easy atom attachment. To obtain the velocity-supercooling function for continuous growth of single-component melts, the growth velocity is typically expressed as a product of a factor involving the thermodynamic driving force for solidification and a kinetic prefactor involving the interface mobility:

$$V(T_i) = V_c(T_i)\left[1 - \exp(\Delta G/RT_i)\right], \tag{36}$$

where T_i is the interface temperature and ΔG is the Gibbs free energy change per mole of material solidified (defined to be negative for solidification). The bracketed term in eq. (36) represents a difference between the "forward flux" (liquid → solid) and the "backward flux". The kinetic prefactor, $V_c(T)$, is the rate of the forward flux alone, and corresponds to the hypothetical maximum growth velocity at infinite driving force. Near equilibrium, the exponential can be expanded, resulting in a linear relation between velocity and supercooling:

$$V(T) = V_c(T_m)\frac{L_m \Delta T_k}{RT_m^2}, \tag{37}$$

that is often written as

$$V = \mu \Delta T_k, \tag{38}$$

where μ is called the linear interface kinetic coefficient.

In conventional modeling of interface kinetics (WILSON [1900], FRENKEL [1932],

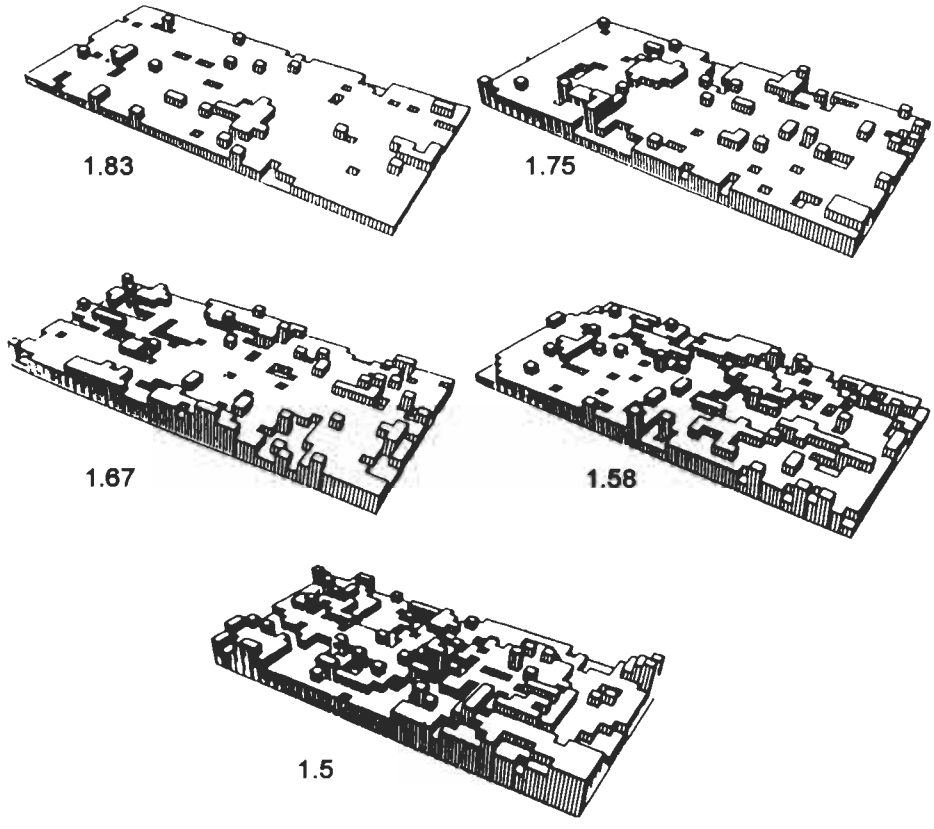

Fig. 17. Surface configuration showing increasing roughness with decreasing values of L_m/RT_m. After LEAMY and GILMER [1974].

TURNBULL [1962], JACKSON [1975]) it is assumed that the rate of the forward reaction, i.e., the rate at which atoms can jump across the interface to join the solid, is similar to the rate at which atoms can diffuse in the melt. Consequently, the kinetic prefactor is assumed to scale with the diffusivity in the liquid:

$$V_c = f_1 D_L/a_0, \tag{39}$$

where a_0 is an interatomic spacing and f_1 is a geometrical factor of order unity. Since the shear viscosity, h_S, of the melt is usually more readily measured, this scaling is often rewritten in terms of h_S using the Stokes–Einstein relation, resulting in:

$$V_c = f_2 k_B T/h_S, \tag{40}$$

where f_2 is another geometrical factor of order unity. Because of the temperature dependence of D_L (or h_S), V will first increase linearly, then go through a maximum and finally decrease as the supercooling increases. This relation has extensive experimental

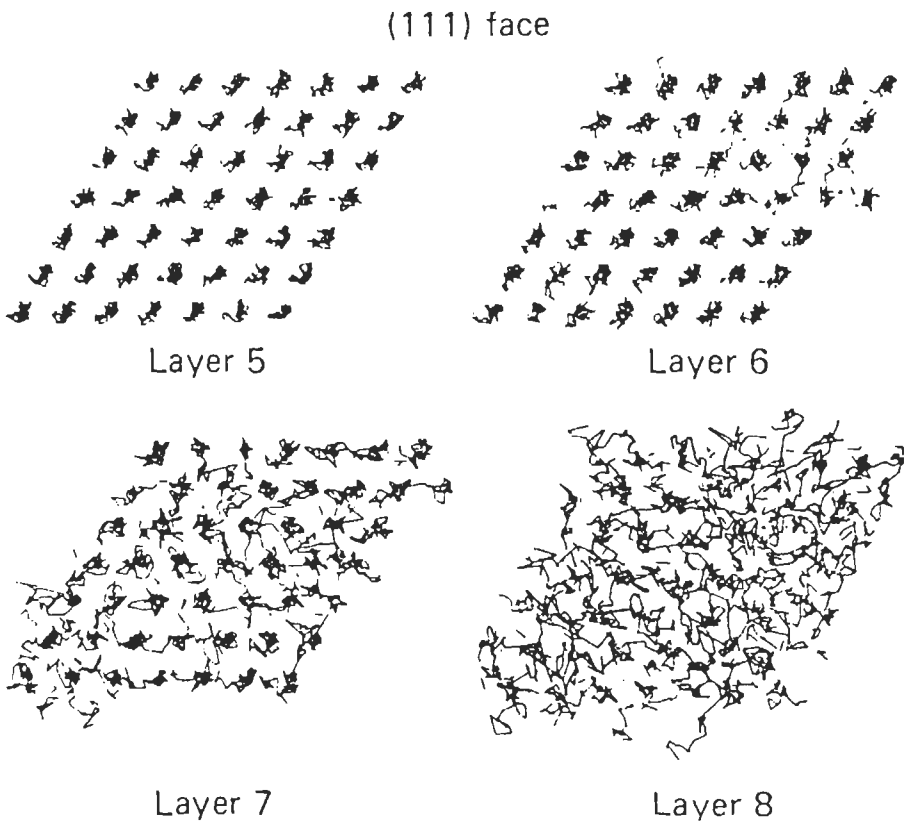

Fig. 18. Trajectories of the molecules in layers parallel to a (111) interface going from solid (layer 5) into the liquid (layer 8) that were obtained by molecular dynamics simulations by BROUGHTON *et al.* [1981].

support for the crystallization of oxide glasses and other covalent materials (JACKSON *et al.* [1967]). However a prefactor that scales with viscosity has never been verified for monatomic melts such as liquid metals (BROUGHTON *et al.* [1982]).

TURNBULL and BAGLEY [1975] pointed out that for simple molecular melts in which the intermolecular potential is largely directionally independent, crystallization events may be limited only by the impingement rate of atoms with the crystal surface and therefore can be much more rapid than diffusive events. According to their *collision-limited growth model*,

$$V_c = f_3 V_S, \tag{41}$$

where V_S is the velocity of sound and f_3 is another numerical factor of order unity. The important consequence is that V_S is about three orders of magnitude greater than D_L/a_0 for typical metallic melts, resulting in a correspondingly more mobile crystal/melt

interface. In addition no maximum is expected in the velocity-supercooling curve. The collision-limited growth model has been confirmed by the analysis of the velocities of rapidly growing dendrites growing into pure Ni melts (CORIELL and TURNBULL [1982]), by molecular dynamics calculations on Lennard–Jones systems (BROUGHTON *et al.* [1982]) and by pulsed laser melting experiments on Cu and Au (MCDONALD *et al.* [1989]). In the molecular dynamics simulation of growth, BROUGHTON *et al.* [1982] approximate their results by eq. (36) with V_c given by $(3k_BT_m/m_w)^{1/2}$ where m_w is the atomic weight. This speed is the average thermal velocity and corresponds to the velocity at which atoms can strike the lattice sites. For Ni at its melting point, this velocity is 8.6×10^4cm/s which is only slightly less than the speed of sound for liquid Ni estimated by CORIELL and TURNBULL [1982]. For Ni at small supercoolings, this value of V_c yields a kinetic coefficient, μ, of 200cm/sK corresponding to negligible interface supercoolings under ordinary solidification conditions. In addition, RODWAY and HUNT [1991] using the Seebeck effect to measure the velocity-interface supercooling relation for Pb have obtained a value of 28 cm/sK for μ that agrees well with that predicted by BROUGHTON *et al.* [1982] using the average thermal speed for this lower melting point material. Both values are orders of magnitude greater than would be predicted for interface kinetics governed by diffusive jumps.

5.1.3. Growth of a diffuse interface

Another approach to modelling continuous growth comes from the consideration of a diffuse interface. MIKHEEV and CHERNOV [1991] have estimated the kinetic coefficient for Pb using this approach. For a gradual transition in the density of atomic planes, the model predicts that the kinetic coefficient is proportional to the thickness of the transition width. Thus a diffuse interface propagates faster at a given level of supercooling than a sharp interface. Spatial and temporal frequency data obtained from bulk liquid structure factor measurements, obtained with neutron scattering experiments on simple monatomic liquids, are employed to estimate the transition width and rate at which atoms can readjust into correct atomic positions. The estimate of the linear kinetic coefficient of 28 cm/sK for Pb is in excellent agreement with the data of RODWAY and HUNT [1991].

An earlier model for a diffuse interface (CAHN [1960], CAHN *et al.* [1964]) also shows the interface mobility to increase with interface thickness. This concept was also incorporated into models for lateral growth (see item 5.1.4.) involving diffuseness of the step edge. In all cases, the diffuseness increases the mobility of the interface over what would be expected for a sharp interface.

5.1.4. Two dimensional nucleation controlled growth

If the interface is atomically smooth and free of any defects, the growth rate is limited by the nucleation of surface clusters. These clusters must form on the interface in order to create the necessary surface steps for lateral growth. The lateral spreading rate is assumed to occur quite rapidly at a speed determined by the continuous growth law described above. The classical theory of two-dimensional nucleation was developed by VOLMER and MARDER [1931]. The growth law (for the formation of cylindrical surface clusters) has the form:

$$V \sim \exp\left\{\frac{-\pi\gamma_e^2 h T_m}{L k_B T \Delta T_k}\right\} \tag{42}$$

where γ_e is the ledge energy per unit area and h is the step height. In the classical theory the constant of proportionality scales with the diffusion coefficient but it could scale with the speed of sound as does the prefactor for continuous growth. According to eq. (42) the growth rate is effectively zero at small supercooling and increases sharply at some critical supercooling. HILLIG [1966] has found that the "constant" of proportionally may in fact depend on ΔT_k. When the number of nuclei is extremely high, the growth is better described by the continuous mechanism.

5.1.5. Growth by screw dislocations

If one or more screw dislocations emerge at the S–L interface it is not necessary to nucleate new layers to provide the sites for lateral attachment. The step generated by each dislocation moves one plane each time it sweeps around the dislocation (FRANK [1949]). It was shown by HILLIG and TURNBULL [1956] that the distance between neighboring turns of the spiral is inversely proportional to ΔT_k, and therefore the total length of step is directly proportional to ΔT_k. For small supercooling, the rate of growth, therefore, will be

$$V \sim (\Delta T_k)^2, \tag{43}$$

because the rate of growth per unit length of step should also be proportional to ΔT_k (CHALMERS [1964]). Figure 19 schematically shows the growth laws for continuous, 2D-nucleation, and screw dislocation-assisted growth laws.

Another source of steps at the S–L interface is the reentrant angle resulting from the emergence of twin planes at the S–L interface. This mechanism is found to be important for Si and Ge. See FLEMINGS [1974].

5.1.6. Transition between continuous growth and facetted growth

The model of CAHN [1960], CAHN *et al.* [1964] predicts a smooth transition from lateral growth at low supercooling to continuous growth at high supercooling. The transition begins at a critical supercooling, ΔT_k^*, and ends at $\pi\Delta T_k^*$. The critical value depends on the surface energy and the degree of diffuseness. For a material with a very diffuse interface, ΔT_k^* may be so small that lateral growth is impossible to observe. An experiment showing the transition predicted by the theory has been performed by PETEVES and ABBASCHIAN [1986] on Ga. The transition to continuous growth occurs at a supercooling of about 4K and a growth rate of about 5 mm/s for the (111) face.

With increasing supercooling other models can also predict a transition to continuous growth. CHERNOV [1984] considers the nucleation of a disk on an otherwise facetted interface. If $L_m/RT_m > 2$ the edge energy is nonzero and the surface is facetted and the growth will be lateral. At some value of increased supercooling, the driving force is comparable to the work of creating a new disk and the moving interface becomes rough. This kinetic roughening then permits growth to proceed in a continuous manner.

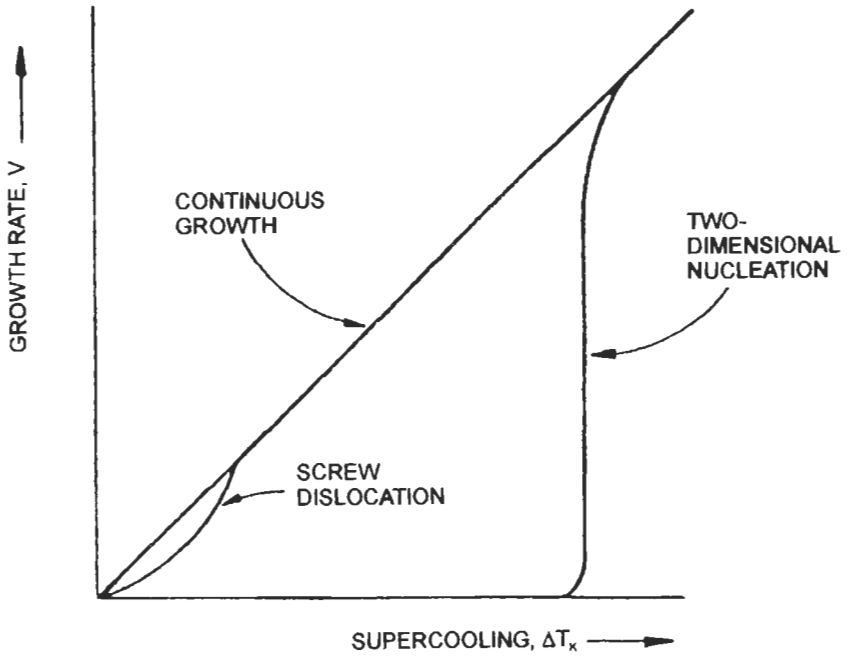

Fig. 19. Growth rate versus interface supercooling according to the three classical laws of interface kinetics.

5.2. Binary alloys

BAKER and CAHN [1971] described the general formalism for the interface conditions for solidification of a *binary* alloy in terms of two response functions. One choice for these functions describes the interface temperature, T_i, and the composition of the solid at the interface, C_S^*. Neglecting orientation effects, these response functions can be written as follows:

$$T_i = T\left(V, C_L^*\right) - T_m \Gamma K_m \tag{44}$$

and

$$C_S^* = C_L^* k\left(V, C_L^*\right), \tag{45}$$

where V is the local interface velocity. The functions $T(V, C_L^*)$ and $k(V, C_L^*)$ must be determined by a detailed kinetic model for the interface. At zero velocity they are very simply related to the phase diagram: $T(0, C_L^*)$ is the equation for the phase diagram liquidus and k(0, C_L^*) is the equation for the equilibrium partition coefficient k_0, which can depend on composition. The dependence of k on curvature is thought to be negligible (FLEMINGS [1974]). The possible forms for the functions T and k are constrained by the condition that $\Delta G < 0$ as described in fig. 7 above. The kinetic partition coefficient can also depend on the crystallographic orientation of the growing interface. If a crystal

grows with a S–L interface having regions that are curved and facetted, the incorporation of solute into the crystal behind the facet can be quite different from the rest of the crystal. BRICE [1973] calls this the *facet effect*. This effect will be neglected in the remainder of this chapter.

Several models for the dependence of the partition coefficient on velocity, eq. (45), have been formulated for continuous growth. The model formulated by BAKER [1970] is quite general. Other theories predict that the partition coefficient changes monotonically from its equilibrium value to unity as the growth velocity increases. In these models the interface partition coefficient is significantly changed from the equilibrium value, k_0, only when a dimensionless growth velocity, V/V_D approaches one. Here V_D is the diffusive speed for atom exchange between the crystal and the liquid. V_D is a ratio of a diffusion coefficient, D_i, for that exchange to the interatomic distance, a_0. The value of this diffusion coefficient should be bounded by those of the liquid and the solid, but experimentally appears to be closer to that of the liquid. Using a value for a liquid diffusion coefficient typical of metals (2.5×10^{-5} cm^2/s) and a length scale of 0.5 nm, V_D should be less than 5 m/s. Experimental evidence (SMITH and AZIZ [1994]) suggests that V_D is in the range between 6 and 38 m/s. Thus in ordinary solidification where $V \ll 1$ m/s the local equilibrium assumption is valid. The functional form of the models of AZIZ [1982] and of JACKSON *et al.* [1980] for non-facetted growth is given by

$$k = \frac{k_0 + V/V_D}{1 + V/V_D}. \tag{46}$$

This expression is valid only for dilute alloys where the composition dependence of k_0 can be neglected. At a velocity of V_D, the partition coefficient is the mean of the equilibrium partition coefficient and unity (see fig. 28a). Because eq. (46) has no dependence on composition, it cannot treat the situation shown in fig. 7b), in which partitionless solidification is impossible for some compositions. The Aziz model has been generalized to treat non-dilute alloys by AZIZ and KAPLAN [1988] and to include the possibility that solute drag dissipates some of the available free energy.

In the continuous growth model of Aziz, the process that accomplishes the formation of the crystal structure from the liquid and the process that establishes the compositions at the interface are considered to be distinct. Indeed for metals, the former may only be limited by the rate at which atoms hit the interface (collision limited growth) whereas the latter process requires diffusive interchanges between liquid and solid to reach equilibrium partitioning. It is this separation of time scales that permits solute trapping at high velocity where there is insufficient time for the diffusive rearrangements before the solute is buried under additional crystal. For this reason the $k(V)$ expression given above involves a diffusion coefficient, whereas the model assumes that the interface temperature equation can be obtained in an identical manner to a pure material, eq. (36), employing eq. (41). It is however necessary to use the value for ΔG obtained for alloys, eq. (20) rather than the simple expression based on ΔT_k.

For dilute solutions, an analytical expression for the interface temperature can be obtained (BOETTINGER and CORIELL [1986]. In this case ΔG from eq. (20) can be given by

$$\frac{\Delta G}{RT_i} = \frac{1-k_0}{m_L}\left(T_m + m_L C_L^* - T_i\right) + C_L^*\left[k_0 - k\left(1 - \ln\left(k/k_0\right)\right)\right]. \tag{47}$$

Expanding eq. (36) for small ΔG gives $V = -V_c(\Delta G/RT_i)$ where V_c is taken here as the speed of sound. One can then summarize the two response functions for a flat interface as follows:

$$T_i = T_m + m_L(V)C_L^* - \frac{RT_m^2}{L_m}\frac{V}{V_c} \tag{48}$$

and

$$C_S^* = kC_L^*, \tag{49}$$

where $m_L(V)$ is given by

$$m_L(V) = m_L\left\{1 + \frac{k_0 - k\left(1 - \ln k/k_0\right)}{1-k_0}\right\}, \tag{50}$$

with k (i.e. $k(V)$) given by eq. (46). For a curved interface, eq. (48) must include an additional term for the Gibbs–Thomson effect. Note that for $V=0$, eq. (48) and (49) revert to the local equilibrium conditions. As k goes to unity, the term in the large brackets in eq. (50) changes the effective liquidus slope from the equilibrium value of m_L to the slope of the T_0 curve, which is $m_L[(\ln k_0)/(k_0-1)]$. The last term in eq. (48) can be identified as a interface kinetic supercooling necessary to drive the formation of the lattice.

Figure 20 shows a plot of the response functions obtained using eqs. (46), (48)–(50) superimposed on a phase diagram including the liquidus, solidus, and T_0 curves. The plot gives the liquid composition at the interface and the interface temperature as a function of interface velocity for a fixed solid composition. This would be the case for directional solidification at different but constant velocities. The figure is based on a phase diagram for Ag–Cu with $T_m = 960°C$, $k_0 = 0.44$ and $m_L = -5.6$ K/at.%, $C_S^* = 5$ at%Cu, $V_D = 5$ m/s, and $V_c = 2 \times 10^3$ m/s. At zero velocity, the composition of the liquid lies on the liquidus curve, a situation that corresponds to local equilibrium. At intermediate velocities (about 1 m/s) the composition of the liquid moves towards the composition of the solid but with an increased interface temperature. At higher velocities the liquid composition continues to approach the solid composition but the interface temperature drops below the T_0 curve. At still higher velocities, where the partition coefficient is essentially unity, the temperature drops sharply with increasing velocity.

This analysis provides a pair of thermodynamically consistent response functions for dilute alloys. For concentrated alloys no simple expressions can be written because k_0 depends on composition. However, given a thermodynamic description of the liquid and solid phases and values for the two kinetic parameters V_D and V_c, the response functions can be calculated numerically (AZIZ and KAPLAN [1988]). Figure 21 shows the result for all compositions of an ideal binary alloy. Effective liquidus and solidus curves are shown for several interface velocities. These curves give the combinations of C_L^*, C_S^*, and T_i

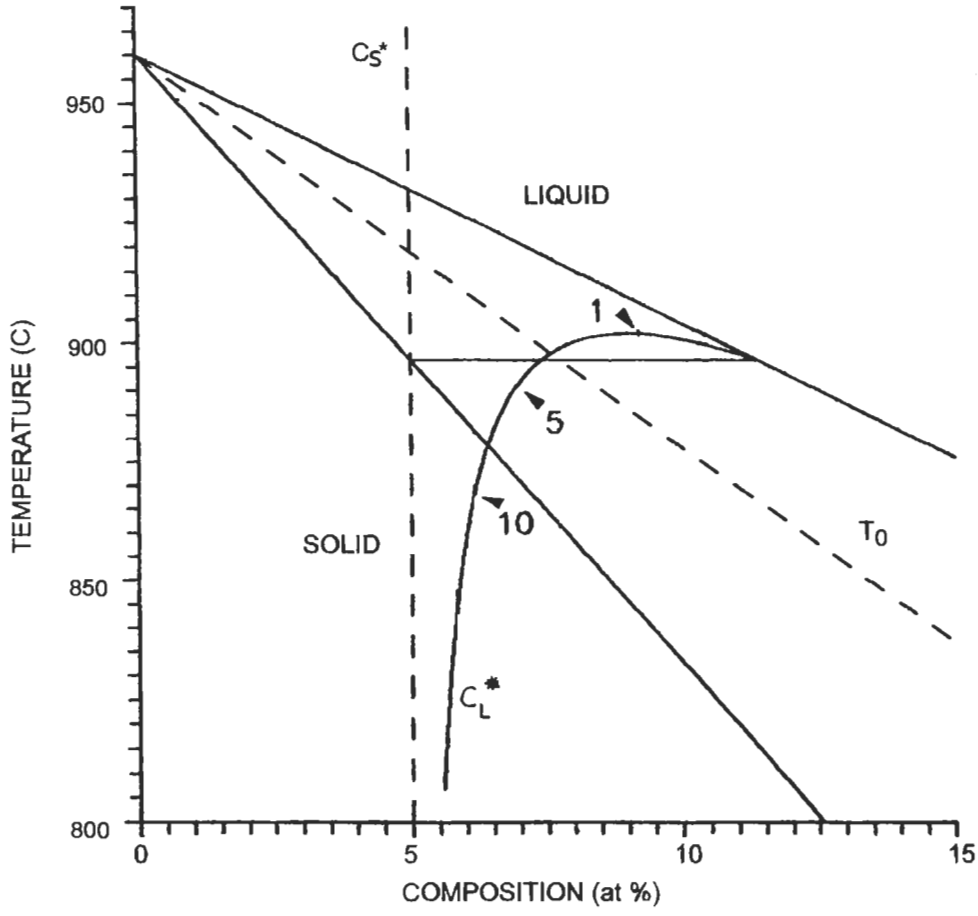

Fig. 20. Plot of interface temperature vs. liquid composition at the interface for a fixed solid composition, (=5 at %), forming at the indicated velocities (in m/s) superimposed on the phase diagram.

possible as interface conditions at the indicated velocities. A related model, which includes solute drag (AZIZ and KAPLAN [1988]), can also be reduced to a simple analytical expression for dilute alloys (AZIZ and BOETTINGER [1994]). Extensive experimental research has been focused on testing these models (KITTL *et al.* [1994]).

These solute trapping ideas have been extended to ordered intermetallic phases by BOETTINGER and AZIZ [1989]. Rapid solidification experiments indicate that some compounds, which are normally ordered at the solidus, can be forced to solidify into the chemically disordered form of the crystal structure (INOUE, *et al.* [1984], HUANG, *et al.* [1986], BOETTINGER *et al.* [1988a)], HUANG and HALL [1989]). The theory treats the trapping of disorder by a consideration of solute trapping on each sublattice of the ordered phase. At high rates, there is insufficient time to proportion the solute onto each

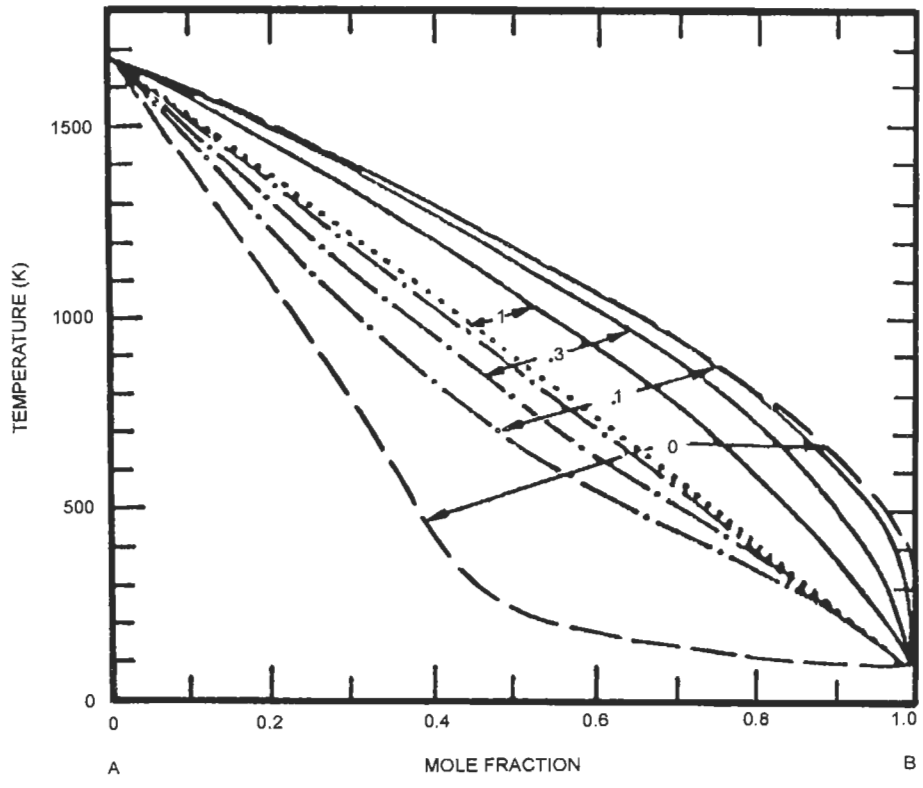

Fig. 21. Kinetic interface condition diagram for ideal liquid and solid with pure component melting points as shown, pure component entropies of fusion equal to R, and $V_C/V_D = 100$. Dashed lines: equilibrium liquidus and solidus labeled zero, dash-dot lines: kinetic liquidus and solidus at different interface velocity given as values of V/V_D, dotted line: T_0 curve. AZIZ and KAPLAN [1988].

sublattice and a chemically disordered crystal can be formed. Often however, this disordered phase reverts to the equilibrium ordered phase during solid state cooling with a resultant microstructure consisting of a high density of antiphase domains. An approximate expression giving the solidification velocity at which the long range order parameter, η, at the liquid solid interface goes to zero is given by

$$V_{\eta\to 0} = V_D[T_c/T_m - 1], \tag{51}$$

where T_m is the melting point of the ordered phase and T_C is the temperature where the solid phase would disorder during heating if melting could be prevented; i.e. the metastable critical temperature for the order–disorder reaction. Clearly the closer T_c is to the melting point, the lower is the velocity to obtain disorder trapping. Strongly ordered compounds cannot usually be disordered by rapid solidification techniques.

References: p. 830.

6. *Solidification of alloys with planar and nearly planar S–L interfaces*

The analysis of the shape of the S–L interface on a scale larger than atomic dimensions begins with a consideration of plane front growth. Plane front growth is used extensively to control the solute distribution that remains in a solid after freezing, especially in the area of crystal growth of materials for electronic applications. It is also important as a starting point to understand the more complex interface shapes involving cellular and dendrite growth. To achieve planar growth, it is necessary to obtain a S–L interface that is both macroscopically and microscopically planar. The former is achieved by controlled directional solidification with good furnace design and avoiding convection in the melt. The latter is achieved by avoiding interface instabilities due to constitutional supercooling (C.S). This section will summarize important work in these two areas.

6.1. General formulation of diffusion controlled growth

In general, the transport of solute during directional solidification in the absence of convection with a planar S–L interface growing in the z-direction is described by the one dimensional diffusion equation

$$\frac{\partial^2 C}{\partial z^2} = \frac{1}{D}\frac{\partial C}{\partial t}, \tag{52}$$

that must be solved for the composition C in the liquid and solid subject to conditions at the interface given by

$$C_S = k_0 C_L \tag{53}$$

and

$$D_S \frac{\partial C_S}{\partial z} - D_L \frac{\partial C_L}{\partial z} = V(C_L - C_S). \tag{54}$$

The use of k_0 in eq. (53) corresponds to the local equilibrium assumption and can be modified for rapid solidification using eq. (46).

6.2. Solute redistribution during one dimensional solidification

Four limiting cases of the diffusional transport and the resultant solute distribution can occur during unidirectional plane front solidification of a rod (fig. 22).

6.2.1. Equilibrium freezing

Here the S–L interface advances so slowly that diffusion in both phases maintains global equilibrium at all time (see § 3). If the phase diagram predicts the solid to be a single phase for the bulk alloy composition, any difference in solid and liquid composition occurring during the solidification process will disappear after solidification is complete (fig. 22a). In more quantatative terms, a *Peclet number* (Pe), defined by

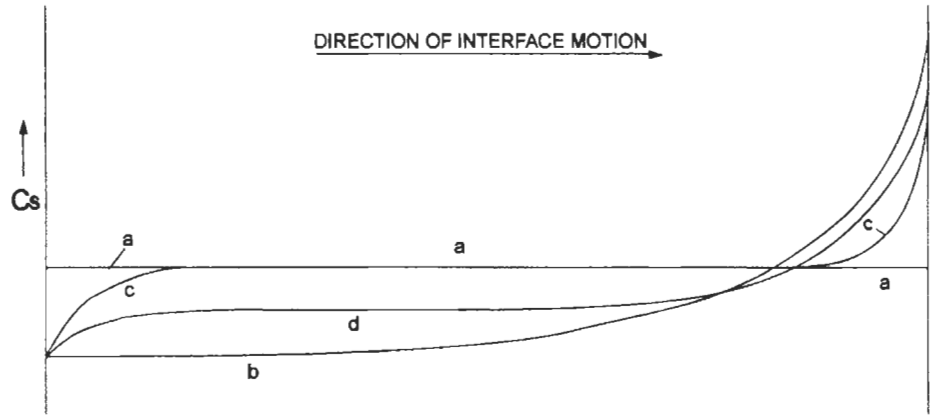

Fig. 22. Solute distribution remaining in the solid *after* one-dimensional solidification: (a) complete diffusion in solid and liquid; (b) complete mixing in liquid-no solid diffusion; (c) diffusion in liquid only; (d) partial mixing in liquid, including convection.

$$P_e = \frac{L_0 V}{D}, \tag{55}$$

for each phase, especially the solid, must be much smaller than unity, where L_0 is the length of the sample. Only under unusual circumstances can the *lever rule* be expected to apply during solidification. One such case is Fe–C growing at very low velocity because of the high solid state diffusivity of C in Fe. In substitutional alloys, equilibrium freezing does not occur in any practical casting or crystal growth situations.

6.2.2. Complete liquid mixing, with no solid diffusion

The conditions considered in this limiting case are: i) complete mixing of the liquid; ii) no solid state diffusion; iii) constant and equal solid and liquid densities; iv) local equilibrium at the S–L interface. The assumption of complete liquid mixing and no solid diffusion is often made because diffusion in the liquid is typically orders of magnitude faster than in the solid. In this case eq. (52) is replaced by a statement of solute conservation. When a fraction of the rod, f_S, is solidified, the concentration of the remaining liquid is found to obey the following differential equation

$$\frac{dC_L}{C_L} = \frac{1 - k_0}{1 - f_S} df_S, \tag{56}$$

which is easily integrated for constant k_0 to

$$C_L = C_0 (1 - f_S)^{k_0 - 1}, \tag{57a}$$

where C_0 is the nominal alloy composition. After freezing is complete, this process leaves a solute distribution in the solid (fig. 22b) given by

References: p. 830.

$$C_S = k_0 C_0 \left(1 - f_S\right)^{k_0 - 1}, \tag{57b}$$

where now f_S is taken as the fractional distance down the rod. Indeed in this model, the rod geometry with a planar interface is not a necessary assumption if the Gibbs–Thomson effect can be neglected, and the equations are valid for any interface shape as long as f_S is taken as volume fraction. The temperature of the interface can be simply obtained by substituing eq. (57a) into eq. (18).

GULLIVER [1922], HAYES and CHIPMAN [1938], SCHEIL [1942] and PFANN [1952] all developed the same type of equation, also called the "*nonequilibrium lever rule*". Equations (57) can only be considered a limiting case since most real systems have at least some solid state diffusion and some level of incomplete liquid mixing. For alloys containing a eutectic (see § 8) the liquid composition may reach the eutectic composition. In this case, the remaining liquid will freeze as a eutectic mixture. For cases when k_0 depends on composition, eq. (56) can be numerically integrated.

6.2.3. Solid diffusion during solidification

BRODY and FLEMINGS [1966] were the first to account for diffusion in the solid. They retained the assumption of complete liquid mixing, approximated the solute concentration gradient in the solid at the S–L interface and derived the following expressions:

$$C_S^* = k_0 C_0 \left[1 - \frac{f_S}{\left(1 + \alpha_\theta k_0\right)}\right]^{k_0 - 1} \tag{58}$$

and

$$C_S^* = k_0 C_0 \left[1 - f_S\left(1 - 2\alpha_\theta k_0\right)\right]^{\left(k_0 - 1\right)/\left(1 - 2\alpha_\theta k_0\right)}. \tag{59}$$

Equation (58) considers the case where V is constant and eq. (59) considers the case where the growth is parabolic, i.e. $V \sim t^{-1/2}$. The parameter α_θ is a measure of the extent of diffusion of solute in the solid and is defined as:

$$\alpha_\theta = \frac{D_S t_f}{L_0^2}, \tag{60}$$

where t_f = local solidification time, that in the simplest case, where V = constant, is given by V/L_0. BRODY and FLEMINGS [1966] also obtained numerical solutions of the solid diffusion equation.

Equations (58) and (59) are good approximations only when $\alpha_\theta << 1$, i.e., with limited solid diffusion during the solidification process. However problems occur when α_θ becomes larger, as has been demonstrated by FLEMINGS *et al.* [1970]. KURZ and CLYNE [1981] postulated an empirical variable, Ω, applicable for the parabolic growth law, given by

$$\Omega = \alpha_\theta \left[1 - \exp\left(-\frac{1}{\alpha_\theta}\right) - \frac{1}{2}\exp\left(-\frac{1}{2\alpha_\theta}\right)\right]. \tag{61}$$

The value for Ω is then used to replace α_θ in eqs. (58) or (59). This new variable was postulated because it provides two limiting cases corresponding to the ordinary Scheil Equation (no solid diffusion, $\alpha_\theta = 0$ or $\Omega = 0$) and to the lever rule (complete solid diffusion, $\alpha_\theta = \infty$ or $\Omega = 0.5$) respectively.

Another form for Ω with the proper limits was given by OHNAKA [1986]. He approximately solved the diffusion equation under the assumption that the solute distribution in the solid can be represented by a quadratic curve and has derived another form for Ω valid for parabolic growth, given by

$$\Omega = \alpha_\theta / 1 + 2\alpha_\theta. \tag{62}$$

KOBAYASHI [1988] developed an exact analytical solution involving a slowly converging series and showed that the approximate solutions above always underestimate the solute composition at the S–L interface with large deviations when k_0 is small and α_θ is large. Another useful approximation for solid diffusion has been given by WANG and BECKERMANN [1993].

The above analytical solutions have limitations, because all the physical properties must be constant, and C_S can only be calculated at the S–L interface. While this does permit one to calculate the fraction of solid versus temperature curve that is required for heat flow modelling (eq. (7)), it does not give the solute profile that remains in the solid. Numerical solutions can overcome these limitations. BATTLE [1992] gives a review of the several models developed. Among them the recent model of BATTLE and PEHLKE [1990] has approached the one dimensional problem in a general form. The method combines solution of the diffusion equation for heat and solute through out the entire rod using the technique of MEYER [1981]. GANESAN and POIRIER [1989] used numerical calculations of solid diffusion to point out that α_θ can not be treated as a constant during solidification. Consequently, eq. (59) overestimates the extent of diffusion in the solid. This effect is more pronounced when $k_0 \leq 0.4$. Diffusion during solidification is also important when dendritic or cellular dendritic growth is considered. This will be discussed in § 7.

6.2.4. Steady-state diffusion controlled freezing

Another practically important limiting case of one dimensional solidification occurs when all the assumptions described in § 6.2.2. apply, except item i). In this case mixing in the liquid is not complete and is governed by diffusion. Figure 22c shows the resulting solute distribution along the rod after solidification. Three distinct regions occur: an initial transient, a steady-state region and a terminal transient. The first is required to establish the steady state boundary layer of solute ahead of the interface and the third arises from the interaction of the boundary layer with the end of the specimen. The diffusion boundary layer in the liquid ahead of the S–L interface is a region of the system that transports the solute missing from the initial transient in the solid and maintains a constant solid composition in the central region of the rod. The moving boundary layer changes the liquid interface composition from C_0 to C_0/k_0, and disappears at the end of solidification by "depositing" its solute in the final transient. Figure 23 (KURZ and FISHER [1989]) shows the distribution of solute in the liquid and solid along the rod during unidirectional solidification.

References: p. 830.

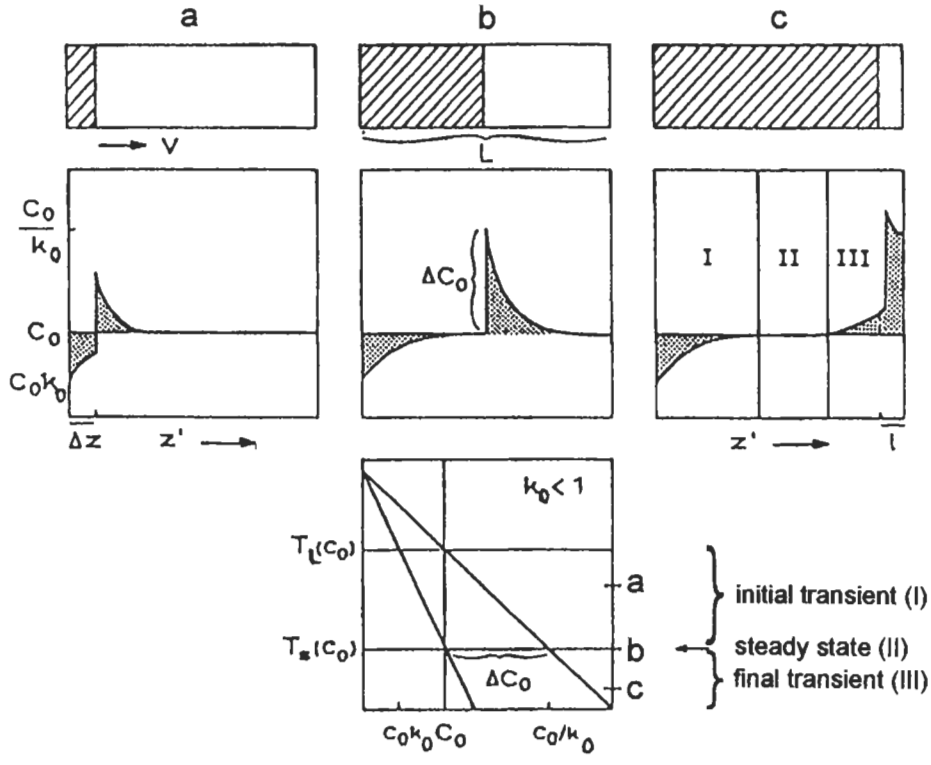

Fig. 23. Development of initial and final transient during steady-state diffusion controlled planar solidification for an alloy of composition C_0. After KURZ and FISHER [1989].

When the steady state condition has been reached in the central region of the bar, the solute distribution in the liquid in front of the interface is given by (TILLER *et al.* [1953]):

$$C_L = C_0\left[1 + \frac{1-k_0}{k_0}\exp\left(-\frac{V}{D_L}z\right)\right], \tag{63}$$

where D_L is the solute diffusion coefficient in the liquid and z the distance from the interface. Note that the liquid concentration at the interface is C_0/k_0 producing a solid composition C_0. In eq. (63) the thickness of the solute rich layer is given by the characteristic distance, D_L/V.

It is quite important to know the extent of each of the three regions shown in fig. 22c. The reader is refered to VERHOEVEN *et al.* [1988], [1989] for a summary of analysis of the initial and final transients.

6.2.5. Convection effects. Freezing with partial mixing in the liquid (Boundary Layer Approach)

Free convection, due to solute or thermal gradients in the liquid, or forced convection,

due to crystal rotation or electromagnetic forces, strongly influence segregation. This subject has been reviewed by various authors: HURLE [1972], CARRUTHERS [1976], PIMPUTKAR and OSTRACH [1981], GLICKSMAN *et al.* [1986], BROWN [1988], FAVIER [1990]. Fluid flow has important technological consequences for the processing of electronic materials where the solute distribution determines the quality of the devices.

The interval between the extreme cases of complete mixing and diffusion controlled freezing was bridged by the pioneering work of BURTON *et al.* [1953]. In this simple approach, a diffusion layer of thickness δ_F is assumed near the interface outside of which the liquid composition is maintained uniform by convection. A general expression for an effective distribution coefficient is then obtained.

$$k_{eff} = \frac{k_0}{k_0 + (1 - k_0)\exp\left[\left(\frac{-V\delta_F}{D_L}\right)\frac{\rho_S}{\rho_L}\right]}. \tag{64}$$

The solute distribution (fig. 22d) is then given by

$$C_S = k_{eff} C_0 (1 - f_S)^{k_{eff}} - 1. \tag{65}$$

Fluid flow affects the solute distribution through the parameter $V\delta_F/D_L$ in eq. (64). For vigorous convection in the liquid, $\delta_F \to 0$, $k_{eff} \to k_0$, and eq. (65) is the same as the Schiel result. For negligible convection, $\delta_F \to \infty$, $k_{eff} \to 1$, and eq. (65) gives a constant solute profile. The model has been quite successful in modeling axial segregation in the presence of laminar and turbulent convection during plane-front growth.

This simple approach, while particularly easy to use, neglects many factors which have been more recently considered. A major effort has been made to include time dependence in the BURTON *et al.* [1953] model when Czochralski and Bridgman crystal growth is considered (WILSON [1978], [1980], FAVIER [1981a], [1981b], (FAVIER and WILSON [1982]). More recently CAMEL and FAVIER [1984a], [1984b] and FAVIER and CAMEL [1986] used an order of magnitude analysis and scaling to examine different flow regimes in terms of dimensionless numbers in Bridgman crystal growth. We defer more complex models of convection until later.

6.2.6. Zone melting

The most important variables in the zone melting process are: (i) zone length; (ii) charge length; (iii) initial distribution of solute in the charge; (iv) vapor pressure and (v) zone travel rate (constant or variable). Manipulation of these variables can produce a large variety of impurity distributions in the solid charge. The most important variation of the method used to obtain high purity metals and semiconductors is *zone refining*. Figure 24 shows a schematic view of a multipass zone refining device, a more efficient system than the single pass system originally developed. The reader is referred to the important contributions of PFANN [1966] concerning this technique as well as the *zone leveling* and the *Temperature Gradient Zone Melting* (TGZM) techniques reviewed by BILONI [1983].

Recently RODWAY and HUNT [1989] established a criterion for optimizing the zone

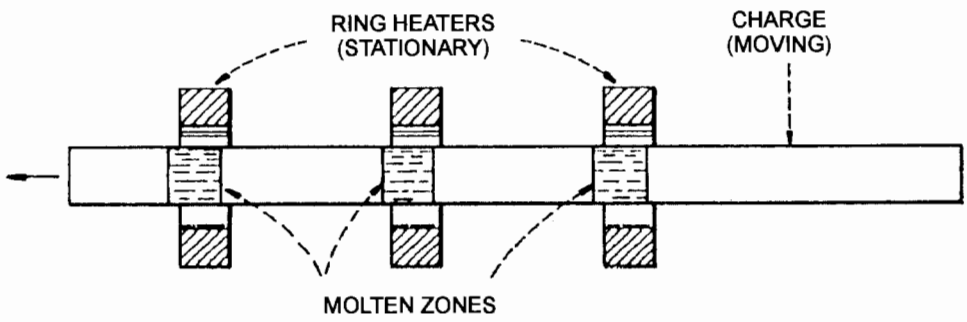

Fig. 24. Schematic of zone-refining, showing three molten zones travelling along an ingot. PFANN [1966].

length during multipass zone refining. The technique has been applied numerically, to model the redistribution in a rod, for various values of k_0. The important conclusions are: (i) a Variable Zone Size along the bar (VZS) during the process, causes a considerable increase in the rate at which the ultimate distribution is approached, compared to a fixed zone size process. This leads to a significant improvement in the usable fraction of the rod. (ii) the optimum zone length at any stage in the process is independent of the k_{eff} value. Consequently for a material containing many impurities with different k_0 values ($k_0 < 1$ or $k_0 > 1$), the VZS is optimum for all of them.

6.3. Lateral segregation

In the previous discussion we have assumed the interface to be planar. In the event that the thermal distribution of the crystal growth apparatus is not perfect, macroscopic curvature of the interface can develop. If convective mixing can be neglected, CORIELL and SEKERKA [1979], and CORIELL *et al.* [1981] have modeled the lateral segregation that will be present for a given shape. Their numerical and analytical results treat the segregation in terms of the distance that the interface deviates from planarity (δ_p), the sample width, the characteristic diffusion distance (D_L/V) and the partition coefficient, k_0. The radial segregation is greatest when k_0 is small and when $\delta_p/(D_L/V) \gg 1$. Detailed calculations of lateral segregation due to convection driven by longitudinal and radial gradients, typical of Bridgman growth upward and downward, are described by CHANG and BROWN [1983]. Experiments performed by SCHAEFER and CORIELL [1984] in the transparent succinonitrile–acetone system show the effect of radial gradients at a S–L interface.

6.4. Morphological stability of a planar interface

In § 6.2 it was assumed that the S–L interface was microscopically planar during solidification. Thus the composition profile induced in the solid varied only in the direction of growth. However even if the heat flow is controlled to be unidirectional and the isotherms are planar, a planar interface may be unstable to small changes in shape. Lateral composition variations can then be induced in the solid on a scale much smaller than the sample width. The morphological stability theory defines the conditions under

which this instability can occur. Instability of the interface utimately leads to the development of cellular and dendritic structures. An excellent review of the stability theory has recently been presented by CORIELL and MCFADDEN [1993].

6.4.1. Theory

The temperature and solute profiles for $k_0 < 1$, as a function of the distance, z, from a planar S–L interface for growth at velocity V (constrained growth) are shown in fig. 25. A linear stability analysis was first applied to a growing sphere and later to the plane by MULLINS and SEKERKA [1963], [1964] and SEKERKA [1967] under the conditions of local interface equilibrium and isotropic surface energy. One of the first extensions of this approach came when CAHN [1967] treated anisotropic kinetics and surface energy. Many other assumptions of the original theory have been relaxed over the years as summarized by SEKERKA [1986].

The analysis begins by perturbing the shape of a planar S–L interface growing in the z direction by

$$z = \delta \exp(\sigma t + 2\pi i x/\lambda), \tag{66}$$

where δ is the perturbation amplitude, λ is the wavelength, and σ is the growth (or decay) rate of the perturbation. The value for σ is determined by solving the steady-state heat flow and diffusion equations with appropriate boundary conditions for small values of δ (linear theory). The planar interface shape is stable if the real part of σ is negative

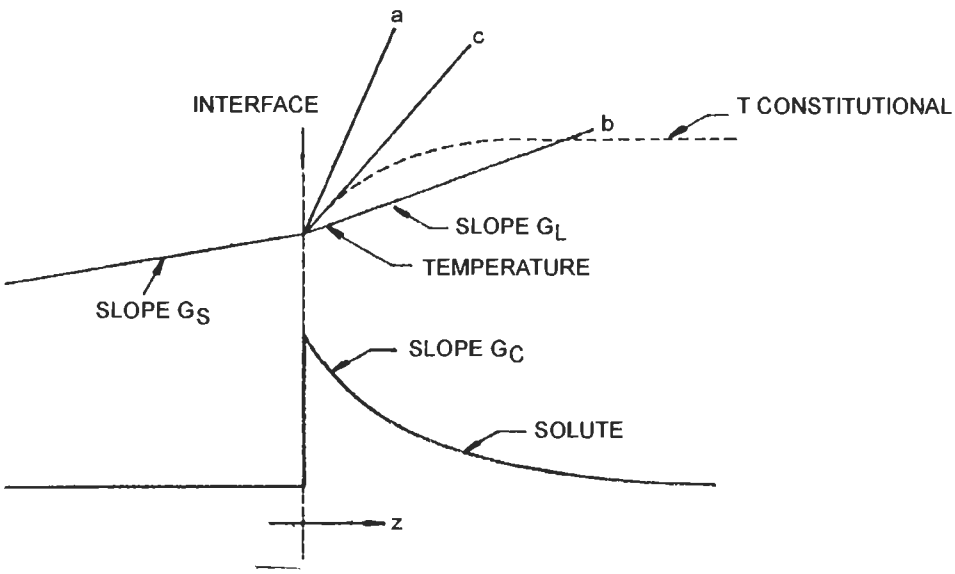

Fig. 25. Temperature and solute profile for $k_0 < 1$ as a function of distance z measured from the S–L interface when constrained growth at a velocity V occurs for a binary alloy. The concept of constitutional supercooling is included.

for all values of λ. The conditions giving the stability–instability demarcation ($\sigma = 0$) reduce to an equation with three terms corresponding to the three factors contributing to the overall stability of the interface, the thermal field, the solute field and the capillarity forces. The stability equation is

$$G - m_L G_C \xi_C + \frac{4\pi^2 T_m \Gamma}{\lambda^2} = 0. \tag{67}$$

The parameter G is the conductivity weighted temperature gradient given by

$$G = \frac{K_S G_S + K_L G_L}{2\bar{K}}, \tag{68}$$

where $\bar{K} = (K_L + K_S)/2$ is the mean of the liquid and solid thermal conductivities. The parameter G_c is the composition gradient in the liquid, which for a planar interface moving at constant velocity, is obtained from eq. (63) and is given by

$$G_C = \frac{VC_0(k_0 - 1)}{k_0 D_L}. \tag{69}$$

The parameter ξ_c can usually be set equal to unity. However ξ_c may deviate significantly from unity under rapid solidification conditions, where $V\lambda/2D_L \gg 1$. In general its value is given by

$$\xi_C = 1 + \frac{2k_0}{1 - 2k_0 - \left[1 + \left(\frac{4\pi D_L}{V\lambda}\right)^2\right]^{1/2}}. \tag{70}$$

Technically eq. (67) is correct only when $V\lambda/2a$ is small, where a is the liquid or solid thermal diffusivity. This condition is almost never violated even during rapid solidification. See KURZ and FISHER [1989] for a complete description of this detail.

If the left hand side of eq. (67) is positive, the interface is stable. The first term is stabilizing for positive temperature gradients; if the temperature gradient is negative (growth into an supercooled melt), this term is destabilizing. If a pure material is considered, this is the only possible destabilizing term. Thus a planar interface in a pure material is only unstable for growth into an supercooled melt. The second term represents the effect of solute diffusion in the liquid and, being negative, is always destabilizing. The third term, involving capillarity, has a stabilizing influence for all wavelengths, though its effect is largest at short wavelengths. This is the sort of stabilizing effect to be expected from surface energy which tends to promote an interface shape with the least area, namely a plane.

Figure 26 shows a plot summarizing the stability of a planar interface for dilute Al–Cu alloys. Figure 26a shows the value of σ vs. λ for selected values of G_L, V, and C_0 (200 K/cm, 0.1 cm/s and 0.1 wt%Cu). Under these conditions a range of wavelengths have positive σ, and are therefore unstable. The smallest unstable wavelength is usually referred to as the marginal wavelength and the wavelength with the largest value of σ is

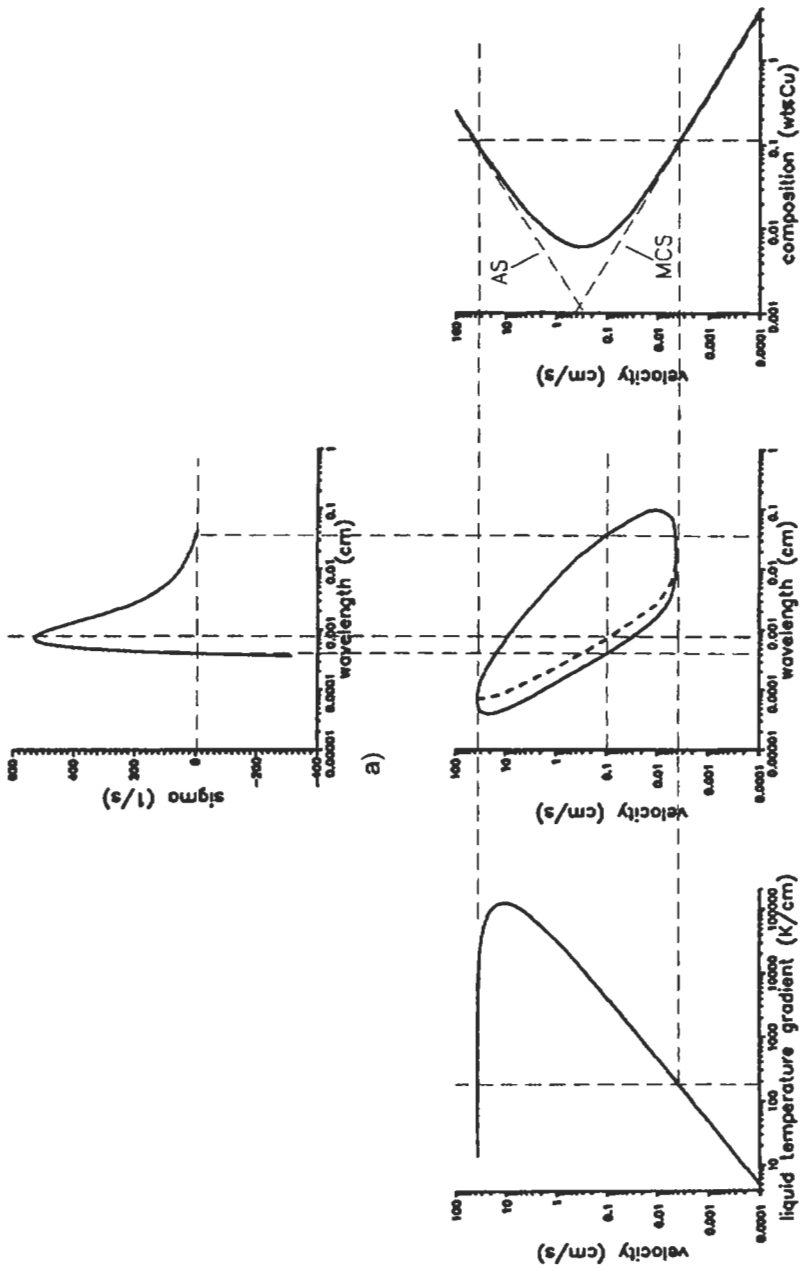

Fig. 26. Summary of the results of interface stability theory for Al-rich Al–Cu alloys. CORIELL and BOETTINGER [1994].

References: p. 830.

called the fastest growing wavelength. For some velocities, $\sigma < 0$ for all λ, and the interface is said to be stable. Figure 26c shows a closed curve of λ and V values for fixed G_L and C_0 (200°K/cm, 0.1 wt%Cu) for which $\sigma = 0$. At values of V and λ inside the closed curve the interface is unstable. Note that instability only exists over a range between two critical velocities. Outside this range, $\sigma < 0$ for all λ and the interface is always stable. Also shown dashed is the wavelength that corresponds to the fastest growing wavelength. Figure 26d shows the two critical velocities as a function of C_0 for fixed G_L (200 K/cm). The curves for the two velocities merge into a smooth curve for low C_0. Instability occurs to the right of the curve. Figure 26b shows the critical velocities as a function of G_L for fixed C_0 (0.1 wt%Cu). Note the insensitivity of the upper velocity stability limit to the value of G_L.

The upper and lower critical velocities may be approximated by two different limiting cases:

(i) If the interface grows at slow velocities, the capillarity forces are small and can be neglected; the stability criterion becomes:

$$G \geq m_L G_C. \tag{71}$$

If, in addition, eq. (68) is coupled with eq. (3), and $VL << 2K_L G_L$, the stability criterion becomes:

$$(K_L/\bar{K})G_L \geq m_L G_C, \tag{72}$$

which is called the *modified constitutional supercooling criterion*. For $K_S = K_L$ this reduces to the *constitutional supercooling criterion* (to be examined in more detail in 6.4.2).

(ii) If the interface grows at high velocity, unstable wavelengths become small and capillarity dominates. In this case, stabilization due to the temperature gradient is negligible and one obtains the *absolute stability condition*:

$$m_L G_C \leq k_0 T_m \Gamma (V/D_L)^2 \tag{73}$$

or

$$V \geq \frac{m_L C_0 (k_0 - 1) D_L}{k_0^2 T_m \Gamma}. \tag{74}$$

The modified constitutional supercooling criterion and the absolute stability criterion serve as asymptotes to the exact result at low and high velocity respectively shown in fig. 26d.

6.4.2. Relationship to constitutional supercooling

The constitutional supercooling criterion obtained by TILLER *et al.* [1953] before the morphological stability theory was developed, serves as a model to understand the major cause of instability. The theory determines if any part of the liquid ahead of a moving interface is supercooled with respect to its local liquidus temperature. The theory considers the solute distribution in front of the interface given by eq. (63) and the

corresponding liquidus temperature for the composition at each point in front of the interface given by

$$T_L(z) = T_m + m_L C_0 \left[1 + \frac{1 - k_0}{k_0} \exp\left(- \frac{V}{D_L} z \right) \right]. \tag{75}$$

The temperature in the liquid ahead of the unperturbed interface due to the temperature gradient, G_L, is

$$T(z) = T_m + \frac{m_L C_0}{k_0} + G_L \, z. \tag{76}$$

Figure 25 considers three possible profiles of the actual temperature. For case (b), the actual temperature is less than the local liquidus temperature $T_L(z)$ (labelled $T_{constitutional}$) for a range of values of z and the liquid is said to be constitutionally supercooled; as a consequence the S–L interface is unstable. Case (a), where the actual temperature exceeds $T_L(z)$, corresponds to a stable S–L interface. Case (c) is the critical condition. It can easily be demonstrated that the interface will be stable for

$$\frac{G_L}{V} \geq \frac{m_L C_0}{D_L} \frac{k_0 - 1}{k_0}. \tag{77}$$

Even though the stability criterion derived from this simple method is very similar to that derived from the more complex treatment, it does not yield any information about the size scale of the instability.

6.4.3. Experiments

Low V — The decrease of the parameter G_L/VC_0 controls [eq. (77)] the evolution of the S–L interface from plane to dendritic. Even when the evolution of the instability is continuous it is possible to recognize discrete stages of the substructure, as shown by many authors using various experimental techniques. BILONI *et al.* [1966] and BILONI [1968] summarize the various methods used: optical observations after liquid decanting, radioactive tracers, and anodic oxidation to produce interference colors. The last method is one of the most sensitive even when extremely dilute alloys such as 99.993% and 99.9993% purity Al were studied (BILONI *et al.* [1965a]). In addition, a quenching technique is often used in order to detect the morphology of the S–L interface through suitable metallography, as used among others by AUDERO and BILONI [1972]. All the techniques are based on the fact that the interface instabilities produce a redistribution of solute that can reveal the origin and development of the instabilities. With increasing CS, corresponding to a decreased value of G_L/VC_0, the following discrete stages may be defined: (i) planar S–L interface; (ii) nodes or depressions at the interface; (iii) elongated or bidimensional cells; (iv) regular hexagonal cells; (v) distorted or branched cells; (vi) dendritic cells or arrayed dendrites.

Many authors have determined experimentally that the CS criterion corresponds reasonably well to the transition from plane to unstable interfaces (CHALMERS [1964],

FLEMINGS [1974]). BILONI *et al.* [1966], through critical experiments with Sn–Pb ($k_0 < 1$) and Sn–Sb ($k_0 > 1$) alloys, were the first to establish that depressions at the S–L interface rather than projections are the first sign of interface instability. Current knowledge of the origin of the instability and its evolution can be summarized as follows:

(i) The first sign of instability is segregation associated with depressions at the interface: grain boundaries, striation boundaries and isolated depressions or *nodes*. These nodes occur in an ordered arrangement in tetragonal Sn base alloys (BILONI *et al.* [1966]) and fcc Pb–Sb alloys (MORRIS and WINEGARD [1969]). However, in Zn–Cd hexagonal close-packed alloys, the first array of nodes is disordered (AUDERO and BILONI [1973]). Alloy crystallography as well as crystal orientation have a large influence on the morphology of the interface formed after the breakdown of the planar interface.

(ii) The grooves associated with grain boundaries and striation boundaries act as built-in distortions of the plane front, and interface breakdowns begin here, spreading outward to other portions of the crystal (SCHAEFER and GLICKSMAN [1970]). The same effect occurs adjacent to the container surface (SATO and OHIRA [1977]).

(iii) The evolution from nodes or depressions at the interface into a regular or hexagonal substructure is obtained as the CS increases. This occurs by the formation of interface depressions that connect the nodes to initially form elongated cells and finally a hexagonal arrangement. This process depends on the alloy crystallography (MORRIS and WINEGARD [1969], BILONI *et al.* [1965b], BILONI *et al.* [1967], AUDERO and BILONI [1973]). Figure 27 corresponds to the evolution from a planar interface to a cellular interface shown by the shape of the decanted interface and by metallographic sectioning slightly behind the interface.

High V — With the development of techniques for rapid solidification over the past twenty five years, the ability to produce microstructures free of cellular and dendritic segregation by increasing the interface velocity as predicted by theory became possible. NARAYAN [1982] summarized the morphological stability results obtained with pulsed laser melting and resolidification in Si alloys. The transition velocities observed were in the m/s range and good agreement with the predictions of the absolute stability velocity if the velocity dependent value of the partition coefficient was used (see section 6.4.4). BOETTINGER *et al.* [1984] showed that in Ag-1 and 5 at% Cu alloys, a transition from cellular structures to plane front growth could be obtained by increasing the growth velocity beyond 0.3 and 0.6 m/s, respectively. These velocities are a factor of two larger than the calculated absolute stability values. However in view of the uncertain materials parameters, the agreement is reasonable. More recently HOAGLUND *et al.* [1991] performed a detailed study using pulsed laser melting and resolidification of Si–Sn alloys. Figure 28 shows the values of $k(V)$ determined and the fit to the morphological stability theory using these measured values of $k(V)$.

6.4.4. Further theoretical developments

Morphological stability theory remains an active area of research. The theory has been extended to include nonequilibrium solute trapping by CORIELL and SEKERKA [1983]. Complex temporally oscillatory instabilities are found. A first order approximation of the results suggests that the absolute stability condition is modified by

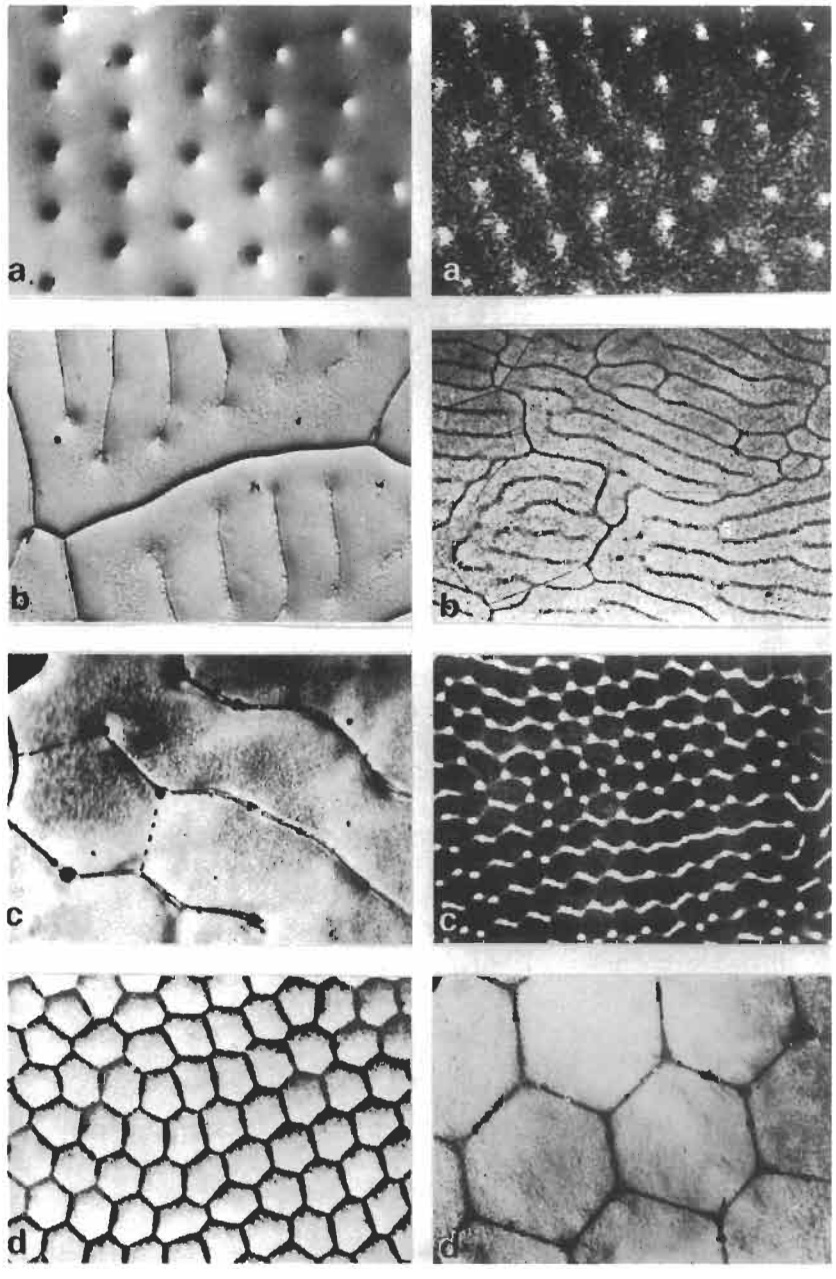

Fig. 27. Evolution of the segregation substructure as a function of constitutional supercooling shown by decanting the interface (left) and slightly behind it by metallographic sectioning (right). The amount of CS increases from (a) to (d). Magnifications: a) left: × 100, right: × 100; b) left: × 100, right: × 50; c) left: × 150, right: × 50; d) left: × 50, right: × 150. BILONI [1970].

References: p. 830.

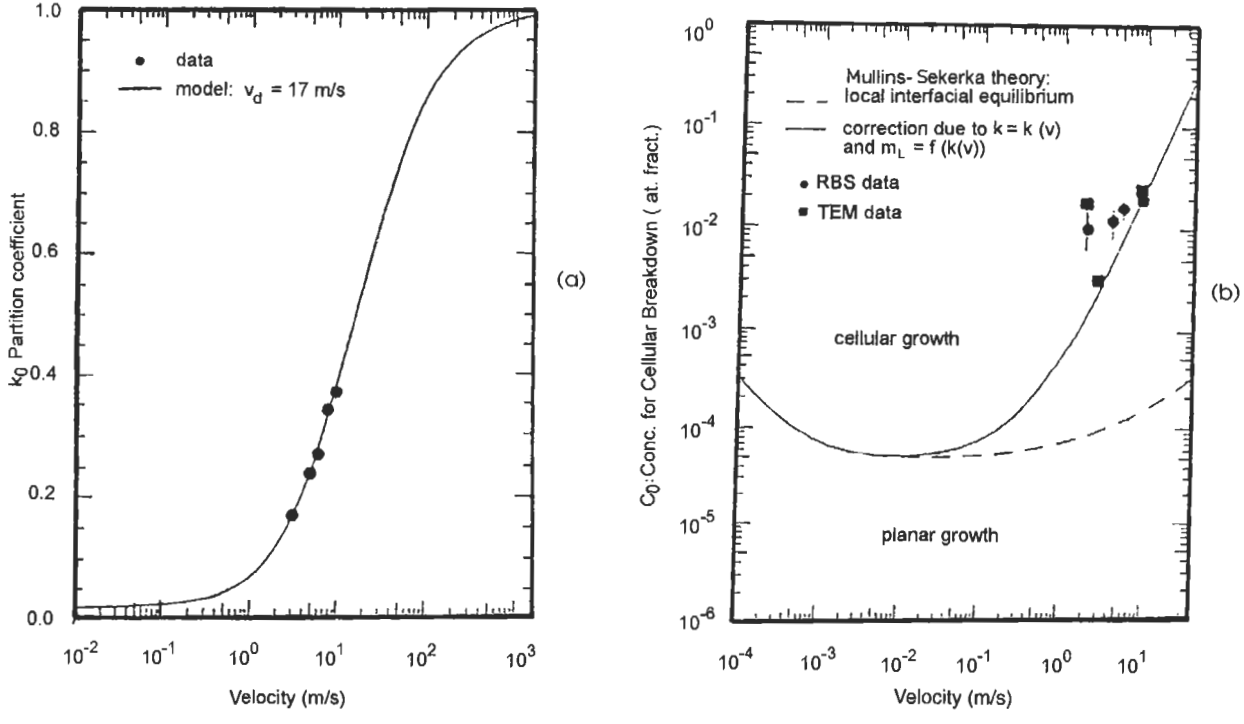

Fig. 28. (a) Velocity-dependence of measured partition coefficient of Sn in (100) Si. $k_0 = 0.016$. Data are fit by eq. (46) with $V_D = 17$ m/s. (b) Critical concentration above which cellular breakdown occurs: dashed curve stability theory using k_0; solid line, stability theory using velocity dependent $k(V)$ and $m_L(V)$. HOAGLUND *et al.* [1991].

substituting the $k(V)$ expression from eq. (46) into eq. (74) and solving implicitly for the critical velocity. This effect reduces the absolute stability velocity compared to what would be calculated on the basis of an equilibrium partition coefficient. The oscillatory instabilities exposed in this analysis and in more detailed studies are related to the banded microstructures observed at high solidification velocities (BOETTINGER *et al.* [1984]) (See § 8.1.7). Other modifications to the linear stability theory include extension to multicomponent alloys (CORIELL *et al.* [1987]), anisotropic thermal conductivities (CORIELL *et al.* [1990]), modification of the latent heat due to heat of mixing effects (NANDAPURKAR and POIRIER [1988]).

Methods for dealing with finite amplitude perturbations and the transition to cellular structures near the lower critical velocity corresponding to the constitutional supercooling condition have been summarized by CORIELL *et al.* [1985]. Two types of behavior are found depending primarily on the value of the partition coefficient (WOLLKIND and SEGAL [1970], CAROLI *et al.* [1982]). If k_0 is near unity, the transition (bifurcation) is supercritical; i.e., a small increase in the velocity past the critical value leads to interface shapes that are only slightly deformed. The wavelength of the instability is close to the fastest growing wavelength of the linear theory. For small values of k_0, the bifurcation is subcritical; i.e., a small increase above the critical value of the linear theory leads to interfaces deformed by a large amount. The wavelength is 2 to 4 times smaller than the fastest growing wavelength predicted by linear theory. The available data on the planar to cellular transition have been reviewed by CHEVEIGNE *et al.* [1988]. Agreement with the above bifurcation concepts was demonstrated. However it has been argued by LEE and BROWN [1993] that the range of velocity where the subcriticallity exists may be too small for experimental observation. They attribute the observation of spacings much smaller than the fastest growing wavelength to the fact that, at velocities only a few percent above the critical velocity, wavelengths up to factors of four smaller than the critical are also unstable. The instability of these smaller wavelengths is evident in the flatness of the bottom of the closed curve in fig. 26c. Indeed the spacing and amplitude of cells that form very close to the critical velocity are very complex (ESHELMAN *et al.* [1988]). However, few practical situations involve velocities that are so carefully controlled. A more detailed discussion of cell and dendrite shapes is deferred to § 7.

6.5. Coupled interface and fluid flow instabilities

Fluid flow is often present during solidification and upsets the diffusion of solute and heat assumed above. Fluid flow during solidification can be caused by the density difference between liquid and solid (shrinkage flow), or by the action of gravity on density gradients within the fluid phase itself. Temperature gradients as well as composition gradients due to solute rejection at the interface induce density gradients. Near a free surface between liquid and gas, temperature and composition variations can lead to gradients in surface energy that can induce flows (Marangoni Effect). This last effect has been shown to be important in some welding situations. Fluid flow can alter the morphological stability of planar interfaces and alter the composition within the interdendritic zone of castings. Flow in the mushy zone will be deferred to § 9.

References: p. 830.

HURLE [1969] and CORIELL *et al.* [1976] first treated the impact of fluid flow on interface stability using the simple boundary layer approach described in § 6.2.5. The thickness of the diffusion boundary layer, δ_F, in front of the planar interface was assumed to be reduced due to flow of an unspecified origin. This reduction increases the value G_c and if δ_F is much larger than the interface perturbation wavelength, alters the stability simply through eq. (67). FAVIER and ROUZAUD [1983] improved this approach with a deformable boundary layer. Flow resulting from radio frequency electromagnetic stirring might be treated using this boundary layer approach.

Complete coupling of the fluid flow and diffusion phenomena near a S–L interface lead to many complex results that influence morphological and fluid stability. These have been summarized by CORIELL and MCFADDEN [1990]. When directional solidification is performed with the liquid above the solid, rejection of a less dense solute can cause a liquid density that increases with height near the interface if the temperature gradient is not sufficiently large and thus cause fluid flow. However even if the overall density decreases with height, convection can still occur when a light solute is rejected. This is termed *double-diffusive convection* due to the fact that heat and solute diffuse with vastly different rates during the flow. A physical argument for the instability can be obtained by considering the forces that act on a small packet of liquid that is given a displacement upward away from the interface into a region of hotter fluid that contains less solute. Because heat transfer is more rapid than solute transfer, the packet will become hotter but remain approximately of the same composition. The displaced packet then finds itself surrounded by liquid of the same temperature but with less solute. The packet is thus less dense than its surroundings and continues to rise. Generally the wavelength of an unstable interface that forms due to the fluid instability are much larger than those of the ordinary morphological instability. However under some conditions, the wavelengths are comparable and complex time dependent oscillations can occur.

Another case of instability can occur even when the rejected solute is more dense than the solvent. Figure 29 shows experiments by BURDEN *et al.* [1973] in which a macroscopic deformation of the S–L interface was observed during growth at very slow rates (1 μm/s). Although these observations were made during cellular and dendritic growth, an analysis by CORIELL and MCFADDEN [1989] for a noncellular interface seems to apply. Instability occurred for wavelengths of the order of millimeters in this case and were determined to be due primarily to the difference in thermal conductivity of the liquid and solid phases. The creation of a slight radial temperature gradient by long wavelength perturbations induces a flow that ultimately leads to the more dense solute accumulating in the depressions in the interface. In the experiments of BURDEN *et al.* [1973], these depressions occurred at the walls of the container and the wavelength was approximately twice the container diameter.

MURRAY *et al.* [1991] studied the effect of time variations of the gravitational force during solutal convection. In the context of experiments in microgravity, this research permits an assessment of the effects of so-called *g-jitter* that occurs during space flight. In space, surface tension driven flows can also become important.

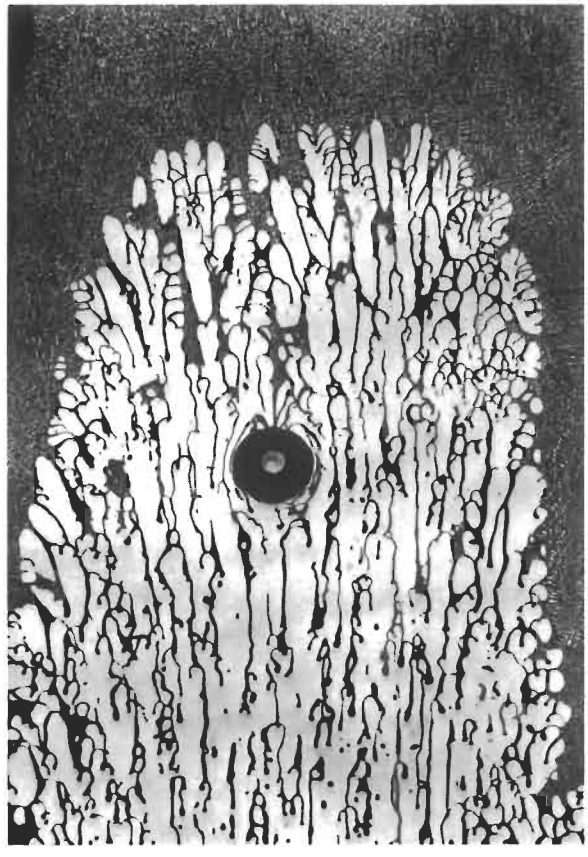

Fig. 29. Macroscopic interface shape across the full sample diameter of 4 mm for an Al-10%Cu alloy grown at $V = 2.8 \times 10^{-4}$ cm/s and $G_L = 60$ K/cm due to solute convection. BURDEN *et al.* [1973].

7. *Cellular and dendritic solidification*

The instability of the planar shape of the liquid solid interface described in § 6.4 leads to solidification by a cellular mechanism and, at conditions further from stability, by a dendritic mechanism. After the passage of the solidification front, a variation of composition remains in the solid on a length scale characteristic of the cellular or dendritic growth that is called microsegregation. This microsegregation pattern typically remains frozen in the solid due to the small ratio of the solute diffusion coefficients in the solid and liquid ($\sim 10^{-4}$ for substitutional solid solutions). In many cases the composition variation is so severe that a second solid phase solidifies in the intercellular or interdendritic regions even though none would be predicted based on a consideration of global equilibrium. The focus of this section is the prediction of the spacings associated with cellular and dendritic growth and the degree of microsegregation produced by that

growth. These spacings are important in the selection of heat treatment times and temperatures for the homogenization of ingots as well as the properties of as-cast materials. Thus the prediction of the microsegregation pattern is a fundamental goal of solidification modeling. Control of practical casting defects such as macrosegregation, porosity and hot tearing must start from an understanding of cellular and dendritic growth.

We will first focus on the theory of growth of an isolated *alloy* dendrite. The case of a pure material can be recovered from this theory by letting the composition go to zero and the reader is referred to a review of dendritic growth of pure materials by GLICKSMAN and MARSH [1993]. For alloys, the relations between dendrite tip velocity, radius, composition and supercooling will be established and compared to existing experiments. TRIVEDI and KURZ [1994] have recently reviewed alloy dendritic growth. The important expression for the tip composition will permit subsequent estimates of the degree of microsegregation. We will then consider the growth of arrays of cells and dendrites and develop an understanding of the factors that control the primary and secondary spacings of fully developed cells and dendrites. Finally we describe microsegregation.

7.1. Alloy dendritic growth

7.1.1. Theory of the tip region

Typically only the region of a growing dendrite near the tip is modelled. Two cases are distinguished: free growth and constrained growth. The model for free dendritic growth treats the situation where an isolated nucleus initiates growth into an uniformly supercooled melt and is often applied to the growth of an equiaxed grain in a casting. The melt temperature far from the dendrite can be taken as the nucleation temperature, T_N and the temperature gradient is negative; i.e., the latent heat flows into the supercooled liquid. The goal is to predict the dendrite tip velocity, V, tip radius, r, tip solid composition, C_S^*, and tip temperature, T^*, as functions of bulk liquid composition C_0 and the bulk supercooling, ΔT, below the liquidus temperature, given by

$$\Delta T = T_m + m_L C_0 - T_N. \tag{78}$$

The model for constrained growth most accurately treats the situation that occurs during directional solidification, where the heat flow is controlled by a moving furnace, and approximates the situation of dendritic growth of columnar grains where heat flows to a cold mould wall. The goal is to predict the dendrite tip radius, tip solid composition and tip temperature for a given liquid alloy composition as functions of velocity and temperature gradient. For constrained growth, the temperature gradient is positive, i.e., the latent heat flows into the solid.

For both free and constrained growth, the diffusion of solute into the liquid ahead of the growing dendrite is treated by assuming that the dendrite tip region has the shape of a paraboloid of revolution. By solving the diffusion equation in the liquid and neglecting solid diffusion, IVANTSOV [1947] has shown that the liquid composition at the dendrite tip C_L^* is given by

$$C_L^* = \frac{C_0}{1-(1-k_0)Iv(P_c)}, \tag{79}$$

where $P_c = Vr/2D_L$, and is called the solute Peclet number. The Ivantsov function, $Iv(P)$, is equal to $P\exp(P)E_1(P)$ where $E_1(P)$ is the first exponential integral of P, a function that is easily available from mathematics tables or software subroutine libraries. (The case of a 2-D (plate) dendrite was also treated and involves complementary error functions.) The composition gradient in the liquid at the tip, G_c^*, is given from the conservation of solute flux condition at the tip as

$$G_c^* = -\frac{V}{D_L}(1-k_0)C_L^*. \tag{80}$$

The treatment of the temperature field is handled differently for free or constrained growth. For free dendritic growth, heat flow in the solid can be neglected, and an Ivantsov solution for the temperature field can be obtained in the liquid. The temperature T^* at the dendrite tip is then given by

$$T^* = T_N + (L/C)Iv(P_t), \tag{81}$$

where $P_t = Vr/2a$ is the thermal Peclet number. The gradient in the liquid at the tip, G_L^*, is given from the conservation of heat flux at the tip as

$$G_L^* = -(2/r)(L/C)P_t = -\left(\frac{L}{C}\right)\left(\frac{V}{a}\right). \tag{82}$$

For constrained growth, the temperature gradient is assumed to be to that imposed by the furnace.

Regardless of the direction of heat flow, the dendrite tip temperature, T^*, must be given by the local interface condition equation evaluated at the velocity and liquid composition present at the tip, viz.,

$$T^* = T_m + m_L(V)C_L^* - \frac{2T_m\Gamma}{r} - \frac{RT_m^2}{L_m}\frac{V}{V_c}. \tag{83}$$

This expression is the same as eq. (48) except for the inclusion of the Gibbs–Thompson supercooling $2T_m\Gamma/r$ for a tip radius of r and includes interfacial non-equilibrium solute trapping effects that are important at high velocity as described in § 5. Letting $m_L(V) = m_L$ and $V_c = \infty$ recovers the local equilibrium condition valid for slow solidification.

For free growth (BOETTINGER *et al.* [1988b]), a combination of eq. (78), (79), (81) and (83) yields

$$\Delta T = \frac{L}{C}Iv(P_t) + m_L C_0\left[1 - \frac{m_L(V)/m_L}{1-(1-k_0)Iv(P_c)}\right] + \frac{2T_m\Gamma}{r} + \frac{RT_m^2}{L_m}\frac{V}{V_c}. \tag{84}$$

This equation connects the values of dendrite growth rate and tip radius that are possible for each value of ΔT. A plot of the relationship is shown in fig. 30. The curve

References: p. 830.

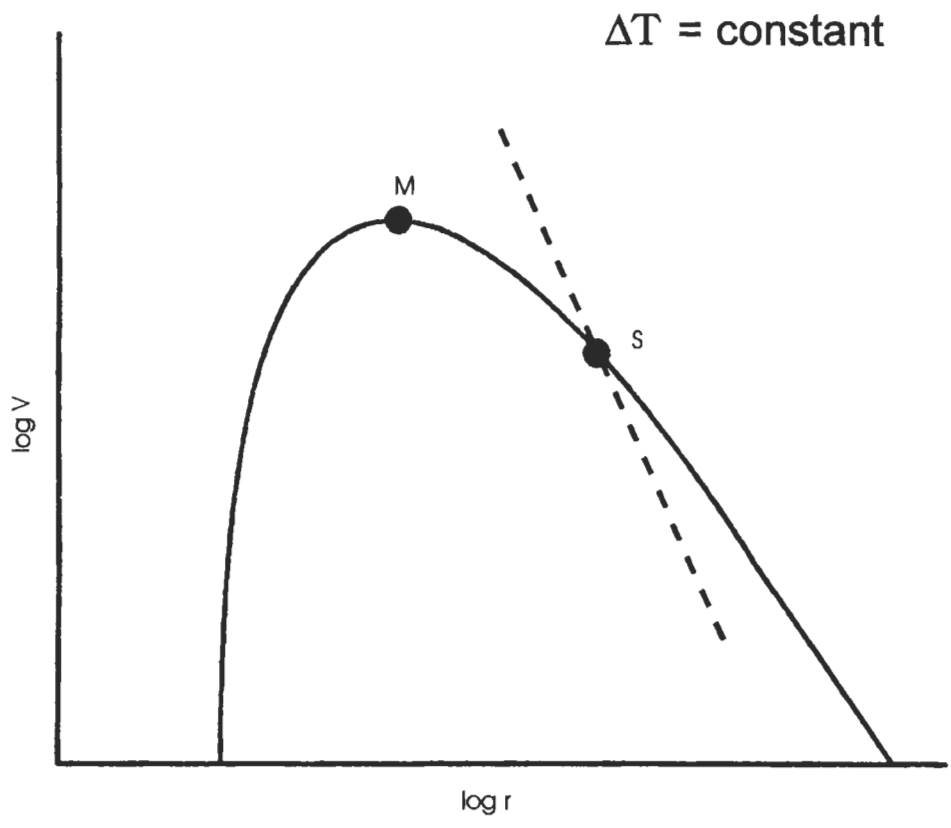

Fig. 30. Relationship between growth velocity and tip radius for dendritic growth for a fixed bulk supercooling as given by eq. (84). Point *M* corresponds to the maximum growth rate hypothesis and point *S* is the operating point of the dendrite correspond to the marginal stability hypothesis, eq. 85, shown dashed.

shows that the growth velocity would be low for small and large values of radius and exhibits a maximum velocity at intermediate values of the radius. At small values of r, the creation of a dendrite tip with high curvature (high surface area) retards growth. At large values of radius, the build-up of heat and solute at the blunt tip is so severe that growth is retarded. Thus intermediate values of radius permit higher growth rates. Experiment has shown that a unique value of velocity and tip radius occur for each value of supercooling. Thus an additional condition is necessary to uniquely specifiy V and r for each supercooling. Similarly for constrained growth, prescribed values of G_L and V also fail to specify the tip radius of the system.

The additional condition required to select the operating point of the dendrite has been the subject of much research. For many years a maximum growth rate hypothesis was employed corresponding to point *M* in fig. 30. Careful experiments by GLICKSMAN

et al. [1976] showed that this hypothesis gave dendrite tip radius values that were too small. Ideas concerning the stability of the tip were first considered by OLDFIELD [1973]. The marginal stability condition of LANGER and MUELLER–KRUMBHAAR [1978] is now commonly used and has been the subject of some experimental validation. It equates the operating tip radius with the minimum unstable wavelength prediction from linear stability theory for a planar interface growing at the same velocity with temperature and composition gradients that are present at the dendrite tip. (These values of the gradients will not in general correspond to those present for planar growth of an alloy of composition C_0). An equation for the tip radius, r, valid for small and large Peclet numbers (BOETTINGER and CORIELL [1986], LIPTON *et al.* [1987]) is given by

$$r^2 = \frac{T_m \Gamma/\sigma^*}{m_L G_c^* \xi_c - G\xi_t} \tag{85}$$

where

$$\xi_t = 1 - \frac{1}{\left(1 + \left(\sigma^* P_t^2\right)^{-1}\right)^{1/2}} \tag{86}$$

and

$$\xi_c = 1 + \frac{2k(V)}{1 - 2k(V) - \left(1 + \left(\sigma^* P_c^2\right)^{-1}\right)^{1/2}}. \tag{87}$$

The parameter σ^* is $1/4\pi^2$. ξ_t and ξ_c can be set equal to unity if P_t and $P_c \ll 1$, but may deviate from unity as the velocity approaches either the constitutional supercooling or absolute stability condition. The parameter G is the conductivity weighted temperature gradient given by

$$G = \frac{K_S G_S + K_L G_L}{K_S + K_L} \tag{88}$$

If the conductivities are equal, G is simply the mean of the liquid and solid temperature gradients. For free dendritic growth, $G_S = 0$, and

$$G = G_L^*/2. \tag{89}$$

For constrained growth, G is determined by the imposed temperature gradient of the furnace. Point S in fig. 30 shows the operating condition given by the marginal stability hypothesis.

Using the marginal stability condition, eq. (85), a complete specification of the dendrite tip can be obtained for free growth or for constrained growth. In the former case, eqs. (79, 80, 82, 89) are used in eq. (85) and solved simultaneously with eq. (84) to numerically determine the tip radius and velocity for a given value of ΔT. For constrained growth, the prescribed values of G and V are used in eqs. (79) (80) and (85) to implicitly give the radius. The radius and velocity are then used to determine C_L^*

References: p. 830.

using eq. (79) and T^* using eq. (83). We refer to the results of this theory as *IV/MS* after the Ivantsov solution using the marginal stability criterion for tip radius selection. A simplified version of this theory for free growth that assumes local equilibrium is given by LIPTON *et al.* [1984].

An example of the results of this theory for free growth into a supercooled melt using corrections for high Peclet numbers and for nonequilirium interface conditions for temperature and compositions is shown in fig. 31 for a Ag-15 wt% Cu alloy (BOETTINGER *et al.* [1988b]). Figure 31a shows the growth velocity versus supercooling relation. The dendrite velocity increases with supercooling. Note the more rapid increase

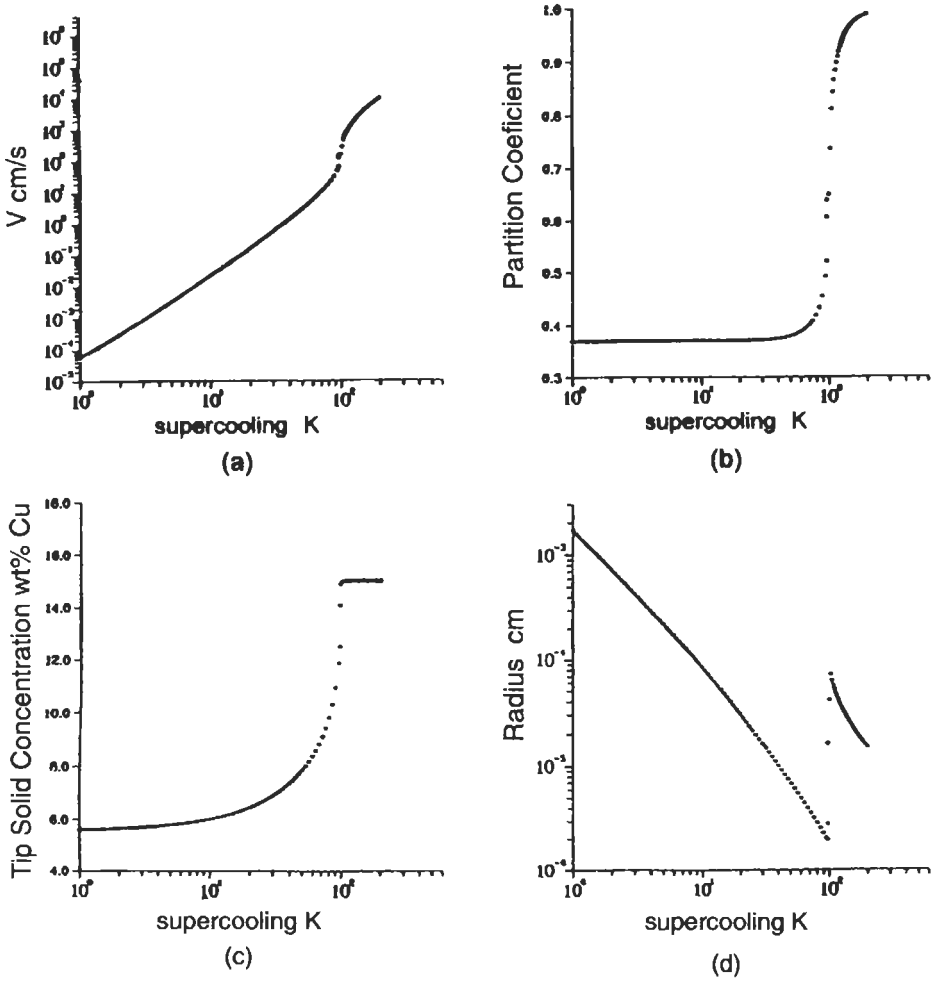

Fig. 31. Results of dendritic growth calculations for free dendritic growth of Ag-15 wt% Cu for various supercoolings below the liquidus, ΔT: (a) growth velocity, V; (b) non-equilibrium partition coefficient, k(v); (c) solid composition at the dendrite tip, ; and (d) tip radius r. BOETTINGER *et al.* [1988b].

in velocity near $\Delta T = 100$ K. Figure 31b shows how the nonequilibrium interface partition coefficient at the tip increases very sharply towards unity due to solute trapping at this same level of supercooling. This indicates the transition to partitionless solidification for the tip. In fact for supercoolings greater than 200 K the dendritic growth rate is the same as that for a pure metal with a melting point equal to the T_0 temperature for a Ag-15 wt% Cu alloy. Figure 31c shows how the composition of the solid at the dendrite tip depends on supercooling. The composition rises from 5.5 wt% Cu (k_0C_0) for low supercooling to 15 wt% Cu for $\Delta T = 100$K. This plot shows how microsegregation in dendritic structures can be reduced by increased supercooling. Finally, fig. 31d gives the dendrite tip radius. The general decline in radius with increased supercooling is sharply arrested at $\Delta T = 100$K as the dendrite tip changes from solute controlled length scales to the larger thermally controlled length scales corresponding to $k(v) \rightarrow 1$.

An example of the results of this theory for constrained growth during directional solidification of Ag–Cu alloys assuming local equilibrium is shown in fig. 32 from KURZ *et al.* [1986]. The calculated tip radius and tip temperature as a function of imposed growth rate for a temperature gradient of 10^5K/cm are given. The general trend for the radius follows $Vr^2 =$ constant for each alloy. However near the constitutional supercooling and absolute stability velocities the tip radius approaches infinity (planar interface) and deviates from this simple law. The tip temperature is close to the liquidus at intermediate velocities and approaches the solidus temperatures at low and high velocity. A very important result from this theory is that the solid composition at the center of a dendrite, $k_0C_L^*$ is only slightly greater than k_0C_0 at intermediate velocity but increases toward C_0 as the velocity approaches the constitutional supercooling and absolute stability velocities. This result impacts the discussion of microsegregation below.

7.1.2. Anisotropy

Clearly anisotropy is important in dendritic growth. Dendrites in cubic materials grow in [100] directions. In the context of the dendrite tip model described above this can be understood by a consideration of the small, but important, anisotropy of the liquid solid surface tension that was neglected above. BLODGETT *et al.* [1974] measured the anisotropy of the liquid–solid surface energy of succinonitrile. They determined that the surface energy had maxima in the [100] directions. To determine the Gibbs–Thomson coefficient, $T_m\Gamma$, for a anisotropic material with surface energy γ_{sL} that depends on orientation θ, the surface energy γ_{SL} is replaced by $(\gamma_{SL} + d^2\gamma_{SL}/d\theta^2)$. This quantity is smallest when γ_{SL} is largest. Therefore through eq. (85), the tip radius would be smaller for growth in the [100] direction than, for example, growth in the [110] direction. This smaller radius leads to more rapid growth in the [100] direction. A more complex expression is necessary if γ_{SL} depends on two angles, as would be the case for a three dimensional dendrite tip.

Despite the success of the marginal stability argument, the choice of the *minimum unstable wavelength (maximum stable wavelength)* rather than a smaller stable value remains somewhat arbitrary. Further analyses by many researchers has been summarized by BILLIA and TRIVEDI [1993]. This work indicates that by including the effect of anisotropic surface energy, only one shape preserving solutions is found to the diffusion

References: p. 830.

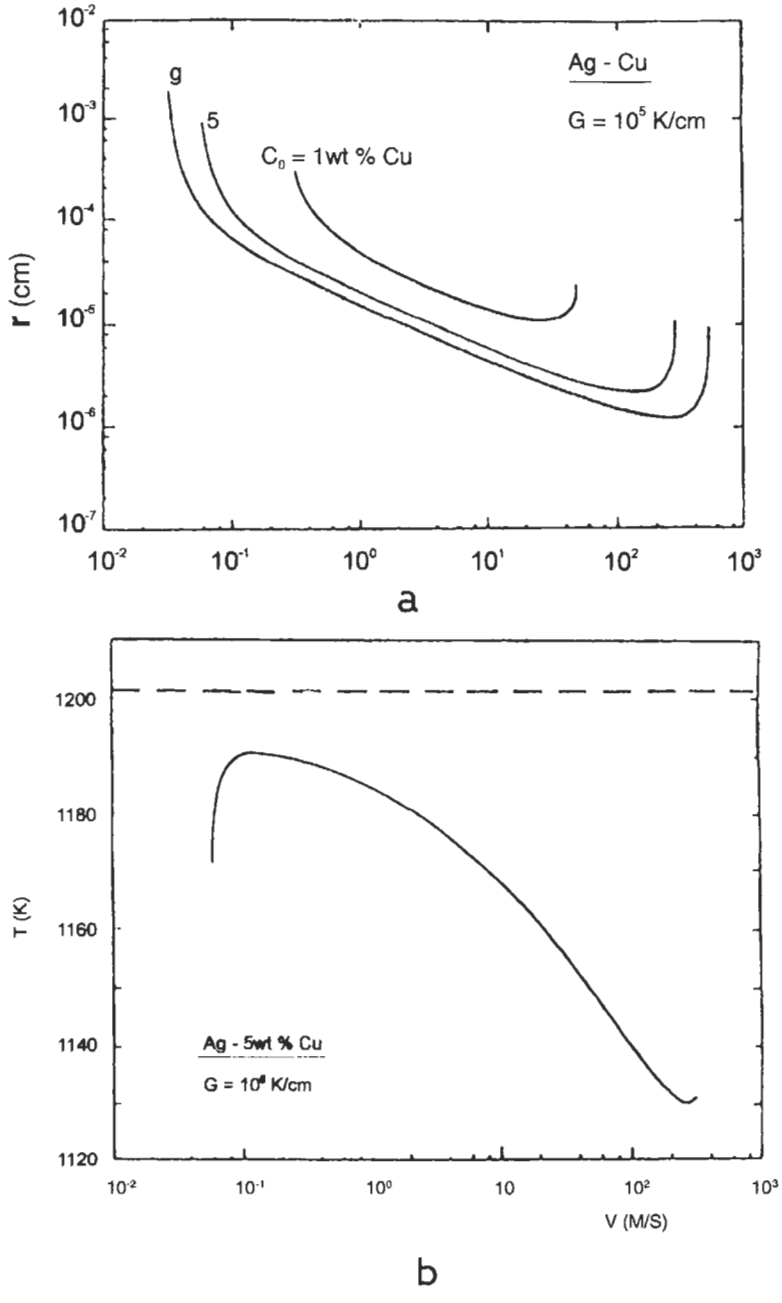

Fig. 32. Calculated dendrite tip radius (a) and tip temperature (b) for Ag–Cu alloys of the noted compositions as a function of velocity for constrained growth at a temperature gradient of 10^5 K/cm. In (b) the liquidus temperature is shown dashed. Local equilibrium was assumed. KURZ *et al.* [1986].

equations that is stable with respect to tip splitting. These considerations are called *microscopic solvability* and specify a unique value of the tip radius. Microscopic solvability predicts that the tip radius will follow essentially the same relationship given by stability analysis except that the value of σ^* depends on the degree of anisotropy in the surface energy. Tests of this model are inconclusive to date.

7.1.3. Approximate theory for low supercooling

For low supercooling, the model presented above can be simplified. For low values of P_c, local equilibrium can be assumed and $Iv(P_c)$ can be approximated by

$$Iv(P_c) \approx P_c, \tag{90}$$

an expression called the hemispherical approximation (KURZ and FISHER [1981]). This approximation leads to a particularly simple expression for the dendrite velocity as a function of supercooling

$$V = \frac{D_L}{\pi^2 m_L C_0 (k_0 - 1) T_m \Gamma} \Delta T^2 \tag{91}$$

with a tip radius given by

$$r = \left(\frac{D_L T_m \Gamma / \sigma^*}{m_L C_0 V (k_0 - 1)} \right)^{1/2}. \tag{92}$$

These relations can be applied to free growth or to constrained growth. However for the latter, the expressions are only valid when the temperature gradient is small. In this case the supercooling, ΔT, in eq. (91) is the difference between the liquidus temperature for the bulk alloy composition and the dendrite tip temperature.

7.1.4. Experiments on dendritic growth

CHOPRA *et al.* [1988] have compared the results of the LIPTON *et al.* [1984] theory to experiments using succinonitrile–acetone transparent alloys. Their results are shown in fig. 33. One of the most interesting results of the theory and experiments is that the addition of a small amount of solute actually increases the growth rate of the dendrites above that for the pure material for fixed bath supercooling below the liquidus. This effect is due to the destabilizing influence (through G_c^* in eq. (85)) of the solute on the dendrite tip. The solute pushes the marginal wavelength and consequently the tip radius to a smaller value and permits the dendrite to grow at a higher speed. With further increased levels of solute, the transport difficulties associated with the solute begin to dominate and the dendritic growth rate slows for a fixed supercooling below the liquidus.

For high supercoolings (100–300 K), several groups have obtained dendritic growth rate data as a function of bulk supercooling for alloys using carefully designed experiments in levitated samples (WU *et al.* [1987] and ECKLER *et al.* [1992]). Good agreement between theory and experiment has been obtained. Figure 34 shows a summary of data and theoretical predictions of the model that incorporates non-equilibrium interface

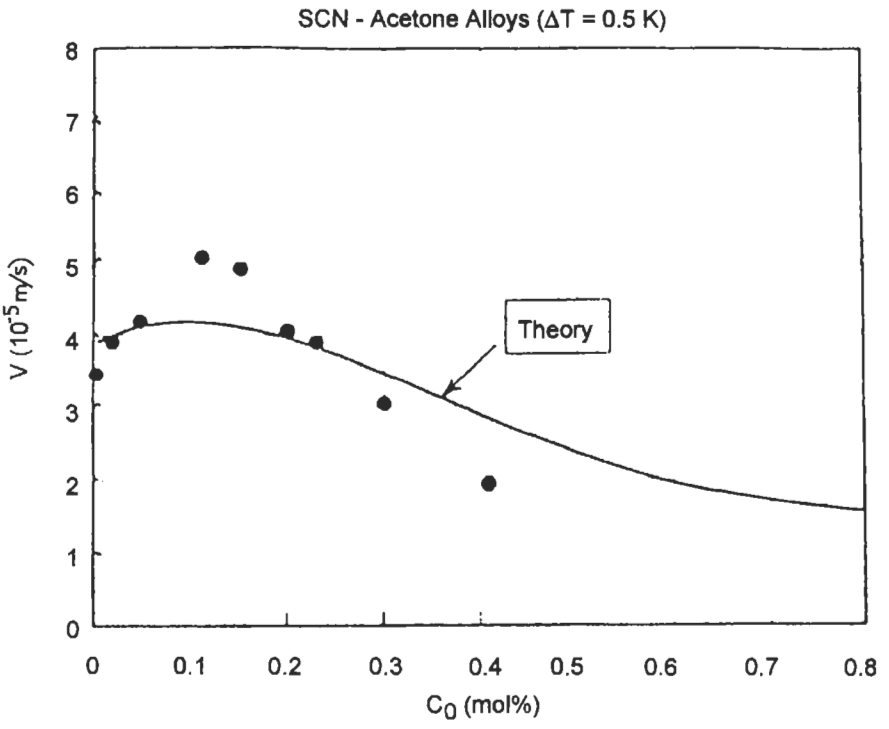

Fig. 33. Comparison of theory and measured dendrite growth velocities as a function of alloy composition for a fixed bulk supercooling below the liquidus of 0.5 K for succinonitrile-acetone alloys. CHOPRA *et al.* [1988].

kinetics for pure Ni and for Ni–B alloys by ECKLER *et al.* [1992]. The abrupt increase in velocity at high supercoolings is associated with the transition from solute controlled dendritic growth to thermally controlled growth brought about by the solute trapping (velocity dependent partition coefficient).

The predictions of the theory for constrained growth have been compared by KURZ *et al.* [1988] to measurements of cell compositions for Ag-15 wt% Cu alloy samples prepared by moving electron beam melting performed by BOETTINGER, *et al.* [1987]. Figure 35 shows bars corresponding to the observed range of composition across cells of the Ag-rich phase as a function of growth velocity. The solid curve shows the results of the present theory. The curve marked IV/MS is the same theory without the inclusion of the velocity dependence of the partition coefficient. The curve BH is the older dendritic growth theory of BURDEN and HUNT [1974a], [1974b] which uses the maximum growth rate hypothesis rather than the marginal stability analysis. It can be seen that the present formulation is closer to the observed experimental data.

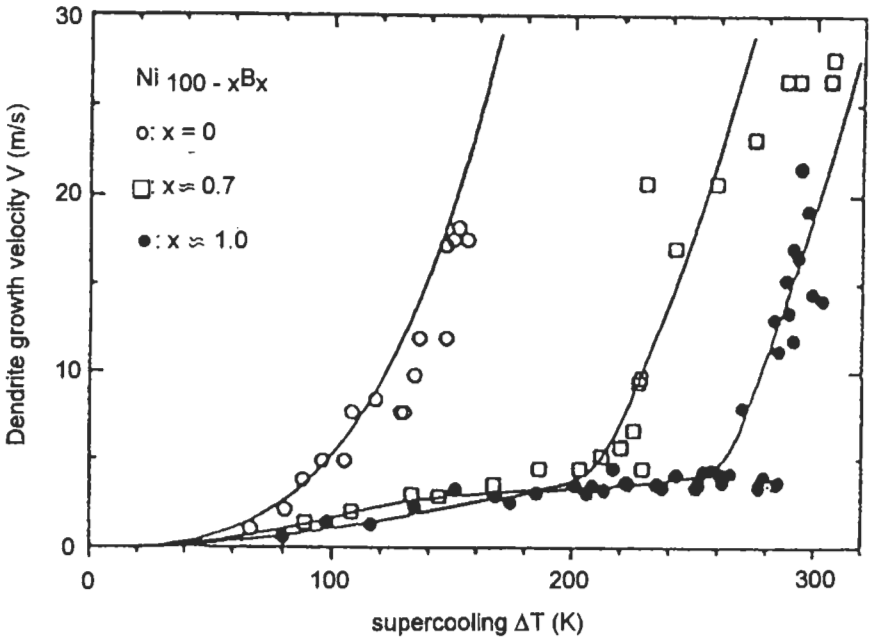

Fig. 34. Comparison of theory and measured dendrite growth velocities as a function of bulk supercooling below the liquidus for pure Ni and two Ni–B alloys. ECKLER *et al.* [1992].

7.2. Cell and dendrite spacings

7.2.1. Numerical calculations of arrayed cell and dendrite primary spacings

During constrained growth cells and dendrites form arrays with a characteristic spacing transverse to the growth direction called the primary spacing. To model the primary spacing, interactions with neighboring cells/dendrites must be considered. In a series of papers, HUNT [1990], LU and HUNT [1992] and LU *et al.* [1994] have performed finite difference calculations to study cell/dendrite shapes and primary spacings during constrained growth. The diffusion equation for solute in the liquid is solved employing local equilibrium. More recently LU *et al.* [1994] use the non-equilibrium interface conditions, eq. (46) and (48), for similar calculations. Computations are performed for single cells and dendrites with radial symmetry in a cylindrical computational domain of various diameters. This geometry is used to approximate a hexagonal array of cells or dendrites with a primary spacing equal to the cylinder diameter. Two classes of solutions were obtained; those with rounded nearly hemispherical interface shapes and those with parabolic interface shapes. The authors associate these two shapes with cells and dendrites respectively. Side branching was not simulated in the dendrite calculations. Multicell calculations where also performed to examine the stability of arrays of cells and dendrites with various primary spacings.

For a very wide primary spacing, only dendritic solutions were obtained and a unique

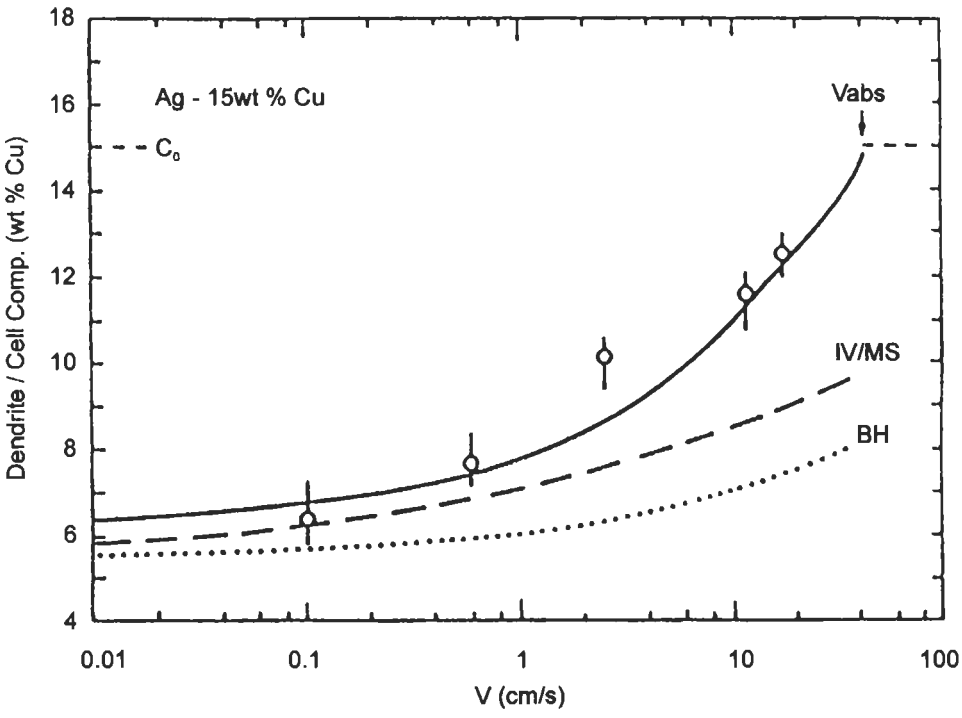

Fig. 35. Measured average composition (circles) of cells of the Ag-rich phase in a Ag-15 wt% Cu alloy as a function of solidification velocity (BOETTINGER *et al.* [1987]). The bars at each velocity represent the range of composition observed for each profile measured by STEM. The three curves are: i) the predictions of dendritic growth theory with velocity dependent partition coefficient, (solid curve), ii) without the velocity dependent partition coefficient, curve labeled IV/MS, iii) the older Burden–Hunt model of dendritic growth (labeled BH). KURZ *et al.* [1988].

value of tip radius was determined for a given set of growth conditions. This computational regime is thought to approximate isolated dendrites. Although the original work (HUNT [1990]) indicated that anisotropic surface energy was not necessary to obtain this unique solution, it was later determined that slight anisotropy was induced by the calculation mesh. Later work (LU and HUNT [1992]) confirmed the important role of anisotropy on the selection of the radius of the tip. The values of radius determined by these calculations can be approximated by the IV/MS model.

For smaller primary spacings, both cell and dendrite solutions could be obtained for the same growth conditions. For each, solutions could be obtained only over a range of primary spacings. The physical processes that define the allowable range of primary spacings are shown in fig. 36. The minimum stable cell spacing is determined by overgrowth of one cell by the adjacent cells. The maximum cell spacing occurs when the cell tips become very flat and on the verge of splitting. For dendrites, the minimum

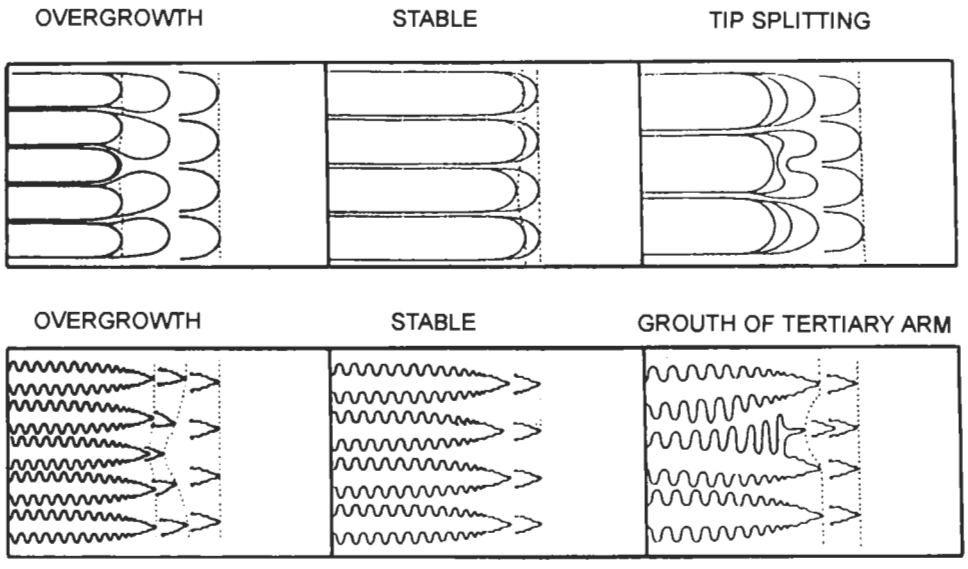

Fig. 36. Schematic illustration of primary spacing adjustment mechanism for cells and dendrites. LU and HUNT [1992].

spacing is also determined by overgrowth. The maximum spacing is assumed to be twice the minimum spacing based on an argument regarding the transition of tertiary arms into new primary arms. An example of the range of primary spacing that could be calculated is shown in fig. 37 and 38 along with experimental data for slow and rapid solidification respectively. The existence of a range of spacings for cells for given growth conditions agrees with observations of ESHELMAN and TRIVEDI [1988]. The predictions of the dendrite tip radius from the IV/MS theory presented above are also shown in fig. 38. It is seen that the primary spacing of the cell solutions is approximately twice the dendrite tip radius from the IV/MS value.

The computations described above do not describe the conditions at the root of cells. The walls of adjacent cells never join and a thin layer of liquid persists far behind the cell tips. UNGAR and BROWN [1985] have performed finite element calculations of deep cells using a composite coordinate technique that allows cell walls to fold over and join at the cell roots. In fact small drop-like structures are found to form at the cell roots that may be indicative of the pinch-off and periodic shedding of liquid droplets. Such shedding of liquid droplets may be the cause of spherical second phase particles that occur in some rapidly solidified alloys, BOETTINGER *et al.* [1988c].

7.2.2. Analytical expressions for primary spacings

Analytical theories of primary spacings often yield a power law expression applicable to a range of solidification conditions not too close to the constitutional supercooling or absolute stability velocities that is given by

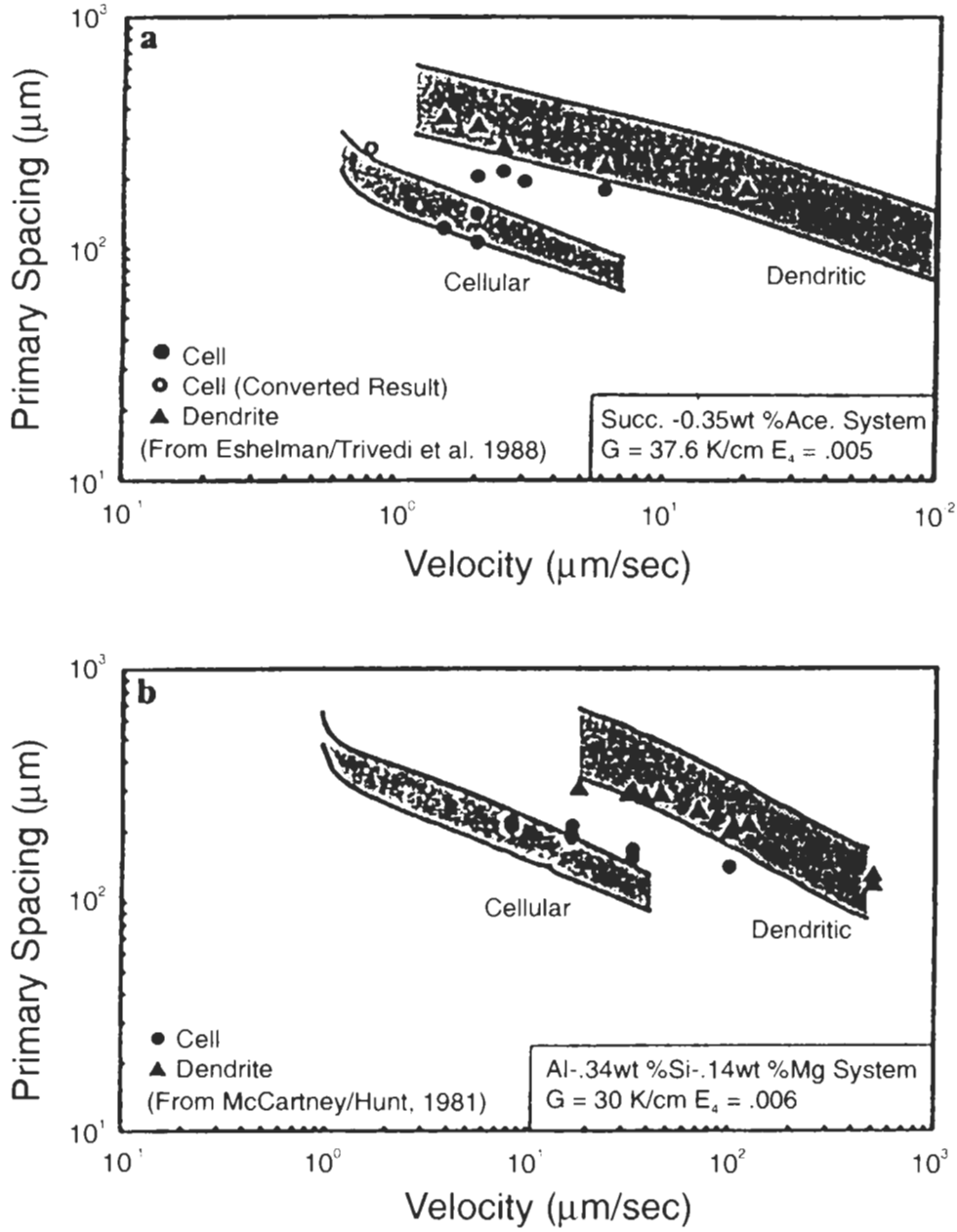

Fig. 37. Comparison of the predicted ranges of cell/dendrite primary spacings with experimental results: (a) succinonitrile-0.35 wt% acetone; (b) Al-0.34 wt% Si-0.14 wt% Mg. E_4 specifies the anisotropy of the surface energy. LU and HUNT [1992].